Dissertation zur Erlangung des Doktorgrades
der Fakultät für Chemie und Pharmazie
der Ludwig-Maximilians-Universität München

S100a4 Secreted by Alternatively Activated Alveolar Macrophages Promotes Activation of Lung Fibroblasts in Pulmonary Fibrosis

Wei Zhang
aus
Handan, China

2016

Erklärung

Diese Dissertation wurde im Sinne von §7 der Promotionsordnung vom 28. November 2011 von Herrn Prof. Dr. Heiko Adler betreut und von Herrn Prof. Dr. Klaus Fürstemann von der Fakultät für Chemie und Pharmazie vertreten.

Ehrenwörtliche Versicherung

Diese Dissertation wurde selbständig, ohne unerlaubte Hilfe erarbeitet.

München, 24.10.2016

Wei Zhang

Dissertation eingereicht am 24.10.2016

1. Gutachter: Prof. Dr. Klaus Fürstemann

2. Gutachter: Prof. Dr. Heiko Adler

Mündliche Prüfung am 08.12.2016

I dedicate this work to my family.

Table of Contents

Zusammenfassung

Idiopathische pulmonale Fibrose (IPF) ist eine progressive und tödliche Lungenerkrankung unbekannter Ätiologie. Charakterisiert wird sie durch die Schädigung der Alveolarepithelzellen, durch eine übermäßige Ablagerung der extrazellulären Matrix (EZM) im Lungeninterstitium und durch die verstärkte Aktivierung und Proliferation von Fibroblasten. Letzten Endes führt dies zur strukturellen Veränderung der Lungenarchitektur und den Verlust der Gas-Austausch-Funktion. Zwei wichtige zelluläre Spieler für die Reparatur des Gewebes und für die Fibrose sind Makrophagen und Fibroblasten. Fibroblasten proliferieren und migrieren in die Wundstelle, werden aktiviert und differenzieren zu Myofibroblasten. Die aktivierten Fibroblasten erzeugen dann, in erster Linie in Form von Kollagen, große Mengen an EZM. Makrophagen zeigen hingegen unterschiedliche Aktivierungszustände. Die häufigsten Phänotypen sind die klassisch aktivierten (M1) und die alternativ aktivierten (M2) Makrophagen. Entzündungen und Gewebeverletzungen werden den pro-inflammatorischen M1-Makrophagen zugeschrieben. Die anti-inflammatorischen M2-Makrophagen hingegen werden durch die Sekretion von profibrotischen Faktoren mit der Gewebereparatur und der Fibrose assoziiert. Die profibrotischen Faktoren induzieren möglicherweise zu einem späteren Zeitpunkt die Proliferation und Aktivierung von Fibroblasten. Neben der bereits bekannten Funktion von Makrophagen und Fibroblasten in der Gewebshomöostase muss die Rolle der von den M2-Alveolarmakrophagen sezernierten parakrinen Faktoren sowie deren Effekt auf die Fibroblasten der Lunge noch weiter erforscht werden, um neue therapeutische Ziele zu finden.

In der vorliegenden Arbeit wurden diesbezüglich MHV-68-infizierte IFN-γR$^{-/-}$ Mäuse als Modell für die Untersuchung der IPF-Pathogenese verwendet. Hierfür wurden Microarray-Analysen von Lungen infizierter IFN-γR$^{-/-}$ und C57BL/6 Mäuse zu unterschiedlichen Zeitpunkten nach der Infektion durchgeführt, um einen allgemeinen Überblick über die transkriptionelle Antwort der Lunge während der akuten und chronischen Infektion zu erhalten und bisher unbekannte, unterschiedlich regulierte Gene, welche an einer pulmonalen Fibrose beteiligt sind, zu identifizieren. Elf potentielle Zielgene wurden ausgewählt und durch qRT-PCR bestätigt. Zusätzlich wurden eine systematische Datenbank-Analyse (PubMed) und ein Vergleich mit

anderen IPF-Tiermodellen durchgeführt. Im Ergebnis wurde das Gen S100a4 für weitere Untersuchungen ausgewählt. Die Untersuchung des gesamten Lungengewebes mittels Western Blot sowie die Analyse der bronchoalveolären Lavage (BAL) Flüssigkeit via ELISA zeigten sowohl in IFN-γR$^{-/-}$ als auch in C57BL/6-Mäusen eine erhöhte Expression von S100a4-Protein während der akuten Entzündungsphase, die während der fibrotischen Phase bei Wildtyp-Mäusen auf das Kontrollniveau zurückging, während sie bei IFN-γR$^{-/-}$ Mäusen erhöht blieb. Darüber hinaus zeigte die Untersuchung der BAL-Flüssigkeit von Bleomycin-behandelten C57BL/6-Mäusen ebenfalls eine erhöhte Expression von S100a4. Die immunohistochemische Färbung des fibrotischen Lungengewebes zeigte, dass S100a4 von M2-polarisierten Alveolarmakrophagen produziert wurde. Folglich wollten wir untersuchen, ob und wie endogenes S100a4 eine profibrogene Funktion ausübt. In vitro Experimente zeigten, dass durch die Stimulation mit rekombinantem S100a4 eine Proliferation und Aktivierung von Lungen-Fibroblasten induziert wird. Darüber hinaus konnte, einhergehend mit den bereits vorausgegangenen Untersuchungen, gezeigt werden, dass Lungen-Fibroblasten, welche konditioniertem Medium von M2-polarisierten primären Alveolarmakrophagen ausgesetzt wurden, eine verstärkte Zellproliferation zeigen. Mit konditioniertem Medium von M2-Makrophagen, die in Anwesenheit einer anti-S100a4 siRNA polarisiert wurden, war dieser Effekt geringer ausgeprägt. Zudem neutralisierten wir das im M2-konditionierten Medium enthaltene S100a4 Protein mit einem anti-S100a4-Antikörper. Die Neutralisation durch den Antikörper führte ebenfalls zu einer Reduktion der Proliferation der Lungen-Fibroblasten. Dies war nicht mit dem mit Isotyp-Kontroll-Antikörper behandeltem M2-konditioniertem Medium der Fall. Zusammenfassend deuten die Daten daraufhin, dass S100a4 eine wichtige Rolle bei der Proliferation und Aktivierung von Lungen-Fibroblasten spielt. Weitere in vitro Experimente zeigten, dass Calcimycin und Niclosamid, zwei S100a4 Transkriptions-Inhibitoren, die S100a4 mRNA Expression in Alveolarmakrophagen während der M2- Polarisation signifikant reduzierten.

Zusammenfassend zeigt die Arbeit, dass das von M2-polarisierten Alveolarmakrophagen produzierte S100a4 eine profibrogene Funktion - durch die Erhöhung der Proliferation und Aktivierung der Lungen-Fibroblasten - ausübt. Dies lässt vermuten, dass eine Hemmung von S100a4 eine potentielle therapeutische Strategie zur Behandlung der idiopathischen pulmonalen Fibrose sein könnte.

Summary

Idiopathic pulmonary fibrosis (IPF) is a progressive and fatal lung disease of unknown etiology. It is characterized by the damage of alveolar epithelial cells, excessive deposition of extracellular matrix (ECM) in the lung interstitium, and enhanced activation and proliferation of fibroblasts, which ultimately leads to the distortion of normal lung architecture and loss of gas-exchanging function. Macrophages and fibroblasts are two major cellular players in tissue repair and fibrosis. Fibroblasts proliferate and migrate into the wound site, and some of these fibroblasts become activated and differentiate into myofibroblasts, which produce large amounts of ECM, primarily in the form of collagen. Macrophages display various activation states, and the main activation phenotypes are classically activated (M1) and alternatively activated (M2) macrophages. The pro-inflammatory M1 macrophages are often associated with inflammation and tissue injury, whereas the anti-inflammatory M2 macrophages are associated with tissue repair and fibrosis by secreting profibrotic factors. The latter may induce the proliferation and activation of fibroblasts. Despite the known association of macrophages and fibroblasts in tissue homeostasis, the role of paracrine factors secreted by M2 alveolar macrophages and their effects on lung fibroblasts still needs to be further investigated in order to determine novel therapeutic targets.

In this thesis, MHV-68-infected IFN-γR$^{-/-}$ mice were used as a model to study the pathogenesis of pulmonary fibrosis. Microarray analysis was performed in MHV-68-infected IFN-γR$^{-/-}$ mice and C57BL/6 wild-type mice at different times post infection in order to obtain a global view of transcriptional responses of the lung during acute and chronic infection, and to identify differentially regulated genes that were sofar not known to be involved in pulmonary fibrosis. Subsequently, eleven potential target genes were selected and validated by qRT-PCR. In parallel with the statistical analysis of the microarray data, a systematic search in the PubMed literature and a comparison with other IPF animal models were also conducted. As a result, the gene *S100a4* was selected for further investigation. Western blot analysis of whole lung tissue and ELISA analysis of bronchoalveolar lavage (BAL) fluids demonstrated that S100a4 was highly expressed during acute inflammation in both IFN-γR$^{-/-}$ mice and C57BL/6 mice, but then declined to the control level in wild-type mice during the fibrotic phase whilst remaining high in IFN-γR$^{-/-}$ mice. In addition, ELISA analysis of

BAL fluids from bleomycin treated C57BL/6 mice also showed high expression levels of S100a4. Immunohistochemistry staining of fibrotic lung tissue revealed that S100a4 was produced by M2 polarized alveolar macrophages. Accordingly, whether and how endogenous S100a4 exerts profibrogenic functions was investigated. *In vitro* experiments revealed that stimulation with recombinant S100a4 induces proliferation and activation of lung fibroblasts. Additionally, lung fibroblasts exposed to conditioned medium from M2 alveolar macrophages showed enhanced cell proliferation. In contrast, conditioned medium generated from M2 macrophages polarized in the presence of anti-S100A4-siRNA showed less proliferation activity. Moreover, neutralization of S100a4 protein in the M2 conditioned medium with an anti-S100a4-antibody also resulted in less proliferation of lung fibroblasts, a phenomenon which was not observed with the isotype control antibody treated M2 conditioned medium. Collectively, all these data suggested that S100a4 plays an important role in lung fibroblast proliferation and activation. Furthermore, *in vitro* experiments using two transcriptional inhibitors of S100a4, calcimycin and niclosamide, showed that 1μM calcimycin or 0.3μM niclosamide significantly reduced the S100a4 mRNA expression level in alveolar macrophages during M2 polarization.

In summary, the study demonstrates that S100a4, produced by M2 polarized alveolar macrophages, exerts profibrogenic functions by enhancing the proliferation and activation of lung fibroblasts. These data suggest that inhibition of S100a4 might represent a potential therapeutic strategy for idiopathic pulmonary fibrosis.

1. Introduction

1.1 Idiopathic Pulmonary Fibrosis

1.1.1 Definitions

Idiopathic pulmonary fibrosis (IPF) is a chronic, fibroproliferative and irreversible interstitial pneumonia of unknown etiology and the most devastating form of interstitial lung diseases (ILDs) (1). The hallmarks of IPF are the increased extracellular matrix (ECM) deposition, fibroblastic foci (activated fibroblasts) and honeycombing predominantly in the subpleural interstitial space suggestive of abnormal tissue repair and aberrant wound healing responses (2-4). When this critical area is saturated with ECM deposition or inflammatory cells, the gas-exchanging function is eliminated and finally results in respiratory failure and death (5). The definite diagnosis of IPF requires the identification of usual interstitial pneumonia (UIP) on surgical lung biopsy (1, 6).

Collectively, lung diseases affecting the interstitium are termed interstitial lung diseases (ILDs) (also known as diffuse parenchymal lung diseases (DPLDs)), and were initially reported by Hamman and Rich in 1944 (7). ILDs are a heterogeneous group of more than 100 distinct disorders resulting in injuries to the lung parenchyma, and frequently share similar clinical presentations and physiological abnormalities (8). The causes of ILDs have been well characterized; they include environmental factors (organic dust or allergens), autoimmune diseases, drug toxicity and sarcoidosis (9). However, a large number of ILDs are of unidentified origin and are categorized as idiopathic interstitial pneumonias (IIPs) (8, 10).

Although there are diverse mechanisms underlying IIPs, many of them possess similar radiological and/or histopathological characteristics. This led the American Thoracic Society and the European Respiratory Society to introduce the criteria for the international classification and diagnosis of IIPs in 2002 (11), and an official update of the guidelines published in 2013 (10) (Table 1.1).

Table 1.1 Revised American Thoracic Society/European Respiratory Society Classification of Idiopathic Interstitial Pneumonias. Adapted from (10).

Major idiopathic interstitial pneumonias
Idiopathic pulmonary fibrosis
Idiopathic nonspecific interstitial pneumonia
Respiratory bronchiolitis–interstitial lung disease
Desquamative interstitial pneumonia
Cryptogenic organizing pneumonia
Acute interstitial pneumonia
Rare idiopathic interstitial pneumonias
Idiopathic lymphoid interstitial pneumonia
Idiopathic pleuroparenchymal fibroelastosis
Unclassifiable idiopathic interstitial pneumonias

1.1.2 Epidemiology and Risk Factors

Because of the rarity and complexity in diagnostic practices of IPF, there are no substantial studies of the prevalence of IPF. A recent study from the United States estimated the incidence rate of 14.6 per 100,000 persons/year by utilizing three algorithms to analyze the database of HealthCore Integrated Research (12). Another study reported that the overall incidence rate was around 4 cases per 100,000 inhabitants/year in the United Kingdom based on the figures for the whole population, and the incidence is rising by 5% per year (13). The occurrence of IPF is higher in males (10.7 cases per 100000/year) when compared to females (7.4 cases per 100000/year) and the incidence or prevalence increases with age (14). The disease is extremely rare in young people, but is primarily seen in people aged 50 years or older with an approximate three-year median survival duration after diagnosis, which is the worst prognosis among the IIPs (9, 15).

Although IPF is, by definition, a disease of unknown etiology and of unknown molecular mechanisms, several potential risk factors have been described: cigarette smoking (16), environmental exposures (metal/wood dust, plant/animal dust) (17-19), gastroesophageal reflux (20), microbial agents (21, 22), and genetic predisposition (23, 24).

1.2 Pathogenesis of IPF

The limited understanding of the mechanisms of IPF is reflected by the lack of effective therapies. Initially, investigations led to the assumption that a chronic inflammatory response to an unclear insult was the possible cause of this disease (25, 26). In the past decade, a new hypothesis has been put forward with a focus on the origins of myofibroblasts, the ultimate effector cells in the pathogenesis of fibrosis. They are morphologically characterized by an elongated spindle or stellate shape and an intermediate feature between smooth muscle cells and fibroblasts, with abundant expression of stress fibers consisting of α-SMA, indicating a role in contractile activity (27, 28). Once the myofibroblasts accumulate in the wound area, they sustain a contractile activity for a long time, and the contraction is maintained by secretion of extracellular matrix, primarily type I collagen, elastins and proteoglycans (29). Moreover, they also play roles in releasing inflammatory cytokines and in epithelial injury. All of these make them the key cells responsible in perpetuating the cycle of wound healing and pathologic lung fibrosis, and the accumulation of myofibroblasts is considered the hallmark of IPF (30). Therefore, a better knowledge of the cellular origin of these cells is thought to be of great significance in order to enhance understanding of fibrosis development and for the development of new therapeutic treatments. Three main potential cellular sources in IPF are proposed: transdifferentiation of epithelial cells to mesenchymal cells (31), activation of resident fibroblasts (32) and recruitment of bone marrow-derived fibrocytes (33). In addition, it is suggested that resident fibroblasts, which comprise 30%-40% of pulmonary cells and function as scaffolds to support alveolar structure by secretion of ECM, are the primary precursors of myofibroblasts (34, 35). However, the precise mechanism underlying IPF remains enigmatic and further elucidation is required to understand the *de novo* genesis of the myofibroblasts. The following mechanisms regarding to the current viewpoints are represented below (Figure 1.1).

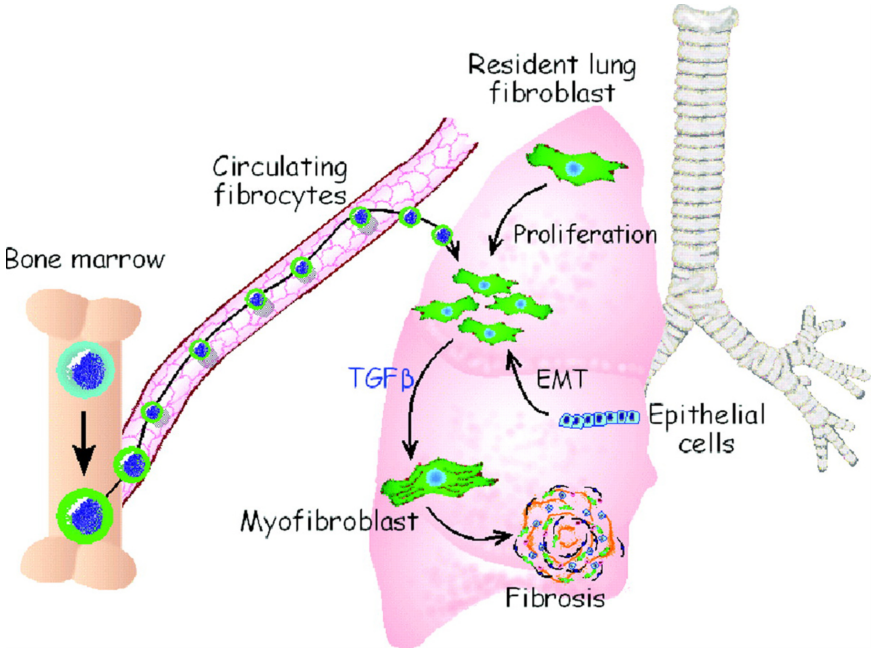

Figure 1.1 Origins of myofibroblasts in IPF. Copied from (36).
Myofibroblasts, the key effector cell type in IPF, are considered to originate from the following: (1) proliferation and differentiation of resident fibroblasts; (2) epithelial-mesenchymal transition (EMT); (3) recruitment of circulating fibrocytes. Diverse cytokines, growth factors, and signaling pathways are involved in these processes.

1.2.1 Epithelium in Fibrosis

An average adult breathes approximate 11,000 liters of air every day. This air not only carries oxygen, but also noxious stimuli like dust or microbial agents that can potentially result in persistent damage to the lung. The alveolar epithelium is the primary site that is exposed to toxic substances or pathogens. The current consensus is that persistent epithelial damage leads to a non-reversing destruction of lung architecture, dysregulation of repair and altered epithelial-mesenchymal crosstalk (37, 38).

Two distinct types of alveolar epithelial cells (AECs) populate the epithelial component of the alveoli, known as alveolar type I and type II cells (Figure 1.2) (39, 40). The type I pneumocytes are squamous, large and flattened cells covering more than 95% of the alveolar surface lining, although they only comprise about one-third of the total AECs. These cells are highly attenuated and branched, forming an interface with pulmonary capillaries through which gaseous exchanges take place. Type I pneumocytes, acting as sentinels, have the ability to sense microbial factors or products and generate inflammatory mediators to recruit or activate immune cells (41, 42). The type II pneumocytes, on the other hand, constitute approximately 15%

of total alveolar cells and make up the remaining 5% of the alveolar surface area. These cells, morphologically appearing as large and cuboidal, are found localized in the corners of alveoli between the type I pneumocytes and contain typical lamellar inclusion bodies and stubby microvilli. The type II pneumocytes are multifunctional cells, and they are the only type of cells which produce, assemble and secret pulmonary surfactant, a lipid-protein complex, to lower the surface tension of the alveolus so that alveolar collapse or overdistension is prevented (43). The type II pneumocytes are also involved in the regulation of alveolar fluid balance both in the normal or pathological lungs (44). In addition, these cells are responsible for lung defense by producing immunomodulatory proteins, including complement, lysozyme and surfactant proteins (SP). SP-A and SP-D, belonging to the “soluble C-type lectin” family, contribute to clearance of diverse microorganisms and resolution of lung inflammation, while SP-B and SP-C exert their functions in reducing alveolar surface tension (43, 45).

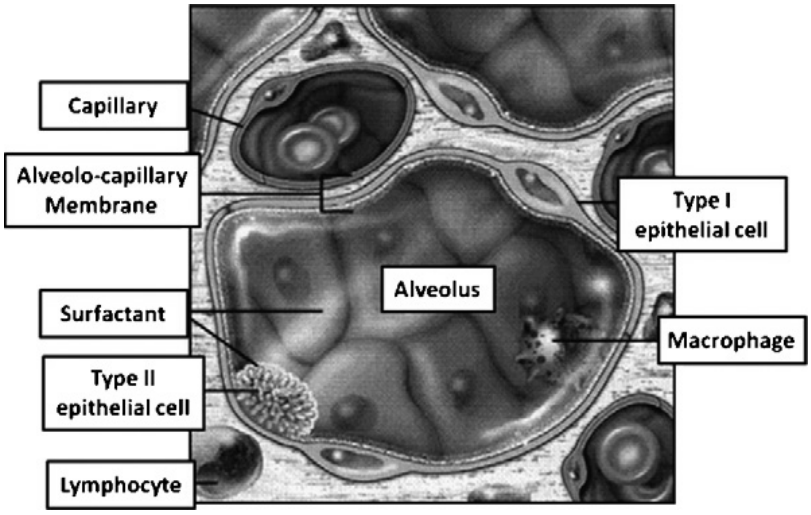

Figure 1.2 Schematic view of the lung alveolus. Copied from (40)**.**

It is commonly assumed that type I pneumocytes are fully differentiated cells and are not able to self-repair when damaged. Type II pneumocytes, on the contrary, are characterized by the potential of both self-maintenance and differentiation and function as progenitor cells for type I pneumocytes (46, 47). Both type I and type II pneumocytes are involved in host defense; however, IPF studies have focused exclusively on type II pneumocytes due to their multiple roles in the immune response.

Repetitive and chronic injury occurring to AECs negatively affects the re-epithelialization process and induces hyperplastic proliferation as well as alterations in the phenotype of type II pneumocytes. The impaired alveolar epithelium serves as a prominent resource of profibrotic mediators, including transforming growth factor-β1 (TGF-β1) (48), tumor necrosis factor-α (TNF-α) (48, 49), endothelin-1 (ET-1) (50) and chemokine (C-C motif) ligand 2 (CCL2) (51). These factors ultimately contribute to the pathogenesis of fibrosis by influencing neighbouring fibroblasts' proliferation and differentiation, ECM deposition or polarization of alveolar macrophages. Furthermore, activated fibroblasts in turn induce injury and apoptosis in alveolar epithelium by secretion of Fas and angiotensin II *in vivo* (52, 53). The alveolar epithelial cells, on the other hand, also respond to TGF-β1 stimulation, which induces apoptosis in type I pneumocytes, whereas type II pneumocytes undergo epithelial to mesenchymal transition (54). In this process, epithelial cells lose their apical-basal polarity, markers such as E-cadherin, and tight junctions Zona Occludens 1 (ZO-1), and acquire mesenchymal markers including α-smooth muscle actin (α-SMA), Vimentin and Fibronectin (55). EMT has been confirmed both in experimental IPF models and in patients that possess a subtype of fibroblasts in the fibrotic lesions, which were demonstrated to be of epithelial origin using co-staining of epithelial and mesenchymal markers (31). Additionally, injured epithelial cells may also secret matrix metalloproteinases (MMPs). These enzymes are able to degrade the varieties of connective tissue matrixes and play a pivotal role in cell proliferation, migration and differentiation (56).

1.2.2 Fibroblasts in Fibrosis

It is believed that persistent epithelial injury might be the initial factor for fibrogenesis. During the normal resolution phase of wound healing, injured type I pneumocytes were replaced by type II pneumocytes to reconstitute the epithelial barrier and cover the exposed basement membrane. However, in IPF, this repairing process is driven by mesenchymal cells such as activated fibroblasts, termed myofibroblasts, that migrate into the alveolar wound area where they contribute to abnormal re-epithelialization, continuously secreting collagen-rich ECMs and forming fibroblastic foci. The uncontrollable increase in numbers of fibroblastic foci indicates a poor prognosis of IPF (57, 58). It has been reported that the myofibroblast is the pathologic fibroblast in IPF (36). Myofibroblasts can degrade basement membranes

through the synthesis of gelatinases A and B (MMP-2 and MMP-9, respectively), consequently leading to the failure of repair of type I pneumocytes and enhancing the migration of fibroblasts (59). Fibroblasts isolated from IPF patients represent increased migration ability and capacity of profibrotic factors production when compared with fibroblasts obtained from healthy lungs (60). Pierce and colleagues revealed that lung fibroblasts from IPF patients possess the property of causing the development of pulmonary fibrosis in immunodeficient mice by adoptive transfer; transfer of normal lung fibroblasts did not cause the development of IPF (61). However, the mechanisms of the enhanced migration and aggressive phenotype remain poorly understood. It is suggested that it may correlate with the expression of α-SMA.

Quiescent resident lung fibroblasts activate, proliferate, and transdifferentiate into myofibroblasts in response to several profibrotic factors, such as TGF-β, IL-4, IL-13 and PDGFs (34, 62, 63).

TGF-β is a well characterized mediator of pulmonary fibrosis (64, 65). TGF-β elicits a diverse range of cellular specific responses, including regulation of inflammation, cell proliferation and differentiation, tissue remodeling, and synthesis of ECM (66). Increased expression of TGF-β is detected in the broncho-alveolar lavage (BAL) fluid and interstitial matrix both in IPF patients and experimental animal model of fibrosis (67-69). Besides injured alveolar epithelial cells, activated alveolar macrophages are the primary source that secrete a TGF-β in fibrotic lung tissues (70, 71). TGF-β regulates fibroblast differentiation through Sma- and Mad-related protein 3 (Smad3), one of the key effectors of the Smad signaling pathway, to regulate the expression of α-SMA. TGF-β is secreted in a latent form, and the integrin $\alpha_V\beta_6$, expressed in AECs, is essential for activation of latent TGF-β into bioactive TGF-β (72). The active TGF-β first binds to the TGF-β receptor type II (TBRII), which recruits and phosphorylates TGF-β receptor type I (TBRI) (Figure 1.3). In the canonical TGF-β-Smad pathway, TBRI then phosphorylates Smad component proteins (Smad2 and Smad3), which subsequently bind to Smad4 and form heterodimeric complexes (Smad2/4 or Smad3/4). These complexes then translocate into the nucleus where they serve as transcription factors by binding to the promoter regions of various profibrotic genes (for instance, α-SMA, collagen type I and fibronectin) (73). Moreover, the non-canonical and Mitogen-activated protein kinases (MAPK)-dependent TGF-β pathway is also involved in fibroblast

differentiation. The MAPK family, including extracellular signal-regulated kinases (ERKs), c-Jun amino-terminal kinases (JNKs) and p38, regulates diverse cellular responses, such as proliferation, differentiation, survival, cytokine secretion as well as apoptosis (74, 75). The activated p38 can induce expression of α-SMA and fibronectin (76). In lung fibroblasts, ERK- and p38-dependent TGF-β signaling pathways have been demonstrated to be involved in the induction of α-SMA and collagens (74). Additionally, TGF-β can also trigger the Wnt-β-catenin-, nuclear factor kB (NF-kB)-and PI3-AKT-signaling pathways (66). Overall, TGF-β plays a central role in the process of lung fibroblast differentiation.

Furthermore, IL-4 and IL-13 are two major Th2 cytokines that are mainly expressed by polarized alveolar macrophages or activated CD4+ T-cells in the fibrotic lung tissue. They stimulate fibroblast differentiation by interfering with the synthesis of prostaglandin E_2 (PGE_2) generator cyclooxygenase 2 (COX-2) (77). Moreover, platelet-derived growth factors (PDGFs) are potent mitogens and chemoattractants for cells of mesenchymal origin. In fibrotic lung tissues, PDGFs are generated by alveolar macrophages and promote fibroblast proliferation and the expression of ECM. PDGFs exert their functions via ligand-dimerization and phosphorylation of PDGFRα and/or PDGFRβ, which activate downstream the MAPK/ERK signaling pathway (34).

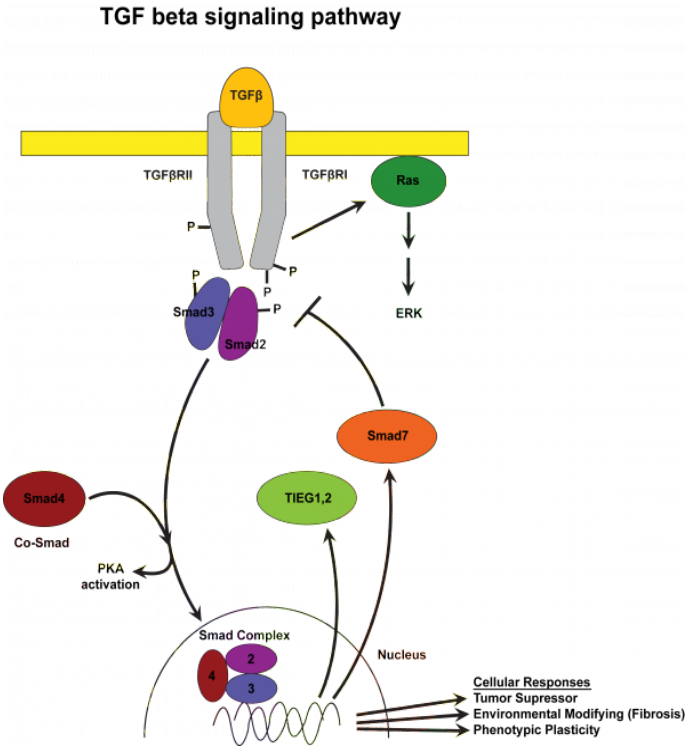

Figure 1.3 TGF-β signaling pathway. Copied from (66).

1.2.3 Fibrocytes in Fibrosis

Fibrocytes, the bone marrow-derived mesenchymal cells, can be recognized in circulation (78, 79) or in the lung parenchyma (80) of IPF patients by the hematopoietic precursor markers CD45 and CD34 along with mesenchymal markers such as α-SMA, collagen I and fibronectin (81). These spindle-shaped cells may home to the injured sites and differentiate into myofibroblasts; hence, fibrocytes contribute to the relentless progression of fibrosis by enhancing ECM deposition (33). Prior investigation has demonstrated that IPF patients have an increased amount of circulating fibrocytes (78-80). The elevated percentage of circulating fibrocytes in total circulating blood leukocytes correlates with exacerbations of IPF (81). Some studies using bone marrow chimeric mice, in which the donated bone marrow cells were labeled with green fluorescent protein (GFP) for tracking purposes, found that after bleomycin instillation more than 20% of the cells in the fibrotic lung tissue were bone marrow-derived (82). Recruitment of fibrocytes is likely mediated via chemokines or cytokines which are expressed by injured tissues, such as CCL2 (83), CCL12 (84), and IL-10 (85). However, the ability of bone marrow-derived fibrocytes to differentiate into myofibroblasts in the fibrotic area still remains controversial. Utilizing α-SMA promoter-driven GFP bone marrow chimeric mice, Yokota and colleagues demonstrated that the bone marrow was unlikely to generate myofibroblasts (86).

2.2.4 Alveolar Macrophages in Fibrosis

1.2.4.1 Origin and Heterogeneity of Alveolar Macrophages

In IPF patients and experimental models, varieties of immune cells were observed in the lung by histological analysis, including alveolar macrophages, lymphocytes, and neutrophils. These cells are thought to contribute to the pathogenesis of fibrosis through secreting numerous profibrotic mediators and play significant modulatory roles in fibrogenesis at different stages of this disease (8). A sampling of the lower respiratory tract reveals that alveolar macrophages account for almost 95% of airspace leukocytes, while lymphocytes and neutrophils represent only 4% and 1%, respectively (87). Therefore, under physiological conditions, alveolar macrophages are the predominant sentinel phagocytic cells of the pulmonary innate immune system which form the first line of host immune defense against any inhaled

xenobiotics, including microorganisms and environmental pollutants. Furthermore, as shown in Table 1.2, regardless of the diverse fibrotic mouse models, alveolar macrophages are the prominent inflammatory cells in injured lungs (88).

Table 1.2 BAL Analysis of Inflammatory Cell Recruitment Following Lung Injury

Agent	Route	Alveolar macrophages	Neutrophils	Lymphocytes
Asbestos	Aerosol	3	2	1
Asbestos	IT	3	2	1
Bleomycin	IN	3	2	1
Bleomycin	IP	3	1	2
Bleomycin	IT	3	2	1
Bleomycin	IV	3	1	2
FITC	IT	3	2	1
Radiation	Thoracic	3	1	2
Silica	Aspiration	3	2	1
Silica	IN	3	3	1
Silica	IT	3	2	1

Least (1) to most numerous (3), IN, intranasal; IT, intratracheal; IP, intraperitoneal; IV, intravenous. Adapted from (88).

Generally, two anatomically distinct macrophage populations are identified in the lower respiratory tract: alveolar macrophages and interstitial macrophages (89). The functions of pulmonary macrophages need to be tailored to their specific micro-anatomical niche. Alveolar macrophages mostly inhabit the alveoli lumen, and it is this unique microenvironment that leads to them possessing a distinct phenotype when compared with interstitial macrophages (90). The alveolar macrophages display a great phagocytic activity and play a vital role in the inflammatory response in the alveoli, but these cells have been shown to be unable to induce T cell antigen-specific responsiveness because of poor antigen presentation competence (91-94). The interstitial macrophages, on the other hand, reside within the parenchymal space (interstitium) where they interact with interstitial lymphocytes and dendritic cells. In contrast to alveolar macrophages, interstitial macrophages are considered to

facilitate an immune response by presenting antigens to T cells (95). However, both types of macrophages can induce inflammatory responses against a broad range of stimuli and share similar morphological phenotypes. Alveolar macrophages can be easily distinguished from interstitial macrophages by surface markers in mice (Table 1.3).

Table 1.3 The phenotypes of mouse macrophages from different sites. Adapted from (96).

Surface marker	Interstitial macrophage	Alveolar macrophage
CD11b	Intermediate expression	Not expressed
CD11c	Not expressed	High expression
CD14	Intermediate expression	Low expression
CD200R	Intermediate expression	High expression
DEC205	Expression unknown	Intermediate expression
F4/80	Low expression	Low expression
Mannose receptor	Intermediate expression	High expression
MHC class II	Intermediate expression	Low expression
SIGLEC-F	Not expressed	High expression

It has long been a controversial issue whether alveolar macrophages originate from bone marrow-derived circulating blood monocytes (97, 98). The current paradigm indicates that tissue macrophages, including alveolar macrophages, derive from embryonic precursor monocytes that seed within the organs and obtain stable phenotypes during the neonatal period responding to instructive cytokines (99-101). Moreover, alveolar macrophages are long-lived cells with a substantial turnover rate of only 40% in 1 year, and like many other tissue macrophages, they autonomously self-renew by homeostatic proliferation through their life (102, 103). However, the signals and molecular mechanisms that underlie the differentiation of fetal monocytes into alveolar macrophages have not yet been completely understood. Schneider and colleagues demonstrated that in the absence of the cytokine granulocyte-macrophage colony stimulating factor (GM-SCF), differentiation of alveolar macrophage precursor cells is abrogated in embryonic lungs, which indicates that GM-CSF is employed in alveolar macrophage development. Moreover,

in the mouse embryo, GM-CSF induced activation of the nuclear receptor PPAR-γ, which is associated with the maturation and differentiation of alveolar macrophages via cholesterol metabolism, lipid transport, storage and degradation (100).

1.2.4.2 Macrophage Activation and Polarization

Macrophages are a heterogeneous group of innate myeloid cells distributed throughout tissues, where they exert their multiple functions in homeostasis, host defense, response to foreign pathogens, and tissue remodeling via their dynamic activities in phagocytosis and bridging innate and adaptive immunity (104-106). To fulfill those functions, macrophages of different origins, including monocytes and tissue resident macrophages, acquire a myriad of phenotypes in response to various stimuli and also depending on their unique physiological compartments. This divergent response by macrophages is termed macrophage polarization. Two distinct subpopulations of macrophages are categorized based upon their functions and distinct cytokine expression profiles, which are classically activated macrophages (M1) and alternatively activated macrophages (M2) (107) (Figure 1.4). It is worth noting that classification of M1/M2 paradigms is analogized with T helper 1 (Th1)/T helper 2 (Th2) dichotomy.

M1 macrophages are induced by pro-inflammatory Th1 cytokines, IFNγ and TNFα, or by bacterial byproducts, such as lipopolysaccharide (LPS, which induces TNFα expression). M1 macrophages have strong anti-microbial functions by generating nitric oxide (NO) and reactive oxygen species (ROS) to stimulate expression of inducible nitric oxide synthase (iNOS) and promoting Th1 immune responses by releasing numerous pro-inflammatory cytokines including IL-1β, TNFα, IL-12 and IL-6 (108). Thus, M1 polarization is mainly presented in acute infectious diseases and inflammation. Nevertheless, ongoing M1 polarization causes excessive inflammation, which leads to increased tissue damage (109). M2 macrophages, comprising of many phenotypes, are further subclassified into M2a (induced by Th2 cytokines, IL-4 and IL-13), M2b (upon exposure to immune complexes in combination with IL-1β or LPS) and M2c (induced by IL-10, TGF-β or glucocorticoids) (110, 111). Putatively, M2 macrophages play a critical role in wound healing, tissue remodeling and resolution of inflammation due to their strong anti-inflammatory activities and high endocytic clearance capacities. This can be beneficial to limit the later stages of inflammatory responses but may also permit chronic infection when associated with

fibrosis or tumors (112, 113). IL-4 or IL-13 are the prototypical inductors of M2a macrophages. They are released by diverse innate cells, such as Th2 cells, mast cells, eosinophils, and even macrophages themselves (114, 115). M2a macrophages are considered to be involved in helminth infestation, tumor progression and tissue remodeling through secretion of anti-inflammatory cytokines (111). They can produce arginase 1, the hallmark of M2a macrophages, which lessens inflammation by inhibiting the expression of proinflammatory NO (116). It has also been reported that they can generate MMP-9, facilitating tumor metastasis (117, 118). M2b and M2c macrophages, also termed M2-like macrophages, are polarized by LPS/IL-1β and IL-10/TGF-β, respectively (119). Both of them exhibit capacities of immune regulation and anti-inflammation. Finally, it has been shown that M2c rather than M2a macrophages induce regulatory T cells (Tregs) from $CD4^{+}CD25^{-}$ T cells in vitro. Therefore, M2c macrophages are more vigorous than M2a macrophages in protecting against tissue injury (120).

In addition, some of the biomarkers used to define M1 or M2 macrophages differ between human and mouse, and most information has emerged from mouse studies (121). For instance, IL-4 or IL-13 elicit up-regulation of arginase 1 (Arg1), chitinase-3-like protein 3/4 (Ym1 and Ym2) and resistin-like molecule α (Fizz1) in mouse M2 macrophages which make them applicable markers. However, they do not have homologs in human M2 macrophages (122). Recently, it has been demonstrated that mannose receptor C type1 (MRC1, CD206) and multifunctional enzyme transglutaminase 2 (TGM2) are conserved biomarkers for both human and mouse M2 macrophages. By the combination of MRC1, TGM2, as well as human specific M2 macrophage markers CD206 (123) and CD68, it is now feasible to identify human M2 macrophages. Moreover, extensive studies have illustrated that M1 and M2 macrophages regulate immune responses and inflammation by expressing a broad repertoire of chemokines and chemokine receptors that recruit other immune cells. Typically, M1 macrophages secrete the chemokines CXCL9 and CXCL10 attracting Th1 cells, and M2 macrophages secrete CCL2, CCL17, CCL22, and CCL24 (124, 125). A list of M1 and M2 markers is provided in Table 1.4.

Table 1.4 A selection of M1 and M2 markers of macrophages. Adapted from (126).

	M1 (IFN-γ)	M2 (IL-4/IL-13)
Human	CD64, IDO, SOCS1, CXCL10	MRC1, TGM2, CD23, CCL22
Mouse	Cxcl9, Cxcl10, Cxcl11, Nos2	Mrc1, Tgm2, Fizz1, Ym1/2, Arg1

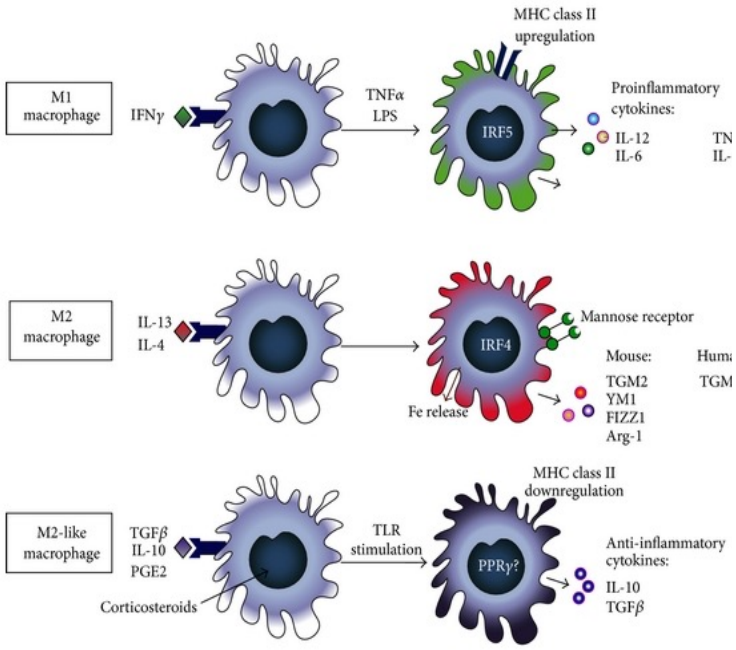

Figure 1.4 Schematic representation of the three macrophage phenotypes and their characteristics (127)**.**

1.2.4.3 Alternatively Activated Macrophages and IPF

During the development of pulmonary fibrosis, the plasticity of alveolar macrophages is required to enable them to polarize into distinct phenotypes responding to the dynamic micro-environment changes in airways. Previously, limited studies investigated the role of M1 alveolar macrophages in IPF. In the initial phases of tissue injury, damaged epithelial or endothelial cells may produce inflammatory factors to promote classical activation of alveolar macrophages. These M1 macrophages release Th1 cytokines and oxygen radicals, which might contribute to the development of fibrosis by their potential capacity to amplify the inflammatory response and cause further tissue injury (127).

Since Th2 inflammatory responses unequivocally play a crucial role in the development of pulmonary fibrosis, substantial studies have illustrated the role of alternatively activated alveolar macrophages in the fibrotic phase of pulmonary fibrosis. Several IPF animal models imply that alveolar macrophages display an

identical phenotype of alternative activation (113, 128, 129). As observed in MHV-68 infected IFN-γR$^{-/-}$ mice, alveolar macrophages accumulated in injured lung and exhibited high Arg1, Ym1/2, Fizz1 and fibronectin, yet were not observed in MHV-68 infected wild-type mice (113).

Likewise, in patients with IPF, high levels of IL-13 are detected in the BAL fluid, correlating with disease severity (129). The clinical data amply indicate that alveolar macrophages disclose an alternatively activated phenotype with high expression levels of CD206 and the pro-inflammatory chemokines CCL17, CCL18 and CCL22, associated with recruitment of CCR4+ T cells (130-132). Furthermore, both human and animal studies have demonstrated that alveolar macrophages are involved in all stages of the perpetuating fibrotic processes owing to their robust roles in pulmonary fibroblast recruitment and activation (133). Alternatively activated macrophages are found to be located in close proximity with ECM-secreting myofibroblasts, and they are an important source of pro-fibrotic mediators, including TGF-β1, PDGF, IL-4 and IL-13, which induce proliferation and activation of resident pulmonary fibroblasts (134). A co-culture system of activated alveolar macrophages obtained from IPF patients with lung fibroblasts evidenced a higher amount of ECMs than those co-cultures with normal alveolar macrophage controls (130). Additionally, alternatively activated macrophages facilitate migration of resident fibroblasts via continuous productions of specific matrix metalloproteinases (135).

Given the significant contributions of alternatively activated macrophages to the development of pulmonary fibrosis, plenty of work has sought to identify a new strategy of therapies by blocking alternative macrophage activation and their products. Administration of antibodies or shRNA against these pro-fibrotic cytokines and cytokine receptor antagonists have been shown to be effective in preventing the development of pulmonary lesions and fibrosis in the experimental models (136). One study demonstrated that application of the IL-13 neutralizing antibody protected mice from bleomycin-induced lung fibrosis (137). Another study revealed that administration of TD139, a novel inhibitor of galactin-3, to bleomycin-treated mice partially attenuated pulmonary fibrosis by inhibiting TGF-β-induced β-catenin activation both in vitro and in vivo (138).

However, there are also some findings highlighting an anti-fibrotic role of M2 macrophages through suppression and resolution of fibrosis as well as elimination of ECM components. A study has shown that arginase-1 and Fizz1 actually

ameliorated pulmonary fibrosis by negatively regulating Th2-dependent inflammation and fibrosis (139). Degradation of ECM components is mediated by different mannose receptors which has been identified in bleomycin-induced fibrosis (139, 140).

To summarize, the above findings demonstrate that both M1 and M2 alveolar macrophages are indispensable in the pathogenesis of fibrotic lung diseases. M1 macrophages are required in the early inflammatory phase, but their presence does not influence the subsequent fibrotic phase, while M2 macrophages play a mechanistic and determined role during the fibrotic phase. Therefore, a thorough understanding how these two phenotypes contribute to different stages of IPF will augment our understanding of this disease and will potentially reveal novel treatments.

1.3 S100a4

1.3.1 Biology of S100a4

The *S100a4* gene was discovered independently by several groups and consequently has various names including fibroblast-specific protein 1 (FSP1), metastasis 1 (Mst1), calcium placental protein (CAPL) and murine placental homolog, 18A2, 42A, p9Ka, pEL98 and calvasculin (141). *S100a4* belongs to the S100 superfamily of EF-hand calcium-binding proteins, which presently is composed of 24 members that usually exist as homo- or hetero-dimers in cells, possessing low molecular mass (10-20kd) (142, 143). “S100” refers to their capacity to be soluble in 100% ammonium sulphate.

The human *S100a4* gene is located, along with other S100 family members, in a frequently rearranged region on chromosome 1q21, and consists of four exons, which are capable of forming two calcium-binding EF-hands after translation (144, 145). Upon the Ca^{2+} loading on the C- and N-terminal, *S100a4* undergoes a conformational transformation and forms two major hydrophobic binding sites, which are essential for recognition and interaction with its potential target proteins and for generating a biological effect (146, 147). Several studies reveal that the transcriptional regulation of *S100a4* varies between cell types. In human cells, several upstream regulatory elements such as β-catenin, methylation status and extracellular factors have been characterized to influence the expression of *S100a4*

(148, 149).

1.3.2 Biological Function of S100a4

S100a4, like other S100 family members, has no enzymatic activity but a broad range of functions both intracellularly and extracellularly by interacting with other target proteins (Figure 1.5). The intracellular S100a4 is associated with calcium transport and cell homeostasis, including cytoskeletal rearrangement, transcriptional activity, protein phosphorylation, cell cycle and migration (150). Moreover, a wide variety of binding partners has been characterized. Direct interactions of S100a4 with intracellular cytoskeletal proteins including actin, non-muscle myosin IIA and IIB (151), liprin-β and E-cadherin (152) and tropomyosin (153) facilitate the remodeling of actin-myosin filaments and alter cell adhesion, thereby enhancing cell motility. For instance, non-muscle myosin II-A is a chemo-mechanical cytoskeleton protein that is involved in cell motility and division. *In vitro* studies demonstrate that S100a4 selectively binds to the myosin II-A in a calcium-dependent manner and thereby inhibits the assembly of myosin II-A monomers into filaments promoting the monomeric, unassembled state (151, 154). The interactions between S100a4 and methionine aminopeptidase 2 (155) or CNN3 (156) have been reported to promote cell proliferation and differentiation. Moreover, the tumor suppressor protein p53 is a newly validated target for S100a4. Co-localization of nuclear S100a4 and p53 was observed in a human colon cancer line, indicating that S100a4 may play a potential role in proliferation and tumor development (157, 158).

There is growing evidence that S100 family members also possess extracellular functions, although the mechanism of secretion has not yet been elucidated (159). When secreted into the extracellular space, S100a4 functions as a cytokine, and several lines of evidence suggest that S100a4 regulates gene expression through activation of transcription factor NF-κB or modulation of MAP kinases, p38, JNK and ERK (158, 160, 161). Extracellular application of S100a4 stimulates MMPs' expression, angiogenesis and cell proliferation, and serves as a moderate prometastatic factor of tumor cells (141). Cell invasion is further facilitated by MMPs which mediate the proteolytic cleavage of ECM proteins. In the mouse, endothelial cells respond to recombinant S100a4 through expression and secretion of MMP-13, thereby influencing the remodeling of ECM and increasing cell invasion (162). Down-regulation of S100a4 in osteosarcoma and neuroblastoma cells was concomitant

with reduced expression of MMP-2 and membrane-type 1 MMP, accompanied by impaired cell invasion (163, 164). In addition, an *in vitro* study indicated that administration of oligomeric S100a4 promotes the invasion ability of human prostate cancer cells, which is mediated by S100a4 inducing activation of MMP-9 (165). The stimulation of the release of MMPs by extracellular S100a4 is dependent on membrane associated receptors (Figure 1.5). One well characterised receptor is the receptor for advanced glycation endproducts (RAGE). S100a4-RAGE mediates cell motility in human colorectal cancer cells via hyperactivated MAPK/ERK and hypoxia signaling (166), and this effect can be arrested by the addition of soluble RAGE, which prevents S100a4 from binding to membrane-associated RAGE (167). However, the capacity of inducing cell invasion by extracellular S100a4 in RAGE-negative cells is still not fully understood, and more cell surface receptors need to be defined (168).

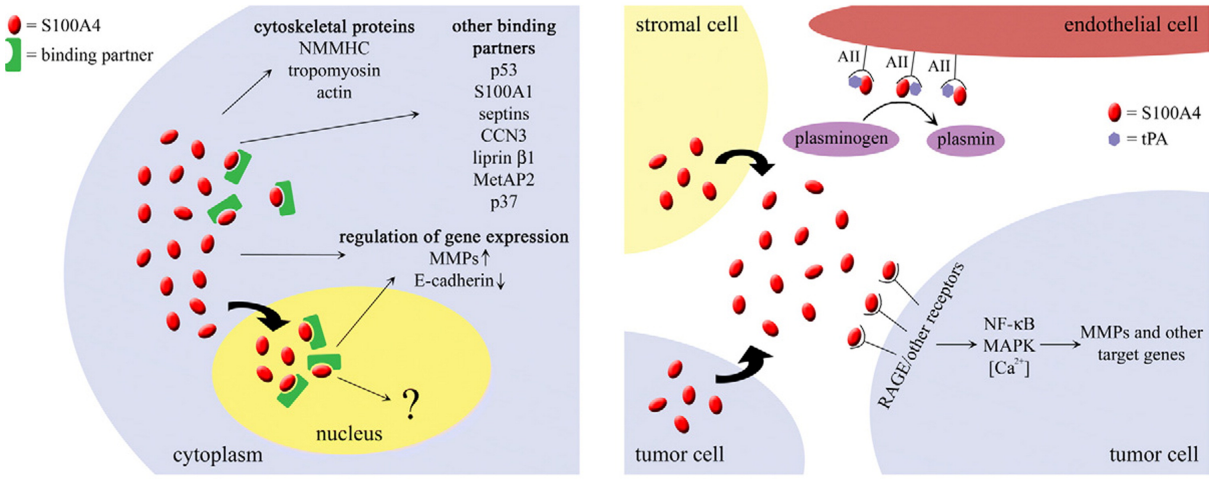

Figure 1.5 Molecular mechanisms associated with intracellular and extracellular S100a4. Copied from (236).

1.3.3 S100a4 and Fibrosis

S100a4 was first characterized a decade ago and its biological function has been studied most intensively with respect to its role in enhancing cancer metastasis; specifically its ability to enhance cell invasion. Excessive expression of S100a4 has been evidenced in most metastatic cancers such as pancreatic (169), ovarian (170), breast (171), prostate (172), colorectal (173), pulmonary (174), bladder (175) and gastric (176) cancers; thus, expression of S100a4 is considered as a marker of poor

survival prognosis in diverse cancer types.

Current studies on S100a4 reveal the novel significant facets of its contribution in non-malignant diseases, particularly in promoting the development of fibrosis. High levels of S100a4 were detected in patients with various fibrotic diseases (177-179). The role of S100a4 might be very similar to that in cancer metastasis, specifically during the early induction of EMT (180, 181). The expression of S100a4 can be induced by growth factors, including TGF-β1, epidermal growth factor and fibroblast growth factor-2 (180, 182). On the transcriptional level, S100a4 is regulated by several regulatory elements and transcription factors, such as β-catenin and KRAB-associated protein 1 (149, 183). However, the mechanism of S100a4 secretion remains yet unknown. Curiously, TGF-β1 and epidermal growth factor both elicit the expression of S100a4 in renal proximal tubular epithelial cells *in vitro*, and also promote the concomitant loss of epithelial markers, thus enhance cell motility. When cells are pretreated with S100a4 siRNA, the cell motility induced by TGF-β1 and epidermal growth factor, is restricted (180). Additionally, TGF-β1 induces EMT in mouse kidneys with a continuous increase of S100a4. This may be reversed by treatment with BMP7, an antagonistic protein to TGF-β1, via activation of Smad proteins (184). Furthermore, increased expression of S100a4 was observed in inflammatory myopathies where it might serve as a cytokine-like factor that causes muscle fiber injuries via stimulating the release of pro-inflammatory cytokines from mononuclear cells (177).

1.4 Animal models of Pulmonary Fibrosis

Due to the lack of effective treatment for IPF, animal models are of great importance for identifying and validating new therapeutic targets. Although no current animal model recapitulates all aspects of human pulmonary fibrosis, investigations utilizing murine models have allowed the dissection of mechanisms relevant to fibrogenesis, and theses models have identified many fibrotic mediators and key cells that are presumably involved in humans as well (185). Detailed advantages and disadvantages of each of the available animal models are summarized in Table 1.5 (186). Among these, the virus model is elaborated in details, the other models are feasible but were not employed in the present research.

Table 1.5 Advantages and disadvantages of various animal models of fibrosis. Adapted from (186).

Model	Advantages	Disadvantages
Bleomycin	● Most well-characterized ● Can be delivered intratracheally, intravenously. intraperitoneally, or intranasally ● Clinically relevant ● Time frame for development of fibrosis is 14–28 days	● Fibrosis is reported to be self-limiting after 28 days in the intratracheal model ● Development of fibrosis is limited to Balb/c mice ● Expense
FITC	● Ability to visualize areas of lung injury by characteristic green fluorescence ● Time frame for development of fibrosis is 14–28 days ● Fibrotic response persists for at least 6 months ● Can be used in both C57Bl/6 and Balb/c mice ● Persistent nature of the fibrotic response makes it amenable for studying viral exacerbations of fibrosis post-FITC	● Response can vary depending on the lot of FITC ● Solution must be made fresh each day and vortexed before each injection ● Model is not clinically relevant
Irradiation	● Clinically relevant ● C57Bl/6 mice are irradiation-fibrosis prone	● Fibrosis can take more than 30 wk to develop ● Expensive per diem costs ● C3H/HeJ and CBA/J mice are irradiation-fibrosis resistant
Silica	● Fibrotic nodules resemble those seen in humans exposed to occupational dusts and particulates ● Persistent fibrotic stimulus	● Fibrosis can take 12–16 wk to develop ● Balb/c mice are resistant ● Special instrumentation is needed if delivered via aerosol
Transgenic	● Can study the overexpression of a particular molecule ● Can be expressed under inducible promoters, which allows expression only in adult mice	● Compensations may occur in mice that constitutively express a transgene throughout development ● Amount of product produced may not be physiological
Viral vectors	● Can be used to deliver fibrotic or antifibrotic mediators ● Lentivirus vectors can infect many cell types	● Immune response may prevent repeated dosing with adenoviral vectors ● Adenoviral vectors have tropism only for epithelial cells
Adoptive transfer of human fibroblasts into immune deficient mice	● Can study fibroblasts from various human fibrotic diseases	● Expense of immunodeficient mice required for adoptive transfer of human cells
MHV-68	● See below (1.4.2)	● See below (1.4.2)

1.4.1 Gammaherpesviruses

Herpesviruses are double-stranded DNA viruses with relatively large linear genomes. They are ubiquitous viruses that widely establish infection in most vertebrates and persist for the whole life of hosts and cannot be cleared (187). The life cycles of all herpesviruses in their natural host can be divided into lytic and latent infections. The lytic infections can be either asymptomatic or present with severe symptoms, followed by the establishment of latent infection in which the complete viral genetic information persists without production of infectious virions and cell destruction. The latent virus can reactivate or switch to a lytic phase of replication under certain circumstances such as immunosuppression or stressful conditions.

The herpesviruses are divided into three subfamilies: α-, β- and γ-herpesviruses, based on their biological properties such as hosts, reproductive cycle and latency sites (188). The γ-herpesviruses are initially identified by their cellular tropism for lymphocytes and variable length of reproductive cycles (189). The γ-herpesvirus family possesses double-stranded DNA genomes, enclosed in an icosapentahedral capsid which is comprised of capsomers, and finally is surrounded by tegument and a glycoprotein envelope. The most well-known members are Epstein-Barr Virus (EBV) and Kaposi's sarcoma-associated herpesvirus (KSHV), because of their significant roles in lymphomas and fibrotic disease (21, 190). However, in vivo studies of the pathogenesis of these viruses are difficult and limited because of their restricted host range. Therefore, animal models are needed. Sunil-Chandra and colleagues established the experimental model of murine γ-herpesvirus-68 (MHV-68) to study the pathogenesis of γ-herpesviruses (191). Importantly, chronic pulmonary infection of mice with MHV-68 provides a relevant model to investigate the clinical pathologies of IPF.

MHV-68 is a natural pathogen of murid rodents, and is genetically co-linear with EBV sharing about 80% homology. MHV-68 displays similar infection patterns compared to EBV: epithelial and B cell tropism, virus-induced B cell activation and proliferation, as well as symptoms such as splenomegaly (192). However, the natural routes of infection are not clear in the mouse model; MHV-68 allegedly enters the host via lung epithelial cells after intranasal inoculation, where the viruses initiate replication and protein production, thereby causing acute infection. Thus, viral infection may result in extensive epithelial cell injury and may subsequently provoke inflammatory responses that can lead to the alveolar collapse that, under certain

conditions, would trigger abnormal remodeling of lung architecture similar to those observed in the early stage of IPF patients (193). The lytic infection is cleared around day 10 post infection in immunocompetent mice. Subsequently, viruses migrate to the spleen via the lymph nodes and switch to a dormant state to establish life-long latency in B lymphocytes, and viral latency reaches peak levels around day 14 post infection (194). Except for splenic B cells, studies also suggest lung epithelial cells, macrophages and dendritic cells as major sites of latent infection (195). In addition, immunosuppression is considered to be a primary trigger for viral reactivation.

1.4.2 MHV-68-induced Animal Model of Lung Fibrosis

There is accumulating evidence suggesting that approximately >95% of IPF patients are undergoing chronic pulmonary infections with viruses, particularly with herpesviruses (196). A number of studies have implied that DNA or proteins of herpesviruses, such as Epstein-Barr Virus (EBV), Kaposi's sarcoma-associated herpesvirus (KSHV) and Cytomegalovirus (CMV), are commonly detected in the lungs of patients by qPCR or immunohistochemistry, and 40–60% of IPF patients have evidence of chronic infection with at least two different types of herpesviruses (21, 197). It has been reported that replicating EBV, KSHV and CMV were detected at high frequency in alveolar epithelial cells of IPF patients but none in the control specimens (198). Furthermore, detection of latent membrane protein 1 (LMP-1) of EBV is thought to associate with a poor outcome and high mortality in IPF patients (199). It has also been postulated that occult infection was identified as a potential explanation for acute exacerbation of IPF (200).

C57BL/6 background transgenic mice lacking the IFN-γ receptor, termed Th2-biased mice, develop pulmonary fibrosis following infection with MHV-68 (201). This is intriguing in light of the fact that IFN-γ deficient mice mimic the imbalance between Th1 and Th2 immune responses detected in IPF patients, who exhibited lower levels of IFN-γ than controls (202-204). The virus is persistently replicating in the lungs of immunocompromised mice, resulting in dramatically increased collagen deposition in lung tissue, upregulation of TGF-β, IL-10, IL-4 and IL-13 in serum or BAL fluid and accumulation of myofibroblasts. A detailed comparison of MHV-68-induced IPF in mice and patients with IPF is shown in Table 1.6 (201).

Table 1.6 Comparison of histological patterns and features between IPF patients and MHV-68 chronic infection in IFN-γR$^{-/-}$ mice. Adapted from (201).

	IPF	MHV-68 IFN-γR$^{-/-}$ Mice
Patchy interstitial inflammation	yes	yes
Patchy interstitial fibrosis	yes	yes
Subpleural, peripheral, and paraseptal distribution of fibrosis	yes	yes
Honeycomb	yes	no
Increased TGF-β expression	yes	yes
Myofibroblasts	yes	yes
Hyperplasia of type II lung epithelial cells	yes	yes
Imbalance of Th1/Th2 cytokines	yes	yes
Alteration of surfactant proteins	yes	yes
Vascular changes	yes	yes

This animal model supports the viewpoint that skewed immune responses create a profibrotic microenvironment in the lung tissue and contribute to fibrogenesis as cofactors. Thus, MHV-68 provides an applicable animal model for the dissection of mechanisms involved in clinical fibrotic processes. Further studies are needed in order to investigate the precise roles of γ-herpesviruses in fibrosis development of patients with IPF.

1.5 The MHV-68-induced IPF Model in the Laboratory of Prof. Dr. Adler

Prior to the beginning of this thesis, the MHV-68-induced IPF model, which has been first described by Mora et al. (201), was established in the laboratory of Prof. Dr. Adler by a former postdoctoral fellow, Dr. Shinji Ohno.

In order to investigate the process of fibrogenesis, IFN-γ R$^{-/-}$ and C57BL/6 wild-type mice were intranasally infected with 1×10^5 pfu of MHV-68, and the mice were sacrificed at days 14 (acute phase), 45 and 100 (chronic phases) post infection (p.i.) (Figure 1.6A). Uninfected mice served as a control. To determine fibrosis and architectural changes in the lungs after viral infection, the lungs were harvested at days 14, 45 and 100 p.i. and examined by H&E staining (Figure 1.6B). C57BL/6 wild-

type mice showed moderate immunocyte infiltrates during the acute phase, and by day 45 p.i., these mice showed complete resolution of inflammation. In contrast, IFN-γR$^{-/-}$ mice demonstrated severe interstitial inflammation as well as immunocyte infiltrates during the acute phase, and began to show evidence of fibrosis at day 45 p.i., which further increased at day 100 p.i.. To confirm collagen deposition, picrosirius-red staining and immunostaining against Collagen 1 was performed (Figure 1.6C and D). Only minimal deposition of collagen was found around alveoli or large airways in uninfected mice and MHV-68 infected C57BL/6 mice. In contrast, virus infected IFN-γR$^{-/-}$ mice demonstrated an excessive deposition of collagen in the interstitium. The abnormal transdifferentiation of pulmonary fibroblasts to myofibroblasts was evidenced by immunohistochemical staining of α-SMA, which is a typical marker of myofibroblasts. Positive α-SMA immunostaining was restricted to perivascular areas in MHV-68 infected C57BL/6 mice at day 100 p.i., while intensive α-SMA-characterized myofibroblasts were present in interstitial areas and along alveolar walls in IFN-γR$^{-/-}$ mice infected with MHV-68 at day 100 p.i (Figure 1.6E).

Figure 1.6F presents the total cell counts from BAL fluids obtained from experimental mice. The number of total cells between C57BL/6 and IFN-γR$^{-/-}$ mice was comparable in the uninfected groups. However, during the acute phase, the total cell counts increased four to seven times compared with uninfected animals in both mice stains. In chronically infected mice, the number of cells in BAL fluids remained at a high level in IFN-γR$^{-/-}$ mice; whereas, the number of cell counts decreased to the base line from day 45 p.i. in C57BL/6 mice. In addition, the expression of TGF-β, the hallmark of IPF, was determined in BAL fluid by ELISA. A significant increase of TGF-β in IFN-γR$^{-/-}$ mice at day 45 p.i. and later was observed, whereas an unchanged and minimal expression was found in C57BL/6 mice (Figure 1.6G).

Taken all together, the MHV-68-induced IPF model was successfully established by Dr. Ohno. Using this model, microarray analysis was performed to analyze global gene expression and to elucidate potential mechanisms of disease development. The raw data set originating from their microarray analysis was the starting point of this thesis.

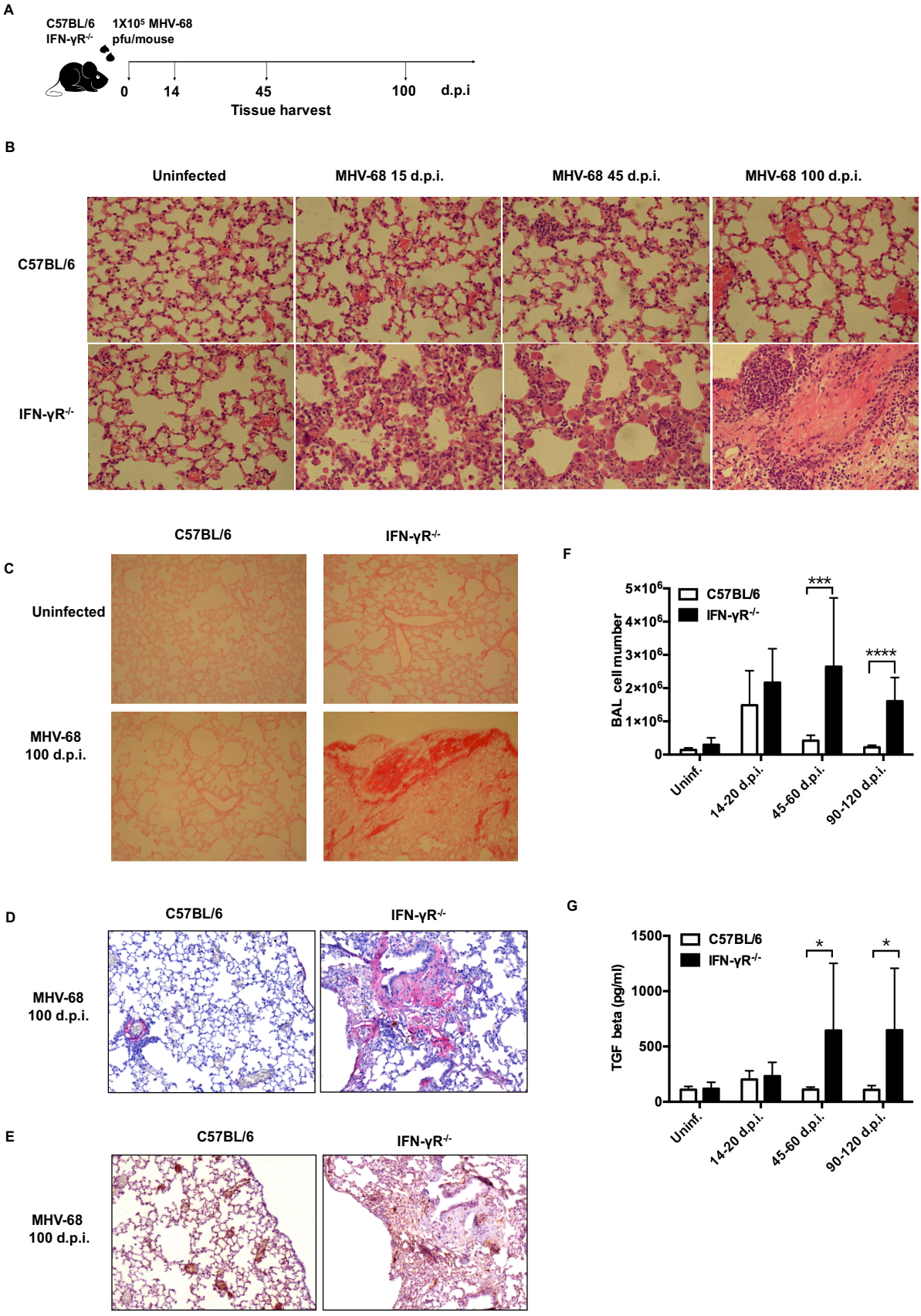
A
C57BL/6
IFN-γR-/-
1X10⁵ MHV-68
pfu/mouse
0
14
45
100
d.p.i
Tissue harvest
B
Uninfected
MHV-68 15 d.p.i.
MHV-68 45 d.p.i.
MHV-68 100 d.p.i.
C57BL/6
IFN-γR-/-
C
C57BL/6
IFN-γR-/-
Uninfected
MHV-68
100 d.p.i.
F
BAL cell number
5×10⁶
4×10⁶
3×10⁶
2×10⁶
1×10⁶
0
C57BL/6
IFN-γR-/-
***
****
Uninf.
14-20 d.p.i.
45-60 d.p.i.
90-120 d.p.i.
D
C57BL/6
IFN-γR-/-
MHV-68
100 d.p.i.
G
TGF beta (pg/ml)
1500
1000
500
0
C57BL/6
IFN-γR-/-
*
*
Uninf.
14-20 d.p.i.
45-60 d.p.i.
90-120 d.p.i.
E
C57BL/6
IFN-γR-/-
MHV-68
100 d.p.i.

Figure 1.6. Establishment of the MHV-68-induced IPF mouse model.
(A) The schematic presentation of the MHV-68-induced IPF mouse model. C57BL/6 and IFN-γR$^{-/-}$ mice were infected with 1×10^5 pfu of MHV-68 intranasally on day 0; the uninfected mice served as negative controls. Subsequently, mice were sacrificed at days 14 (acute phase), 45 and 100 (chronic phases) p.i.. (B) Histological analysis of H&E-stained lung sections from C57BL/6 and IFN-γR$^{-/-}$ mice sacrificed at day 0, 15, 45 and 100 p.i.. Severe inflammatory infiltrates were observed in IFN-γR$^{-/-}$ mice from day 14 p.i. and persisted during the chronic phase of infection, notably significant at day 100 p.i.. In contrast, the C57BL/6 wild-type mice showed moderate immunocytes infiltrate during the acute phase, and by day 45 p.i., these mice showed complete resolution of inflammation. (C) Picrosirius-red stained lung sections from C57BL/6 and IFN-γR$^{-/-}$ mice. Normal presence of collagen around airways is depicted by red staining in the uninfected mice and MHV-68 infected C57BL/6 mice. Extensive expression of collagen was detected in virus infected IFN-γR$^{-/-}$ mice at day 100 p.i.. (D) Immunostaining of collagen 1. The collagen fibers were indicated in red, and the nuclei were stained blue. Pervasive collagen was only detected in lung interstitium of virus infected IFN-γR$^{-/-}$ mice at day 100 p.i.. (E) Immunohistochemical staining of α-SMA. Positive α-SMA immunostainings were often detected in the areas of lung interstitium in the MHV-68 infected IFN-γR$^{-/-}$ mice at day 100 p.i., but were absent in infected C57BL/6 wild-type mice. (F) Total cell counts in BAL fluids after infection. Cells were obtained from the BAL fluids of uninfected controls and MHV-68 infected C57BL/6 and IFN-γR$^{-/-}$ mice, stained with Trypan blue and counted using a hemocytometer. MHV-68 infected IFN-γR$^{-/-}$ mice exhibited significantly more cells in the airways compared to C57BL/6 mice both in the acute and chronic phase. Results are derived from 8 to 21 mice per group and shown as mean ± SD. Unpaired t-test was performed for statistical analysis (* denotes $p<0.05$; ** denotes $p<0.01$; ***denotes $p < 0.001$; ****denotes $p < 0.0001$). (G) The level of TGF-β was measured in BAL fluids by ELISA. Abundant expression of TGF-β in IFN-γR$^{-/-}$ mice starting from day 45 p.i. was observed, while the levels of TGF-β in C57BL/6 mice remained low. Results are derived from 8 to 21 mice per group and shown as mean ± SD. (* denotes $p<0.05$; ** denotes $p<0.01$; ***denotes $p < 0.001$; ****denotes $p < 0.0001$).

1.6 Aims of the Thesis

Idiopathic pulmonary fibrosis (IPF) is the most devastating form of interstitial lung disease with unknown etiology. Although the precise molecular mechanisms that drive the pathogenesis of IPF remains elusive, increasing clinic evidence suggests that viral infection, particularly with γ-herpesviruses, is an important factor in the initiation and/or perpetuation of the development of IPF. Therefore, in this thesis, MHV-68-infected IFN-γR$^{-/-}$ mice were used as a model to study mechanisms of pulmonary fibrosis.

The following objectives were persued:

a. Use microarray analysis to obtain a global view of transcriptional responses of the lung during acute and chronic infection.

b. Identify differentially regulated genes that were hitherto not known to be involved in pulmonary fibrosis.

c. Determine the role of dysregulated target genes in fibrotic lung disease.

d. Analyze the effects of antifibrotic drug treatment toward the target gene.

2. Materials and Methods

2.1 Materials

2.1.1 Laboratory Equipments

Device/Hardware	**Manufacturer**
0.2ml, 1.5 ml and 2ml Tubes	Eppendorf, Hamburg, Germany
100 µm cell strainer	BD Falcon, Heidelberg, Germany
15 ml and 50 ml Tubes	BD Falcon, Heidelberg, Germany
25 cm^2 and 75 cm^2 cell culture flasks	Greiner bio-one, Frickenhausen, Germany
5417C table-top centrifuge	Eppendorf, Hamburg, Germany
6-, 12-, 24-, 96-well cell culture plates	TPP, Trasadingen, Switzerland
Axiovert 25 microscope	Carl Zeiss, Oberkochen, Germany
Electrophoresis power supply	Peqlab, Erlangen, Germany
FastPrep-24 Lysator	MP Biomedicals, Illkirch Cedex, France
Gel Doc 2000 Imaging System	Bio-Rad, Hercules, USA
Heracell™ 150i Incubators	Thermo Fisher Scientific, Waltham, MA, USA
Herasafe KS safety cabinet	Thermo Fisher Scientific, Waltham, MA, USA
Histostar embedding workstation	Thermo Fisher Scientific, Waltham, MA, USA
Inverse microscope	Carl Zeiss, Oberkochen, Germany
Mastercycler gradient PCR machine	Eppendorf, Hamburg, Germany
Megafuge 1.0R	Thermo Fisher Scientific, Waltham, MA, USA
MicroAmp® Fast Optical 96-Well reaction plates	Applied Biosystems, Foster City, USA
Microscope slide cover glasses	Leica, Wetzlar, Germany
Microtome HYRAX M55	Carl Zeiss, Oberkochen, Germany

Mirax micro digital slide scanner	Carl Zeiss, Oberkochen, Germany
Molecular Imager ChemiDoc™ XRS+ system	Bio-Rad, Hercules, USA
NanoDrop® ND-1000 spectrophotometer	Thermo Scientific, Wilmington, MA, USA
Neubauer counting chamber	Carl Roth GmbH & Co, Karlsruhe, Germany
PAGE-electrophoresis	Bio-Rad, Hercules, USA
Pipette	Eppendorf, Hamburg, Germany
Real-Time PCR System 7300 (TaqMan)	Applied Biosystems, Foster City, USA
Semi-enclosed Benchtop Tissue Processor	Leica, Wetzlar, Germany
Tank-blotting chamber	Bio-Rad, Hercules, USA

2.1.2 Commercially Available Kits

Name	**Company**
Cell proliferation kit II (XTT)	Roche, Basel, Switzerland
DNA Mini kit	Qiagen, Hilden, Germany
Fast SYBR® Green Master Mix	Applied Biosystems, Foster City, USA
Pierce ECL Western Blotting Substrate	Thermo Scientific, Wilmington, USA
QIAGEN DNeasy tissue kit	Qiagen, Hilden, Germany
RNeasy Mini Kit	Qiagen, Hilden, Germany
Superscript™ III Reverse Transcriptase kit	Invitrogen, Carlsbad, USA

2.1.3 Recombinant Proteins

Name	**Company**
Recombinant murine IFN-γ	Immuno Tools, Friesoythe, Germany
Recombinant murine IL-4	Immuno Tools, Friesoythe, Germany
Recombinant murine IL-13	Immuno Tools, Friesoythe, Germany
Lipopolysaccharides (LPS) from E.coli	Sigma-Aldrich, Deisenhofen, Germany
Recombinant murine S100a4	R&D System, Minneapolis, MN

2.1.4 Chemicals

Dulbecco's Phosphate buffered saline (DPBS), Dulbecco's Modified Eagle Medium/ F-12 Nutrient mixture (Ham) (DMEM/F-12), RPMI Medium 1640 (1×), Glasgow modified eagle's medium, Fetal Bovine Serum (FBS), HEPES 1 M, L-Glutamine 200 mM (100×), 0.05% Trypsin-EDTA (1×), 2-Mercaptoethanol (50 mM) and antibiotics were purchased from Gibco (Life Technologies, Warrington, UK), Bioconcept (Allschwil, Switzerland) and PAN Biotech (Aidenbach, Germany). All chemicals were purchased from Invitrogen (Karlsruhe, Germany), Sigma-Aldrich (Deisenhofen, Germany), Roche (Mannheim, Germany), Bio-Rad (Munich, Germany), Fluka (Deisenhofen, Germany), Merck (Darmstadt, Germany) and Carl Roth (Karlsruhe, Germany) unless otherwise specified.

2.1.5 Commonly Used Buffers and Stock Solutions

Laemmli SDS loading buffer (2×)	100 mM	Tris/HCl, pH 6.8
	4% (w/v)	SDS
	20% (v/v)	Glycerol
	0.2% (w/v)	Bromophenol blue
	20 mM	2- Mercaptoethanol
RIPA buffer (for protein lysates)	50 mM	Tris-HCl (pH 7.5)
	150 mM	NaCl
	1 mM	Na_2EDTA
	1%	NP-40
	1%	Sodium deoxycholate
	1 mM	ß-glycerophosphate
PBS buffer (10×)	137 mM	NaCl
	2.7 mM	KCl
	10 mM	Na_2HPO4
	2 mM	KH_2PO4
Wash buffer (TBS-T)	1 l	PBS/TBS
	0.05%	Tween-20
Electrophoresis buffer (5×)	15,1 g	Tris
	94 g	Glycine
	50 ml	10% SDS

Transfer buffer (1×)	3,02 g	Tris/HCl, pH 7.5
	14,4 g	Methanol
10% PAGE (4 gels) Resolving	15,9 ml	H_2O
	13,3 ml	30% Acrylamid
	10,0 ml	1.5M Tris, pH 8.8
	400 µl	10% SDS
	400 µl	10% APS
	16 µl	TEMED
5% PAGE (4 gels) Stacking	13,6 ml	H_2O
	3,4 ml	30% Acrylamid
	2,5 ml	1M Tris, pH 6.8
	200 µl	10% SDS
	200 µl	10% APS
	20 µl	TEMED
Wash buffer (PBS-T)	1 l	PBS
	0.05%	Tween-20
Assay buffer (ELISA)	1 g	BSA
	100 ml	1×PBS
Stopping solution (ELISA)	0.18 M	H_2SO_4
H_2O_2 buffer (IHC)	6 ml	30% H_2O_2
	80 ml	Methanol
	14 ml	Distilled H_2O
Target retrieval solution	30 ml	Citrate buffer, pH 6.0
	270 ml	Distilled H_2O

2.1.6 Cell Culture Medium

Cells	**Medium**
Primary alveolar macrophages	RPMI-1640
	10% FBS
	1% Penicillin/Streptomycin
	50 mM 2-Mercaptoethanol
	1% L-Glutamin

Primary lung fibroblasts	DMEM/F12 15% FBS 1% Penicillin/Streptomycin 1% HEPES
BHK-21	Glasgow MEM (BHK-21) 5% FBS 1% Penicillin/Streptomycin 5% TPB 1% L-Glutamin
Cell storage medium	90% FCS 10% DMSO

2.1.7 Enzymes

Enzymes	Company
Proteinase K (for Genotyping)	Qiagen, Hilden, Germany
DNase I	Qiagen, Hilden, Germany
Collagenase A	Roche, Basel, Switzerland
Taq Polymerase	NEB, Frankfurt, Germany

2.2 Methods

2.2.1 Virus Preparation

2.2.1.1 MHV-68 Virus Stock Preparation

The original virus stock of MHV-68 (clone G2.4) was kindly provided by J. Stewart and A. Nash (University of Edinburgh, Edinburgh, United Kingdom). Working stocks of virus were prepared in baby hamster kidney cells (BHK-21) with Glasgow modified eagle's medium (Pan Biotech) supplemented with 10% FBS, 2mM L-glutamine, 5% tryptose phosphate broth (TPB), penicillin (100 U/ml) and streptomycin (100 mg/ml) as previously described (205). Briefly, MHV-68 was amplified in BHK-21 cells by infection at a multiplicity of infection (MOI) of 0.1, followed by incubation at 37°C until cytopathic effect (CPE) was complete. Virus stocks were prepared by freezing and thawing the cells twice, and the supernatant

was collected and cleared of cell debris by centrifugation at 1300×g for 20 minutes at 4°C. Subsequently, virus was pelleted at 26000×g for 2 hours at 4°C. The pellet was resuspended in 1 ml (dependent on the amount) complete medium, homogenized and stored in aliquots at -80°C.

2.2.1.2 Virus Titration

Titers of virus were determined by plaque assay on BHK-21 cells in 24-well plates (5×10^4/well). Stocked virus was 10-fold serially diluted in complete medium from 10^{-1} to 10^{-8}, 0.9 ml each, and adsorbed onto BHK-21 cells, followed by incubation at 37°C for 90 minutes. Each well was overlayed with complete medium containing 1.5% carboxymethylcellulose. Cells were stained with 0.1% crystal violet solution after 5 days and the numbers of plaques were counted. Virus titer was calculated by the following equation:

Titer (pfu/ml) = n (plaque count per well) / 0.9 (volume of diluted virus) × viral dilution

2.2.2 In vivo Experiments

2.2.2.1 Experimental Animals and Husbandry

C57BL/6 and IFN-γR$^{-/-}$ mice on C57BL/6 background were purchased from Charles River Laboratories (Sulzfeld, Germany) and/or the Jackson Laboratory (Bar harbor, Maine, USA), bred and maintained in the Helmholtz Zentrum München. The mice had free-choice access to drinking water as well as chow diet. Mice were maintained at constant temperature (20-24°C) with 45% to 65% relative humidity and a 12/12-hour light-dark cycle. Before experimental treatments, mice were allowed to adapt to the new environment for at least 7 days.

Mice were housed in individually ventilated cages during the MHV-68 infection period. All animal experiments were performed in accordance with the local Animal Care and Use Committee (District Government of Upper Bavaria; permission number 124/08).

2.2.2.2 Genotyping

Tissue from IFN-γR$^{-/-}$ mice or C57BL/6 mice was incubated in Buffer ALT containing 20 µl proteinase K (QIAamp DNA Mini Kit) for 1 to 3 hours at 56°C with

occasional vortexing until the tissue was completely lysed. Genomic DNA was then isolated according to the manufacturer's instruction and subsequently used for PCR assays in 25 µl reaction volumes, containing 10 ng whole genome DNA, 5 µl 5× reaction buffer (NEB Q5 high-fidelity DNA polymerase reaction buffer), 0.5 µl 10 mM dNTP (Thermo Scientific), 0.5 µl of each primer, 0.25 µl DNA polymerase (NEB Q5 high-fidelity DNA polymerase) and sterile distilled water. Primer sequences are shown in Table 3.1. The cycling conditions were according to the recommendations from the Jackson Laboratory (https://www.jax.org/strain/003288).

Table 2.1 Primer sequences for mice genotyping

Accession Number	Primer (5'-3')
oIMR0587	CCCATTTAGATCCTACATACGAAACATACGG
oIMR0588	TTTCTGTCATCATGGAAAGGAGGGATACAG
oIMR6916	CTTGGGTGGAGAGGCTAT TC
oIMR6917	AGGTGAGATGACAGGAGATC

2.2.2.3 Infection of Mice

Eight- to ten-week-old, age and sex matched IFN-γR$^{-/-}$ or C57BL/6 mice were anesthetized with ketamine/xylazine and inoculated intranasally with 1×10^5 plaque forming units (PFU) of MHV-68 diluted in PBS in a total volume of 30 µl. Mock-infected mice were treated with PBS without virus. The mice were immediately euthanized and aborted from the study if they showed severe symptoms such as scrubby furs, loss of weight, or bent back. At the predetermined time points, mice were sacrificed by inhalation of carbon dioxide (CO_2). Subsequently, bronchoalveolar lavage was performed and lung tissues were quartered and processed for the following experiments: the left lobe was inflated and fixed in 10% buffered formalin for histologic and immunohistochemical examination; the remaining lobes were stored at -80°C and used for RNA isolation for microarray analysis and qRT-PCR to determine the gene expression profiles, or for the preparation of whole lung tissue protein extracts and western blot analysis.

2.2.2.4 Bronchoalveolar Lavage (BAL)

Immediately after euthanasia, bronchoalveolar lavage (BAL) was conducted via the introduction of a cannula into the trachea. A 1 ml aliquot of ice-cold Dulbecco's

Phosphate Buffered Saline (DPBS) was flushed into the airway and gently aspirated via a syringe and the tracheal cannula. After the first BAL fluid (BALF) was collected, the BAL continued with seven times of 1.5 ml aliquots of PBS until an additional 7 ml of BALF was collected. The initial BALF was then centrifuged at 1500 rpm for 5 minutes at 4°C, and the supernatant was collected and decanted into a new 1.5 ml microcentrifuge tube and stored at -80°C for biochemical measurements such as cytokine concentration. The remaining lavage fluid was pooled and centrifuged to remove the supernatant. The sedimented cells together with remnant cell pellets from the first lavage wash were subsequently resuspended in 1 ml PBS. Finally, the number of living cells was counted on a standard hemocytometer in the presence of 0.4% trypan blue (Sigma-Aldrich).

2.2.3 Histologic and Immunohistochemical Analysis

2.2.3.1 Histopathological Examination

After BAL harvesting, either the whole lung or the left lobe was inflated by 5 ml 10% phosphate buffered formaldehyde solution (PFA) (AppliChem) and then gently removed and immersed in 10% PFA. An average of three mice per group at each experimental time point was used for histopathological analysis. After fixation for 24 hours, dissected lung tissues were dehydrated through a series of solution with increasing concentrations of ethanol and subsequently embedded in paraffin blocks. 3 µm thick adjacent sections were cut by the microtome (Carl Zeiss), so that all parts of the samples were represented on the slides. Prior to hematoxylin and eosin (H&E) staining, slides were baked at 60°C for 30 minutes. Subsequently, lung sections were prepared for histopathological staining by deparaffinization in Xylene, and rehydration in a decreasing ethanol series (100%, 90%, 80%, 70%) and distilled water. Slides were then stained with hematoxylin and eosin according to the manufacturer’s protocols to determine histopathological changes and fibrosis. Briefly, lung sections were incubated in Mayer's Hemalaun solution (Carl Roth) for 8 minutes, rinsed quickly in 0.3% acid-alcohol solution, washed and then transferred into 0.5% Eosin G solution (Carl Roth) for 8 minutes. Sections were washed in tap water and dehydrated in a graded ethanol series and covered with Entellan (Millipore).

2.2.3.2 Picrosirius Red Staining for Collagen

Additionally, serial sections were also subjected to picrosirius red staining to visualize collagen deposition. Slides were deparaffinized in xylene and rehydrated through decreasing grades of ethanol as described above. Slides were then stained in saturated Picric acid with 0.1% (W/V) Sirius red F3BA (Sigma-Aldrich) solution for 1 hour at room temperature. This was followed by washing briefly with distilled water, staining with Mayer's Hemalaun solution (Carl Roth) for 8 minutes to depict nuclei, differentiation in 0.01 N hydrochloric acid (HCl), alkalinization with distilled water, dehydration through graded ethanol and finally mounting.

2.2.3.3 Immunohistochemistry (IHC) Procedure

Briefly, serial lung tissue sections were processed as follows: slides were deparaffinized and incubated with 3% hydrogen peroxide (H_2O_2) (Spectrum) in 100% methanol for 20 minutes at room temperature to quench endogenous peroxidase activity. Heat-induced antigen retrieval was performed with 0.05% citrate buffer pH 6.0 (Dako REAL Target Retrieval Solution) for 30 seconds at 125°C and 10 seconds at 90°C. Subsequently, blocking was performed with Roden Block M buffer (Biocare Medical, Zytomed) for 1 hour at room temperature to avoid non-specific antibody binding. To identify myofibroblasts or macrophages and products of alternatively activated macrophages, primary antibodies used were against α-smooth muscle actin (α-SMA), arginase I and S100a4, according to the manufacturer’s instructions. The slides were incubated with corresponding secondary antibodies for 30 minutes at room temperature. Vulcan Fast Red Chromogen Kit (Biocare Medical, Zytomed) was used to visualize the positive stained cells and hematoxylin was used as counterstaining for nuclei. Isotype controls were routinely applied.

The primary antibodies used for IHC staining were mouse anti-α-SMA monoclonal antibody (Sigma-Aldrich) diluted at 1:200 in antibody diluent (Zytomed Systems), rabbit anti-arginase I polyclonal antibody (Santa Cruz Biotechnology Inc.) at 1:200 dilution and rabbit anti-S100a4 polyclonal antibody (Abcam) at 1: 250 dilution. The secondary antibody applied was the Rabbit-on-Rodent alkaline phosphatase (AP) polymer (Biocare Medical, Zytomed) and mouse-on-mouse AP-polymer (Biocare Medical, Zytomed).

2.2.4 Gene Expression Analysis

2.2.4.1 RNA Isolation from Lung Tissue

Approximate 20 mg frozen lung tissue was disrupted and completely homogenized in 350 µl TissueLyser LT buffer through the FastPrep-24 Lysator (MP Biomedicals). Total RNA was extracted and purified utilizing the RNeasy Mini Kit (Qiagen) as per the manufacturer's instruction. The concentration and purity of RNA samples were quantified by a Nanodrop ND-1000 spectrophotometer (Thermo Scientific). RNA was stored at -80°C for microarray analysis and quantitative real-time RT-PCR.

2.2.4.2 Microarray Analysis

For each condition, three biological replicates were used:

C57BL/6 mice	IFN-γR$^{-/-}$ mice
Mock-infected	Mock-infected
Day 14 post infection	Day 14 post infection
Day 45 post infection	Day 45 post infection

Total RNA was isolated and subjected to the mouse experimental array ME430 2.0 (Affymetrix) by the Affymetrix Core Facility of the Technical University of Munich. Data analysis was carried out using the Qlucore Omics Explorer software (Qlucore). Differentially expressed genes were identified by Multi Group Comparison (F-test) and visualized by hierarchical clustering and a heat map.

2.2.4.3 cDNA Synthesis

cDNA was generated from total RNA utilizing SuperScript RT III kit (Invitrogen) in a total volume of 20 µl. First-strand synthesis was performed in a total volume of 13.5 µl with 1 µg RNA, 1 µl 10 mM dNTP (NEB), 1 µl random hexamers (50 µM) and RNase-free distilled water. The mixture was incubated at 65°C for 5 minutes and then chilled on ice immediately for at least 1 minute. Thereafter, the following reagents were added to the RNA/hexamers mixture: 4 µl 5×first-strand buffer, 2 µl 0.1 mM DTT and 0.5 µl of Superscript III (200 units). The obtained solution was incubated at 42°C for 1 hour and reverse transcriptase was inactivated by

incubating at 70°C for 10 minutes. cDNA was either stored at -20°C or subjected to quantitative real-time PCR analysis (diluted 1:10 with H_2O before use).

2.2.4.4 Quantitative Real-Time PCR

Quantitative real-time PCR (qPCR) was conducted to verify the microarray data using the ABI Prism 7300 Real-Time PCR System (Applied Biosystems, Life Technologies). Specific primers for the genes of interest were custom designed through the online PrimerBank database (pga.mgh.harvard.edu/primerbank/) and synthesized by Metabion (Martinsried, Germany). The housekeeping genes ribosomal protein l8 (rpl8) or β-actin were used to normalize for the input of loaded cDNA. 1 µl of cDNA was mixed with the appropriate 100 nmol/ml primers and 2×SYBR Green Master Mix (Applied Biosystems, Life Technologies) in a total volume of 25 µl. The sequences of primers are given in Table 2.2. Each qPCR reaction was carried out in a 96-well plate in duplicate with the following program: 95°C for 10 minutes for initial denaturation, 40 cycles of amplification as follows: 1) denaturation at 95°C for 15 seconds, 2) annealing and elongation at 60°C for 1 minute. Melting curve analysis was also done with a continuous temperature increasing from 60°C to 95°C with a rate of 0.1°C/second to assess the specificity of the amplification process.

Relative gene expression levels were calculated using the comparative Ct (ΔΔCt) method (206). ΔCt corresponds to the difference between the threshold cycle (Ct) value for the gene of interest (Ct_{GOI}) and the Ct value for the housekeeping gene (Ct_{HG}) which is:

$\Delta Ct_{GOI} = Ct_{GOI} - Ct_{HG}$

$\Delta Ct_{control} = Ct_{control} - Ct_{HG}$

ΔΔCt reveals the relative quantitation between ΔCt_{GOI} and $\Delta Ct_{control}$:

$\Delta\Delta Ct = \Delta Ct_{GOI} - \Delta Ct_{control}$

Relative expression was then calculated as $2^{\Delta\Delta Ct}$.

Table 2.2 Primer sequences of genes of interest (GOI).

Target gene	Forward primer (5'-3')	Reverse primer (5'-3')
Actb	TCCATCATGAAGTGTGACGT	GAGCAATGATCTTGATCTTCAT
Arg1	GGAACCCAGAGAGAGCATGA	TTTTTCCAGCAGACCAGCTT
Tnf	CACCACGCTCTTCTGTCT	GGCTACAGGCTTGTCACTC
Rpl8	AAGGCGCGGGTTCTGTTTT	GCTCTGTCCGCTTCTTGAATC
S100a4	TCAGCACTTCCTCTCTCTTGG	AACTTGTCACCCTCTTTGCC

2.2.5 Protein Analysis

2.2.5.1 Protein Isolation

Total protein was extracted from lung tissue with precooled RIPA buffer (10mM Tris, 150mM NaCl, 5mM EDTA, 1% sodium deoxycholate, 1% Triton X-100, 1% SDS supplemented freshly with 1 tablet complete protease inhibitor cocktail (Roche) per 10 ml. Samples were homogenized by the FastPrep-24 Lysator (MP Biomedicals) and placed on ice for 30 minutes with vigorous vortexing every 10 minutes. All samples were centrifuged at 14,000 rpm for 15 minutes at 4°C, and supernatants were collected and decanted in new microcentrifuge tubes and stored at -80°C.

For isolation of whole cell extracts, cells were washed with precooled PBS and lysed with cold RIPA buffer for 30 minutes on ice. Cell debris was pelleted at 14,000 rpm for 15 minutes at 4°C and the supernatant was harvested and stored at -80°C.

2.2.5.2 Protein Quantification

Protein concentrations were measured by Bradford assay with coomassie protein assay reagent (Thermo Scientific) according to manufacturer's instructions with BSA (Thermo Scientific) as standards (0, 25, 125, 250, 500, 750, 1000, 1500 and 2000 µg/ml). Absorption at OD 595 was measured with a microplate absorbance reader (TECAN SUNRISE), and the BSA standard curve was applied to calculate concentrations of samples.

2.2.5.3 Western Blot Analysis

Western blot was performed as previously described (207). In brief, 25-50 µg total protein extract per sample was diluted in 4×Laemmli Buffer (Biorad) supplemented with 5% β-mercaptoethanol and incubated for 5 minutes at 95 °C. Samples were resolved in 5-15% sodiumdodecylsulphate polyacrylamide gels (SDS-PAGE) for 90 minutes at 120V in Tris-glycine running buffer in an electrophoresis tank (Bio-Rad). The pre-stained full-range rainbow molecular weight marker (GE Healthcare, Life Science) was used to indicate the protein size. Proteins were transferred to the nitrocellulose membrane (GE Healthcare, Life Science) in blotting buffer at 300 mA for 60 minutes in a Hoefer TE22 Mini Tank (GE Healthcare, Life Science). The membrane was then soaked in 5% milk in TBS-T blocking buffer for 1 hour at room temperature to prevent non-specific binding. Primary antibodies were diluted in 1% milk blocking buffer and incubated overnight at 4°C with agitation in a 50 ml falcon tube. After washing 3 times with TBS-T buffer, the membrane was incubated with the appropriate secondary antibody for 1 hour at room temperature. The membrane was washed three times with TBS-T buffer, and the resulting signals were visualized and captured with Pierce ECL western blotting substrate (Thermo Scientific) and Bio-Rad imaging system (Thermo Scientific). If necessary, initial antibodies could be stripped with Restore Stripping Solution (Thermo Scientific) for 8 to 15 minutes at room temperature. The nitrocellulose membrane was then washed with TBS-T, blocked with 5% milk in TBS-T and reprobed with other antibodies as described above. The antibodies and dilutions employed are shown in Table 2.3.

Table 2.3 Antibodies utilized in western blot assays

Name	Dilution	Company
Rabbit polyclonal anti-S100a4 antibody	1:1000	Abcam, ab27957
Mouse monoclonal anti-S100a4 antibody	1:1000	Abcam, ab93283
Rabbit polyclonal anti-ArginaseI antibody	1:1000	Santa Cruz, sc-20150
Rabbit polyclonal anti-GAPDH antibody	1:1000	Abcam, ab37168
Rabbit polyclonal anti-STAT6 antibody	1:1000	Cell Signaling, #9362
Rabbit polyclonal anti-pSTAT6 antibody	1:1000	Cell Signaling, #9361
Mouse monoclonal anti-β-actin-HRP-conjugated antibody	1:50000	Sigma-Aldrich, A3854
HRP-conjugated anti-mouse IgG secondary antibody	1:5000	GE Health care, 9597364
HRP-conjugated anti-rabbit IgG	1:5000	GE Health care, 356938

2.2.5.4 Enzyme-Linked Immunosorbent Assay (ELISA)

In order to quantify the levels of active TGF-β1 in BALF, the Human TGF-β CytoSetTM (Invitrogen) was utilized according to manufacturer's manual. Specifically, 96-well NUNC MaxiSorp microplates (NUNCTM, Thermo Scientific) were coated with 2 μg/ml TGF-β capture antibody in PBS at 4°C overnight. Plates were blocked with assay buffer (PBS + 5% BSA) for 1 hour at room temperature. In parallel, standard samples were prepared by dilution of recombinant human TGF-β (2000, 1000, 500, 250, 125 and 62.5 pg/ml) and BALF was treated with 1 N HCl at room temperature for 15 minutes and then neutralized with 1 N NaOH. All samples were transferred into designed wells and incubated for 2 hours at 37°C. After washing three times with washing buffer, 0.64 μg/ml detection antibody (Anti-human TGF-β biotin antibody), diluted in assay buffer, was added and incubated at room temperature with continuous shaking (700 rpm). Subsequently, wash three times with washing buffer, and add streptavidin-HRP solution (R&D systems). For colorimetric quantification, TMB substrate reagent (BD Biosciences) was added to each well and reactions were stopped with 2 N H_2SO_4. Absorbance at 450 nm was measured by a microplate absorbance reader (TECAN SUNRISE), and the standard curve was applied to calculate concentrations of samples.

Secreted S100a4 in cell culture supernatants was measured by a sandwich ELISA as described (179). Briefly, 96-well NUNC MaxiSorp microplates (NUNCTM,

Thermo Scientific) were coated with 1 µg/ml mouse anti-S100a4 monoclonal antibody (Abcam) at 4°C overnight. After blocking with assay buffer (PBS + 5% BSA), samples were added and incubated for 2 hours at 37°C, followed by incubation with 1 µg/ml rabbit polyclonal anti-S100a4 antibody (Abcam) at room temperature with continuous shaking (700 rpm). Next, a secondary HRP-conjugated anti-rabbit IgG (GE Healthcare, Life Science) was applied and proteins were detected by TMB substrate.

2.2.6 Cell Culture and Treatments of Cells

2.2.6.1 BHK-21

Baby hamster kidney cells (BHK-21) were maintained in Glasgow modified eagle's medium (Pan Biotech) supplemented with 5% FBS, 2 mM L-glutamine, 5% tryptose phosphate broth (TPB), penicillin (100 U/ml) and streptomycin (100 mg/ml) at 37°C in 5% CO_2. To subculture the cells, the medium was discarded and monolayer cells were washed with PBS once, followed by incubation with 0.25% trypsin (Gibco) until cells were detached from the surface of the flask. A comparable volume of complete medium was used to neutralize the trypsin, and cells were split at a ratio of 1:5 every 3-4 days.

2.2.6.2 Isolation of Mouse Primary Resident Alveolar Macrophages (AMs)

To isolate lung tissue alveolar macrophages, C57BL/6 wild type mice were anesthetized by injection of xylazine (4.1 mg/kg body weight) and ketamine (188.3 mg/kg body weight) intraperitoneally and killed by exsanguination (209). The trachea was exposed, cannulated and the lungs were serially washed with 1 ml sterile PBS 10 times as described previously to harvest lavage fluid. Cell pellets were obtained by centrifugation at 1500 rpm for 10 minutes at 4°C, and 5×10^5 cells per well were seeded in 24-well plates in complete RPMI-1640 medium (Gibco) and incubated at 37°C and 5% CO_2 atmosphere. Cells were allowed to adhere for 60 to 90 minutes and then non-adherent cells were removed by washing twice with PBS.

2.2.6.3 Isolation and Cell Culture of Mouse Primary Lung Fibroblasts

C57BL/6 mice were euthanatized by exsanguination as described above. 15 ml cold PBS was perfused smoothly into the right heart ventricle until the lung got

cleared of blood. The whole lung was removed and rinsed in pre-warmed DMEM/F-12 (Gibco) medium supplemented with 1% penicillin/streptomycin (Gibco), 1% HEPES buffer (Gibco) and 15% FBS (PAA). The lung was diced into 1-2 mm pieces and digested with 0.1 mg/ml Collagenase A (Roche) at 37°C for 2 hours. Digested tissue was then minced using a 100 µm cell strainer (BD, Biosciences). After washing and centrifuging, cells were resuspended in complete DMEM/F-12 medium and incubated at 37°C with 5% CO_2. The culture medium was changed every two to three days to remove unattached cells. After reaching 80–90% confluence, cells were detached by 0.25% Trypsin (Gibco), split at 1:4 and applied to experiments at passages not higher than three.

2.2.6.4 Macrophage Activation Experiments

Isolated primary alveolar macrophages were cultured in 24 well plates (5×10^5 cells/well) in RPMI-1640 medium (Gibco) supplemented with 1% penicillin/streptomycin (Gibco) and 10% FBS (PAA) overnight. The cells were stimulated with LPS (100 ng/ml, Sigma) and/or IFN-γ (20 ng/ml, Immuno Tools) to produce M1 macrophages, or with IL-4 (20 ng/ml, Immuno Tools) to induce M2 macrophage polarization. The application of a 72-hour time course (6, 24, 48 and 72 hours) and increasing doses of IL-4 (10, 20, 50, 100, 200 ng/ml) allowed for the accurate analysis of gene expression profiles and cytokine release without medium change or repeated administration of stimuli. Untreated macrophages incubated in culture medium served as controls. For the analysis of cytokines, supernatants were collected and subjected to ELISA for measurement of S100a4 as described above. Adherent cells were washed with ice-cold PBS and then harvested for total RNA or protein isolation.

2.2.6.5 Immunocytofluorescence Staining

For immunocytofluorescence staining of Arginase I and S100a4, primary alveolar macrophages were seeded on a 24-well plate containing sterile round glass coverslips at a density of 5×10^5 cells/well and cultured in the absence or presence of IL-4 (20 ng/ml). At 48 hours after the initiation of stimulation, adherent cells were washed with precooled PBS and fixed with cold methanol for 10 minutes at room temperature. After washing three times in PBS for 5 minutes, cells were covered with blocking solution (1% BSA in PBS) for 30 minutes at room temperature, and

then incubated with a mixture of mouse anti-S100a4 monoclonal antibody (Abcam) at 1: 300 dilution and rabbit anti-Arginase I polyclonal antibody (Santa Cruz Biotechnology Inc.) at 1: 250 dilution for 1 hour at room temperature. This was followed by an exposure to a mixture of secondary antibodies, a goat anti-mouse IgG Alexa Fluor® 488 secondary antibody (Thermo Scientific) and a goat anti-rabbit IgG Alexa Fluor® 633 secondary antibody (Thermo Scientific), at 1: 500 dilution, in the dark for 1 hour. Stained cells were mounted with Mowiol which contains 4′,6-diamidino-2-phenylindole (DAPI) (Dako) to visualize the nuclei, and images were captured by a fluorescence microscope (LSM 700, Carl Zeiss). The appropriate irrelevant isotype-matched immunoglobulins were employed as negative controls.

2.2.6.6 Cell Proliferation Assay

Cell proliferation was evaluated after different treatments by utilizing the cell proliferation kit II (XTT) (Roche) according to the manufacturer's instructions. Briefly, primary lung fibroblast cells were plated into 96-well plates (3×10^3 cells/well) in complete DMEM/F-12 medium (Gibco) and allowed to accommodate overnight before quiescing by replacing with serum-free medium for a further 12 hours. Subsequently, cells were incubated in 2% FBS DMEM/F-12 medium with or without recombinant S100a4 protein (2 µg/ml) or together with the anti-S100a4 antibody (3 µg/ml) (R&D Systems) for 72 hours. Prior to harvesting, cells were treated with XTT labeling mixture for 4 hours, and the absorbance was quantified at 450 nm with a reference wave length at 650 nm by using a microplate absorbance reader (TECAN SUNRISE).

To verify whether the inhibition of S100a4 in M2 macrophages influence the pro-proliferative effect, M2 macrophage conditioned medium was incubated with S100a4 antibody (3 µg/ml) for 1 hour at room temperature, and then applied on pre-starved primary lung fibroblast cells. Additionly, the conditioned medium from S100a4-siRNA transfected M2 macrophages was also applied on pre-starved cells. After 48 hours, proliferation was evaluated by cell proliferation kit II (XTT) mentioned above.

2.2.6.7 Wound Healing Assay

Cell migration was determined by wound healing assay. Initially, 5×10^4 cells were seeded into a 24-well plate and allowed to adhere overnight until reaching about

70% confluence. Cell monolayers were inflicted by manually scraping with a 200 µl pipette tip and cell debris was removed by washing with PBS. Subsequently, cells were treated with the recombinant S100a4 protein (2 µg/ml) or that pre-incubated with the anti-S100a4 antibody (3 µg/ml) in culture medium supplemented with 2% FBS. Microphotographs were taken at 0 and 24 hours after treatments with an Axiovert microscope (Carl Zeiss). The wound areas were subsequently measured, and each wound healing assay was conducted in triplicates. Finally, the cells were harvested for further analysis.

2.2.6.8 Transfection of Primary Alveolar Macrophages with siRNA

For specific knockdown of the S100a4 gene in primary alveolar macrophages, a set of three siRNAs (1, 2, 3) as well as a non-targeting negative control was purchased from Riboxx (Radebeul, Germany) (NM_011311.2). Prior to the experiments, the siRNA powder was reconstituted with RNase-free water in order to obtain the working solution with a final concentration of 600 nM. Primary alveolar macrophages were prepared as described above and seeded in 24-well plates at a density of 150,000 cells/well approximately 24 hours before transfection. Cells were transfected in duplicates as follows: 3 µl riboxx®FECT transfection reagent diluted in 37 µl Opti-MEM (Gibco) were added to the 20 µl siRNA in 40 µl Opti-MEM. The reaction mixtures were incubated at room temperature for 15 minutes. In the mean time, the cell culture medium was aspirated and replaced with 500 µl fresh complete medium. Then, the mixture was added to each designed well to a final siRNA concentration of 20 nM/well. After transfection for 72 hours, supernatants were harvested for further experiments, and cells were harvested for RNA extraction and subsequent quantitative RT-PCR analysis.

2.2.7 Drugs and Treatments

2.2.7.1 Cytotoxicity assay

The inhibitors of S100a4, calcimycin and niclosamide (2',5-dichloro-4'-nitrosalicylanilide), were purchased from Sigma and were solubilized in dimethyl sulfoxide (DMSO) for in vitro experiments. To exclude adverse effects caused by DMSO, control cells were treated with the equal amount of solvent. Analysis of cell cytotoxicity was performed with the cell proliferation kit II (XTT) (Roche) according to

the manufacturer's instructions. Briefly, cells were seeded at $1x10^4$ cells/well in a 96-well-plate and allowed to accommodate overnight. The cells were exposed to a series of different concentrations of calcimycin or niclosamide for 24 hours. Subsequently, cells were treated with XTT labeling mixture for 4 hours, and the absorbance was quantified at 450 nm with a reference wave length at 650 nm by using a microplate absorbance reader (TECAN SUNRISE). Cell viability was determined by dividing the absorbance ratio of drug treated cells by the ratio obtained from untreated cells which was defined as 100% cell viability.

2.2.8 Statistical Analysis

All statistics and calculations were conducted with GraphPad Prism version 6.0. Values are shown as mean ± SD of at least 3 animals or 3 individual samples in each group if not otherwise indicated. The comparison of two groups was examined by unpaired Student's t-test, and comparisons between several experimental groups were performed by analysis of variance (ANOVA). All significance tests were two-tailed and P values were expressed as follows: $0.05 > p > 0.01$ as *; $0.01 > p > 0.001$ as **; $p < 0.001$ as ***; $p < 0.0001$ as ****.

3. Results

3.1 Gene Expression Profiles of Normal and Fibrotic Lung Tissues

3.1.1 Experimental Approach for Characterization of Differentially Regulated Genes during Pulmonary Fibrosis

Despite intensive research efforts, the underlying mechanisms of idiopathic pulmonary fibrosis remain poorly understood, and there are currently inefficient therapeutic options for this serious complication. While a number of hypothesis-driven investigations have characterized potential profibrotic genes, translation of these into therapeutic targets has been so far mostly disappointing. The characterization of more effective targets in pulmonary fibrosis can be addressed using DNA microarrays. In general, most of these studies have focused on characterizing gene expression in the bleomycin-induced pulmonary fibrosis model.
In this thesis, genes that are involved in the initiation and progression of IPF were identified in the MHV-68-induced fibrosis model, which is the most closely related to human disease.

Previous studies suggested that MHV-68 infection causes pneumonia in both IFN-$\gamma R^{-/-}$ and C57BL/6 wild-type mice during the acute phase of the infection (<14 days post infection (d.p.i.)). However, during the chronic phase, (>45 d.p.i.), wild-type mice had complete resolution of interstitial pneumonia; only the IFN-$\gamma R^{-/-}$ mice started to establish progressive pulmonary fibrosis (113). To uncover the potential molecular mechanisms underlying the pathogenesis of pulmonary fibrosis, a whole genome transcriptional analysis using microarrays was performed at different time points of disease progression in the animal model of MHV-68-induced pulmonary inflammation and fibrosis. Eight- to ten-week-old IFN-$\gamma R^{-/-}$ or C57BL/6 mice were randomly divided into several groups (n=3 for each group), and inoculated intranasally with 1×10^5 plaque forming units (PFU) of MHV-68 or were left uninfected. The mice were sacrificed and RNA from lung samples was isolated at 14 (acute phase) and 45 (chronic phase) days post infection, corresponding to the inflammatory and fibrotic phases of the disease.

As a control, RNA of lung samples was isolated from uninfected littermate mice. After statistical selection of differentially regulated genes, results were compared

with other published microarray data in IPF, both from mice and humans, thus generating a list of likely disease mediators. Furthermore, qRT-PCR, western blot, ELISA and immunohistochemical analysis were performed, respectively. An overview of the experimental approach to identify the differentially expressed genes is represented in Figure 3.1.

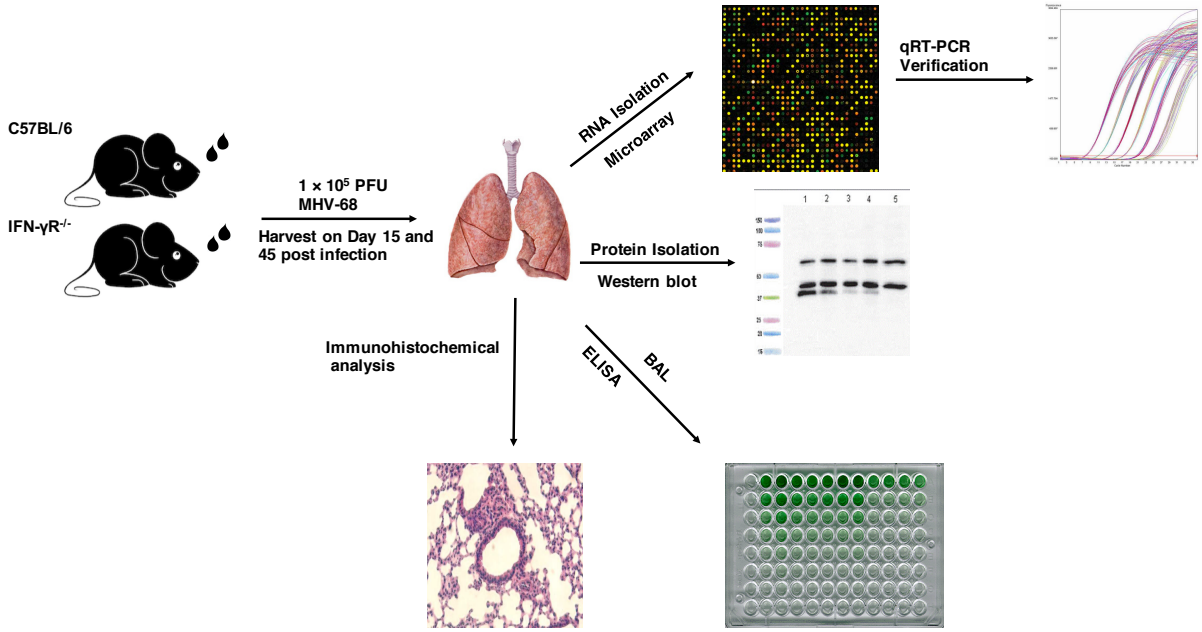

Figure 3.1 Schematic diagram illustrating the characterization and verification of differentially regulated genes in the pathogenesis of pulmonary fibrosis.
Both IFN-γR$^{-/-}$ or C57BL/6 mice were randomly divided into several groups (n=3 for each group). Age and sex matched mice were inoculated intranasally with 1×10^5 PFU of MHV-68 or were left uninfected. At days 14 and 45 post infection, mice were sacrificed and lung tissues and BAL fluid were collected and processed for the following experiments: The left lobe was inflated and fixed in 10% buffered formalin for histologic and immunohistochemical examination; the remaining lobes were used for RNA isolation for microarray analysis and qRT-PCR to determine the gene expression profiles or for the preparation of whole lung tissue protein extracts for Western blot analysis; additionally, protein was measured in the BAL fluid.

3.1.2 Microarray Analysis

The comparison of gene expression profiles between MHV-68 infected IFN-γR$^{-/-}$ and C57BL/6 wild-type mice, together with respective uninfected mice, during acute (day 14) and chronic phase (day 45), was carried out with a multiple group comparison (F test) with a threshold of $p \leqslant 0.001$ by the software Qlucore (Qlucore bioinformatics company, Sweden). This analysis resulted in 216 genes which were found to be differentially expressed (Figure 3.2A). The identified gene clusters were then further illustrated in separate panels (Figure 3.2B-H). Some of the identified

genes were consistently and highly expressed in IFN-γR$^{-/-}$ mice while lowly expressed in C57BL/6 mice or vice versa (Figure 3.2B and C). Although these genes had significant variation between IFN-γR$^{-/-}$ and C57BL/6 wild-type mice due to the genotype of the mice, expression of these genes was not regulated during pulmonary inflammation and fibrosis. Genes in group D and E represented a homogeneous expression pattern. Several genes in these groups are involved in the regulation of the cell cycle, such as Ccnb1, Rrm2, Uhrf1, Tacc3, Ccna2 and Shcbp1. Group F contains a number of genes that were significantly upregulated in the C57BL/6 mice but not in IFN-γR$^{-/-}$ mice. Most of these genes were involved in the IFN-γ signaling pathway, such as Tap1, Sata1, CXCL10, CXCL9, Ido1 and Wars. However, in IFN-γ-receptor-deficient mice, those genes were not able to respond to the induction of IFN-γ. In groups G and H, 38 genes were shown to be differentially expressed during pulmonary inflammation and fibrosis between the IFN-γR$^{-/-}$ and C57BL/6 mice. 35 genes were highly expressed in both strains of mice by day 14 p.i., while they returned to baseline expression levels by day 45 p.i. in C57BL/6 mice but remained elevated above baseline values in the IFN-γR$^{-/-}$ mice (Figure 3.2G). Moreover, the expression levels of Slc5a12, Crispld2 and Gria1 in group H were suppressed in both strains of mice during the acute inflammatory phase (14 d.p.i.) and increased to the baseline expression levels during the chronic phase (45 d.p.i.) in C57BL/6 mice, but remained low and unchanged in the IFN-γR$^{-/-}$ mice during the chronic phase (45 d.p.i.). The expression profiles prioritized these genes in group G and H for further studies.

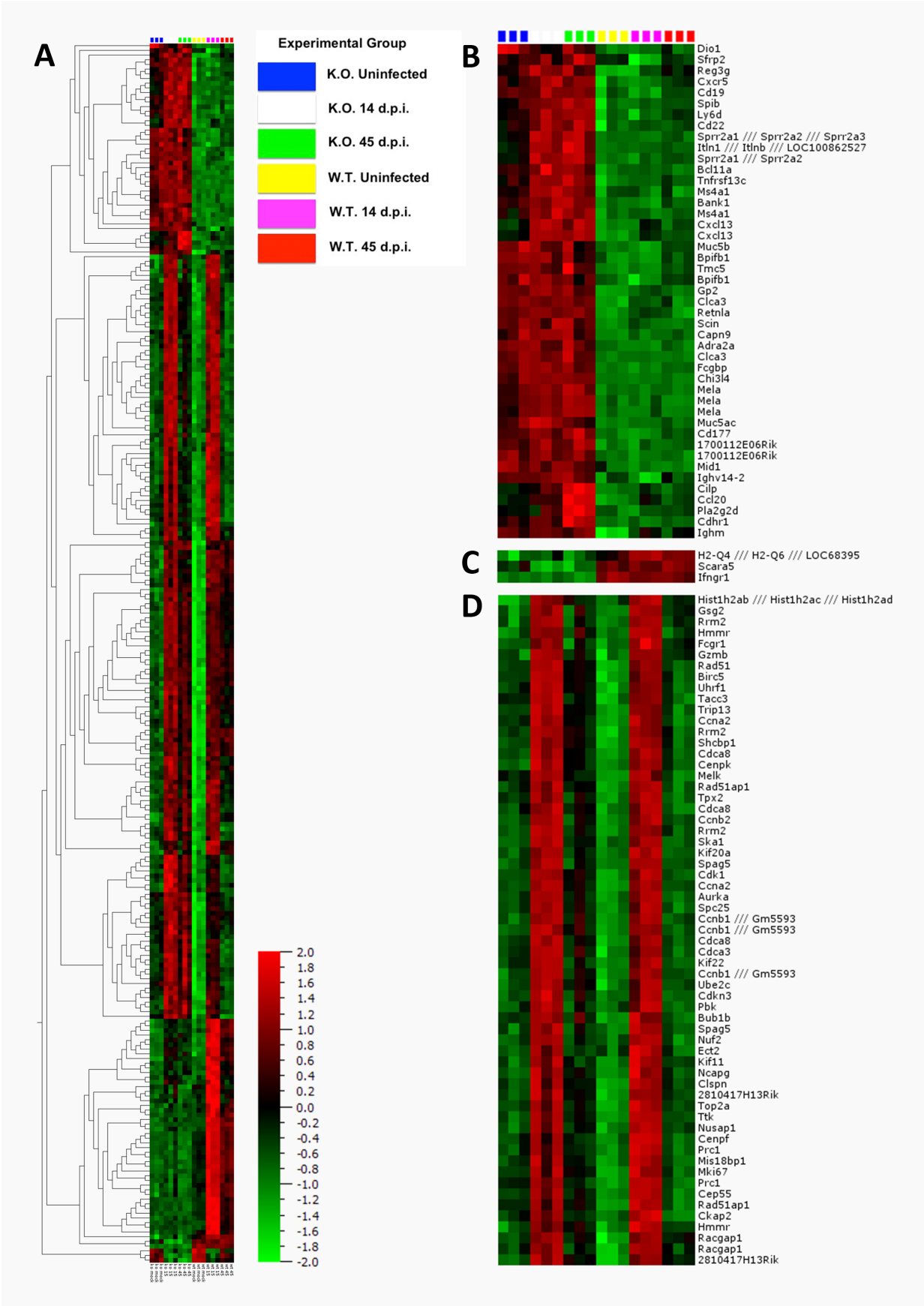
A
Experimental Group
K.O. Uninfected
K.O. 14 d.p.i.
K.O. 45 d.p.i.
W.T. Uninfected
W.T. 14 d.p.i.
W.T. 45 d.p.i.
2.0
1.8
1.6
1.4
1.2
1.0
0.8
0.6
0.4
0.2
0.0
-0.2
-0.4
-0.6
-0.8
-1.0
-1.2
-1.4
-1.6
-1.8
-2.0
B
Dio1
Sfrp2
Reg3g
Cxcr5
Cd19
Spib
Ly6d
Cd22
Sprr2a1 /// Sprr2a2 /// Sprr2a3
Itln1 /// Itlnb /// LOC100862527
Sprr2a1 /// Sprr2a2
Bcl11a
Tnfrsf13c
Ms4a1
Bank1
Ms4a1
Cxcl13
Cxcl13
Muc5b
Bpifb1
Tmc5
Bpifb1
Gp2
Clca3
Retnla
Scin
Capn9
Adra2a
Clca3
Fcgbp
Chi3l4
Mela
Mela
Mela
Muc5ac
Cd177
1700112E06Rik
1700112E06Rik
Mid1
Ighv14-2
Cilp
Ccl20
Pla2g2d
Cdhr1
Ighm
C
H2-Q4 /// H2-Q6 /// LOC68395
Scara5
Ifngr1
D
Hist1h2ab /// Hist1h2ac /// Hist1h2ad
Gsg2
Rrm2
Hmmr
Fcgr1
Gzmb
Rad51
Birc5
Uhrf1
Tacc3
Trip13
Ccna2
Rrm2
Shcbp1
Cdca8
Cenpk
Melk
Rad51ap1
Tpx2
Cdca8
Ccnb2
Rrm2
Ska1
Kif20a
Spag5
Cdk1
Ccna2
Aurka
Spc25
Ccnb1 /// Gm5593
Ccnb1 /// Gm5593
Cdca8
Cdca3
Kif22
Ccnb1 /// Gm5593
Ube2c
Cdkn3
Pbk
Bub1b
Spag5
Nuf2
Ect2
Kif11
Ncapg
Clspn
2810417H13Rik
Top2a
Ttk
Nusap1
Cenpf
Prc1
Mis18bp1
Mki67
Prc1
Cep55
Rad51ap1
Ckap2
Hmmr
Racgap1
Racgap1
2810417H13Rik

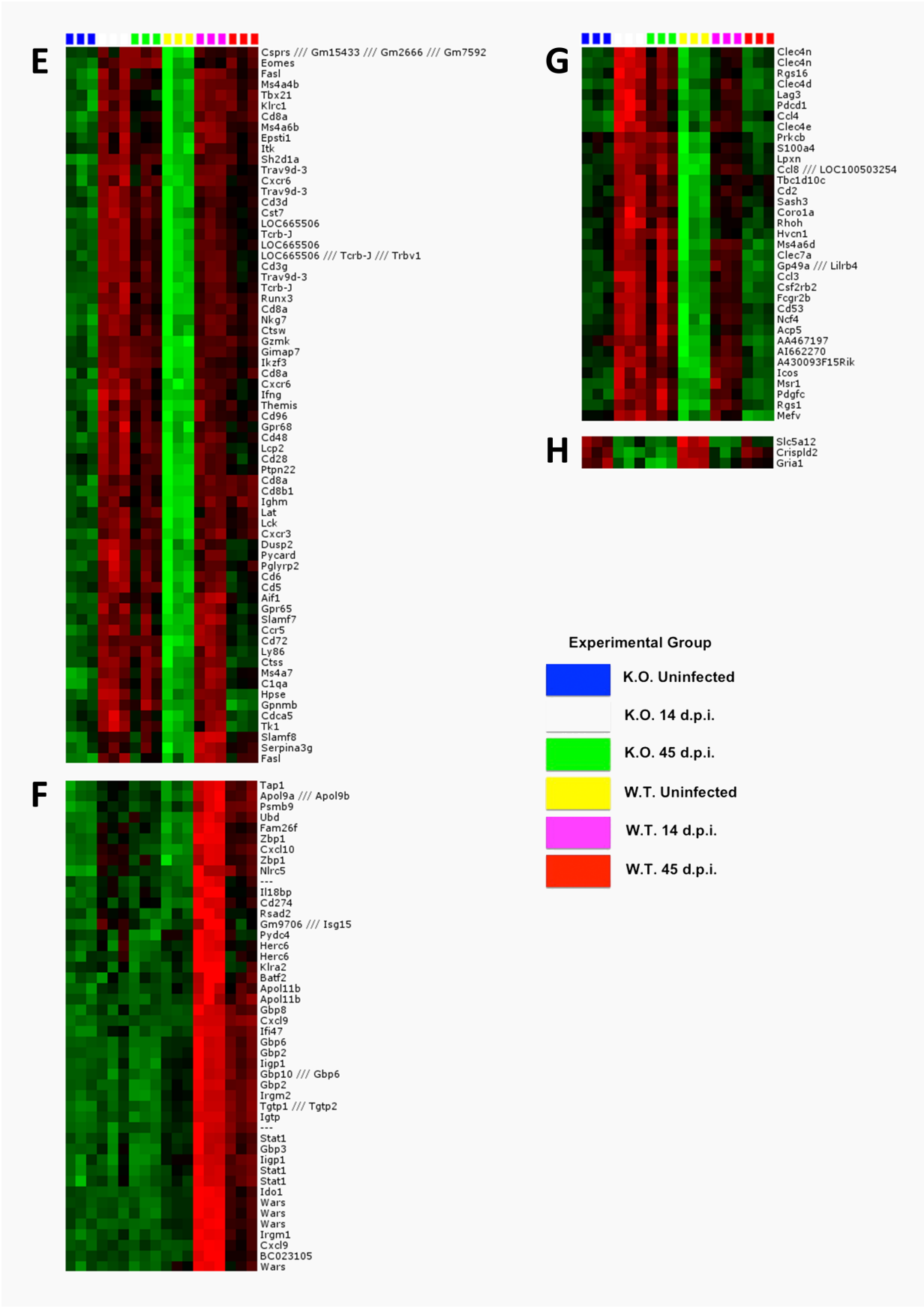
E
Csprs /// Gm15433 /// Gm2666 /// Gm7592
Eomes
Fasl
Ms4a4b
Tbx21
Klrc1
Cd8a
Ms4a6b
Epsti1
Itk
Sh2d1a
Trav9d-3
Cxcr6
Trav9d-3
Cd3d
Cst7
LOC665506
Tcrb-J
LOC665506
LOC665506 /// Tcrb-J /// Trbv1
Cd3g
Trav9d-3
Tcrb-J
Runx3
Cd8a
Nkg7
Ctsw
Gzmk
Gimap7
Ikzf3
Cd8a
Cxcr6
Ifng
Themis
Cd96
Gpr68
Cd48
Lcp2
Cd28
Ptpn22
Cd8a
Cd8b1
Ighm
Lat
Lck
Cxcr3
Dusp2
Pycard
Pglyrp2
Cd6
Cd5
Aif1
Gpr65
Slamf7
Ccr5
Cd72
Ly86
Ctss
Ms4a7
C1qa
Hpse
Gpnmb
Cdca5
Tk1
Slamf8
Serpina3g
Fasl
F
Tap1
Apol9a /// Apol9b
Psmb9
Ubd
Fam26f
Zbp1
Cxcl10
Zbp1
Nlrc5

Il18bp
Cd274
Rsad2
Gm9706 /// Isg15
Pydc4
Herc6
Herc6
Klra2
Batf2
Apol11b
Apol11b
Gbp8
Cxcl9
Ifi47
Gbp6
Gbp2
Iigp1
Gbp10 /// Gbp6
Gbp2
Irgm2
Tgtp1 /// Tgtp2
Igtp

Stat1
Gbp3
Iigp1
Stat1
Stat1
Ido1
Wars
Wars
Wars
Irgm1
Cxcl9
BC023105
Wars
G
Clec4n
Clec4n
Rgs16
Clec4d
Lag3
Pdcd1
Ccl4
Clec4e
Prkcb
S100a4
Lpxn
Ccl8 /// LOC100503254
Tbc1d10c
Cd2
Sash3
Coro1a
Rhoh
Hvcn1
Ms4a6d
Clec7a
Gp49a /// Lilrb4
Ccl3
Csf2rb2
Fcgr2b
Cd53
Ncf4
Acp5
AA467197
AI662270
A430093F15Rik
Icos
Msr1
Pdgfc
Rgs1
Mefv
H
Slc5a12
Crispld2
Gria1
Experimental Group
K.O. Uninfected
K.O. 14 d.p.i.
K.O. 45 d.p.i.
W.T. Uninfected
W.T. 14 d.p.i.
W.T. 45 d.p.i.

Figure 3.2 Heat map analysis of genes differentially expressed in MHV-68 infected C57BL/6 wild type and IFN-γR$^{-/-}$ mice.
(A) Gene expression profiles were analyzed by whole genome expression analysis via Qlucore software using RNA isolated from mock or MHV-68 infected mouse lungs at 14 or 45 days post virus inoculation. 216 differentially expressed genes were clustered across all mouse samples. Red and green denote increased and decreased gene expression levels, respectively. Each column represents an individual mouse (n=3 for each group), and each row is a separate gene. Groups (left to right) are IFN-γR$^{-/-}$ uninfected mice, IFN-γR$^{-/-}$ mice at days 14 and 45 post infection; C57BL/6 uninfected mice, C57BL/6 mice at days 14 and 45 post infection. (B&C) Genes that are consistently and highly expressed in IFN-γR$^{-/-}$ mice while lowly expressed in C57BL/6 mice or vice versa. (D&E) Genes exhibit the same expression pattern in IFN-γR$^{-/-}$ and C57BL/6 mice. (F-H) Genes that are differentially regulated in IFN-γR$^{-/-}$ and C57BL/6 mice during inflammatory and fibrotic phases.

3.1.2 GO and Pathway Analysis

In parallel with the bioinformatic identification of differentially regulated genes, the 216 genes were annotated in the form of GO terms, in the categories of Molecular Function and Biological Process, in order to infer deregulated biological functions from the gene list and define functional criteria for further gene selection. GO term frequencies in the selected gene list were then analyzed and their statistical significance (identified as a P value) were estimated through their hypergeometric distribution (Gene Ontology Consortium). As shown in Table 3.1, a number of well-expected processes and functions were found to be deregulated during the pathogenesis of MHV-68-induced pulmonary inflammation and fibrosis, such as chemokine activity, regulation of leukocyte activation, myeloid leukocyte activation, and regulation of cell proliferation. As anticipated, GO analysis indicated disorders of the immune system as a pathogenic insult that could lead to (or exacerbate) pulmonary fibrosis.

Moreover, the Panther Pathways software (http://pantherdb.org/pathway/) was used for automated gene expression data integration in cellular canonical pathways. The genes were examined for their participation in canonical pathways, followed by a frequencies calculation. The top 12 clustered pathways are shown in Table 3.2. A number of pathways were identified to be deregulated, such as Wnt signaling pathway, angiogenesis and T cell activation. Notably, the inflammation mediated by chemokine and cytokine signaling pathways was ranked first in the list, further supporting the GO analysis results.

Table 3.1 Gene ontology analysis of differentially regulated genes.

Annotation	P value
GO: molecular function	
protein binding	6.16E-14
binding	3.29E-07
chemokine receptor binding	5.15E-04
chemokine activity	2.09E-03
carbohydrate derivative binding	2.23E-03
antigen binding	2.30E-03
protein kinase binding	3.83E-03
kinase binding	4.01E-03
identical protein binding	9.21E-03
CXCR3 chemokine receptor binding	1.73E-02
protein complex binding	2.58E-02
GO: Biological process	
response to other organism	1.15E-08
response to external biotic stimulus	1.15E-08
leukocyte differentiation	1.15E-07
single organism cell adhesion	1.27E-05
positive regulation of leukocyte activation	1.08E-04
regulation of cell proliferation	1.11E-03
regulation of microtubule cytoskeleton organization	1.02E-02
response to molecule of bacterial origin	1.08E-02
negative regulation of cellular process	1.08E-02
myeloid leukocyte activation	1.11E-02

Table 3.2 Pathway analysis of differentially regulated genes.

Pathway	Frequencies
Inflammation mediated by chemokine and cytokine signaling pathway	17 %
T cell activation	7 %
Angiogenesis	5 %
Interleukin signaling pathway	4 %
Interferon-gamma signaling pathway	4 %
Heterotrimeric G-protein signaling pathway-Gq alpha and Go alpha mediated pathway	4 %
Heterotrimeric G-protein signaling pathway-Gi alpha and Gs alpha mediated pathway	4 %
Wnt signaling pathway	4 %
B cell activation	4 %
Apoptosis signaling pathway	3 %
p53 pathway	3 %
EGF receptor signaling pathway	3 %

3.1.3 Verification of Microarray Data Using qRT-PCR

In order to assess the validity of the gene expression differences identified by the microarray analysis, the expression levels of eleven selected genes, including immune regulators, transporters, and cell surface receptor were assessed by qRT-PCR in our original samples used in the microarray study. Figure 3.3 shows that the great majority of these genes (S100a4, Scara5, Bpifb1, LPNX, Muc5b, Cle4n, Slc5a, C1qa, Gria1, Ctss, and Crispld2) demonstrated good correlations between data obtained with the two techniques.

To further identify novel candidates for disease-related differentially regulated genes, we evaluated the genes that were not highlighted or well-studied in the inflammatory response. A very extensive manual literature search with PubMed and a comprehensive comparison of published expression profiling results from other IPF animal models as well as from human patients were performed (208). Most of the inflammation related genes have been well characterized in the regulation of pulmonary fibrosis, such as CXCR3 and its ligands CXCL9 and CXCL10 (209). Noticeably, the gene termed *S100a4* has been found to be highly expressed in the

bleomycin-induced acute lung injury and pulmonary fibrosis dataset with fold changes of 2.4 and 3.7, respectively, compared with mice from control groups (208). Its upregulation across multiple IPF animal models suggested that it may play a role in the common features of disease pathogenesis. In addition, S100a4 was also found to play roles in the immune response (163, 210-212).

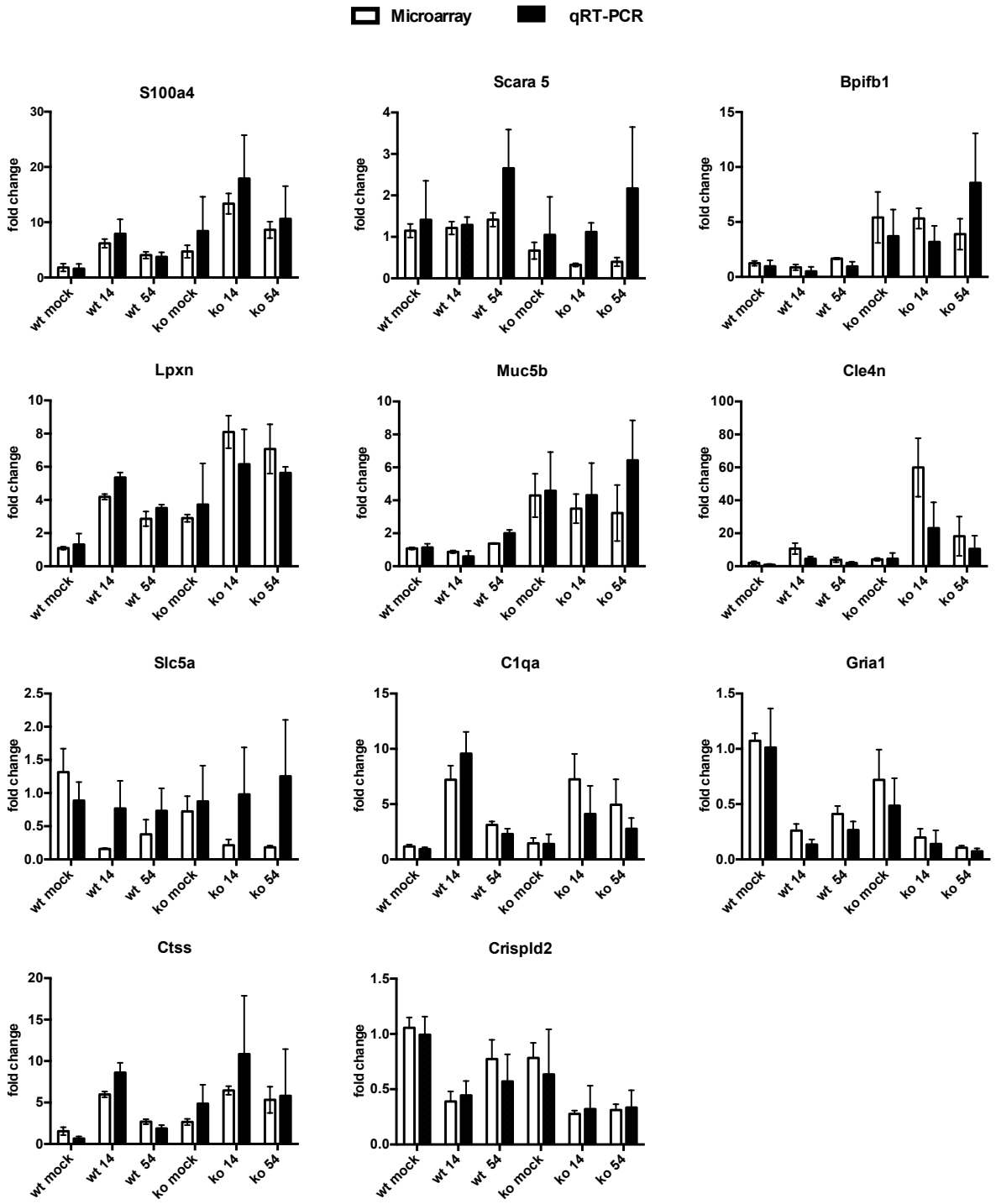

Figure 3.3 qRT-PCR verification of microarray results.
Expression levels of eleven genes selected from the microarray data were measured by qRT-PCR in homogenates from uninfected or MHV-68 infected IFN-γR$^{-/-}$ (k.o) and C57BL/6 wild-type (w.t) mice at days 14 and 45 p.i.. Relative fold changes of selected genes, *S100a4*, *Scara5*, *Ctss*, *Bpifb1*, *LPXN*, *Muc5b*, *Clec4n*, *Slc5a*, *C1qa*, *Gria1*, *Ctss*, and *Crispld2* were analyzed by qRT-PCR. For each sample, the microarray data are plotted on the left with white columns, while the qRT-PCR results are plotted on the right with black columns. The qRT-PCR expression levels were normalized to l8. Results are derived from 3 mice per group and shown as mean ± SD.

3.2 S100a4 Positive Cells Increase during Fibrogenesis

3.2.1 Expression Analysis of S100a4 by Western Blot

As indicated by microarray analysis, S100a4 was extensively expressed at day 14 p.i. (acute inflammation phase) in both IFN-γR$^{-/-}$ and C57BL/6 wild-type mice, then declined to the control level in the wild-type mice at day 45 p.i. (fibrotic phase), whilst remaining high in the IFN-γR$^{-/-}$ mice. Thus, we next assessed whether the changes in S100a4 mRNA level also resulted in respective changes at the protein level. Western blot analysis was performed in an independent set of freshly homogenized lung tissues. The results confirmed the microarray and qRT-PCR analysis. High expression of S100a4 only occurs during the progression phase in both strains of mice, and disappears rapidly at the resolution phase of lung fibrosis in the wild-type mice but not in IFN-γR$^{-/-}$ mice (Figure 3.4).

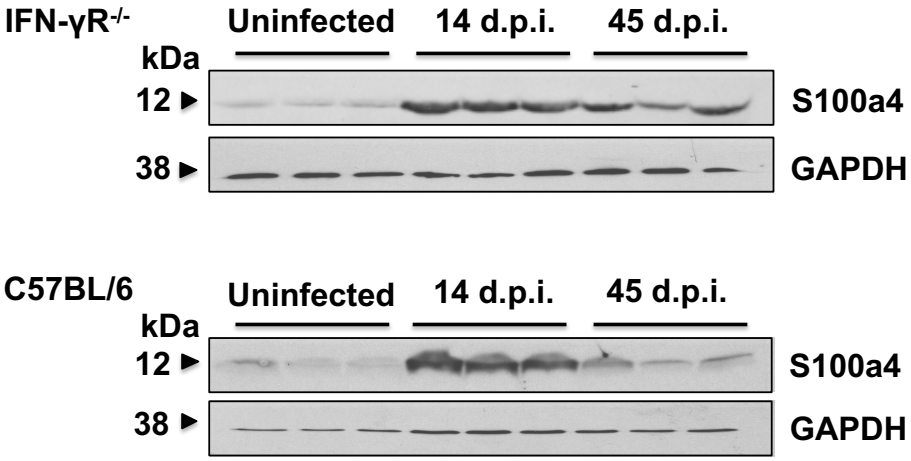

Figure 3.4 Increased S100a4 expression in MHV-68-induced pulmonary inflammation and fibrosis.
Lung homogenates from uninfected mice and MHV-68-infected mice at the indicated time points were subjected to western blot analysis for the S100a4 protein (3 mice per group). Blots were either incubated with an anti-S100a4-antibody or an anti-GAPDH antibody as loading control.

3.2.2 Expression Analysis of S100a4 by ELISA

It has been reported that S100a4 could be secreted extracellularly (159) and therefore ELISA was performed to further analyze the secreted S100a4 protein in the BAL fluid isolated from uninfected and MHV-68 infected IFN-γR$^{-/-}$ and C57BL/6 wild-type mice at indicated time points (Figure 3.5A). As expected, the S100a4 protein

detected in the BAL fluid was in accordance with the western blot analysis: the level of soluble S100a4 protein was elevated during the pulmonary inflammation (day 20 p.i.) in both stains of mice, and remained high during the fibrotic phase (> day 60 p.i.) in IFN-γR$^{-/-}$ mice (k.o), while decreasing in wild-type mice (w.t). In addition, the amount of S100a4 protein was also quantified in BAL fluid obtained from PBS- or bleomycin-treated C57BL/6 mice at 14 days after instillation (Figure 3.5B). An elevated expression level of S100a4 was also observed in the bleomycin-treated mice. These results indicated that a significantly increased level of S100a4 protein in the lung is a common phenomenon during fibrogenesis, independent of the experimental mouse model.

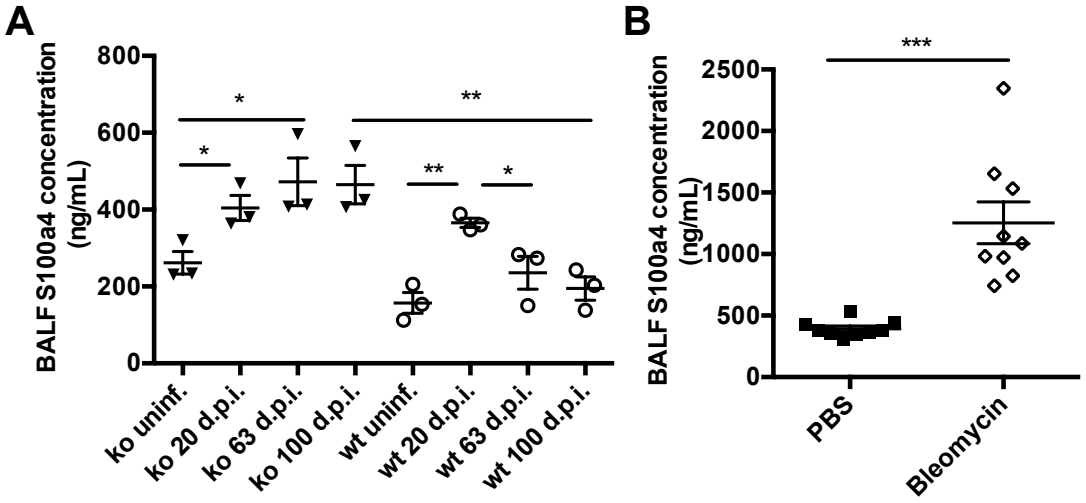

Figure 3.5 Up-regulation of S100a4 protein in BAL fluid of fibrotic mice.
(A) S100a4 protein was measured in BAL fluids from uninfected or MHV-68 infected IFN-γR$^{-/-}$ (ko) and C57BL/6 mice (wt) at days 20, 63 and 100 p.i.. Each symbol represents a mouse. Results are derived from 3 mice per group and shown as mean ± SD. Unpaired t-test was performed for statistical analysis (* denotes $p<0.05$; ** denotes $p<0.01$). (B) Protein levels of S100a4 were measured in BAL fluid from PBS or bleomycin-treated C57BL/6 mice at 14 days after instillation (n=9 per group). Each symbol represents a mouse. Results are derived from 9 mice per group and shown as mean ± SD. Unpaired t-test was performed for statistical analysis (***denotes $p < 0.001$).

3.2.3 Immunohistochemistry Localizes S100a4 to Alveolar Macrophages in Fibrotic Lungs

In previous studies, S100a4 was considered as a marker of fibroblasts in different organs undergoing tissue remodeling including kidney, lung, liver and heart. Additionally, S100a4 is commonly used to demonstrate the EMT process in several tissues during fibrogenesis (213). However, it remains elusive what the origin of

S100a4 secreting cells in the fibrotic lungs is. Österreicher and colleagues reported that S100a4 identifies an inflammatory subpopulation of macrophages in the injured liver (214). In order to characterize the origin of S100a4 in the fibrotic lung tissue, the S100a4 protein was characterized by immunohistochemical staining of consecutive sections. Representative images of immunohistochemical staining of S100a4 are shown in Figure 3.6. In uninfected IFN-γR$^{-/-}$ mice, S100a4 was detected only in a few cells. In contrast, in the sections of fibrotic lungs, S100a4-positive stained cells were widely observed in perivascular lymphocytic infiltrates, areas around small or medium vessels and injured alveoli or airways with enhanced staining of monocytes/macrophages in the early (day 17 p.i.) and advanced stages (day 45 p.i.) of lung fibrosis (Figure 3.6A).

Prior investigations have suggested that alveolar macrophages are the predominant immune cells of the pulmonary innate immune system and play an important role in driving the fibrogenesis process. Additionally, recruited alveolar macrophages showed high expression of Ym1/2, FIZZ1 and Arg1, which indicates that the macrophages were activated by an alternative pathway (113). Hence, we hypothesized that S100a4 was secreted by alternatively activated macrophages. To confirm the above concept, immunohistochemical staining of S100a4 and Arg1 on consecutive lung sections was performed. Careful inspection of serially stained sections demonstrated that S100a4 positive cells were closely localized with Arg1 positive cells at the beginning of fibrosis (Day 45) and also in the remodeling phase (Day 90) (Figure 3.6B), which confirmed our hypothesis that S100a4 co-localized with Arg1 in macrophages.

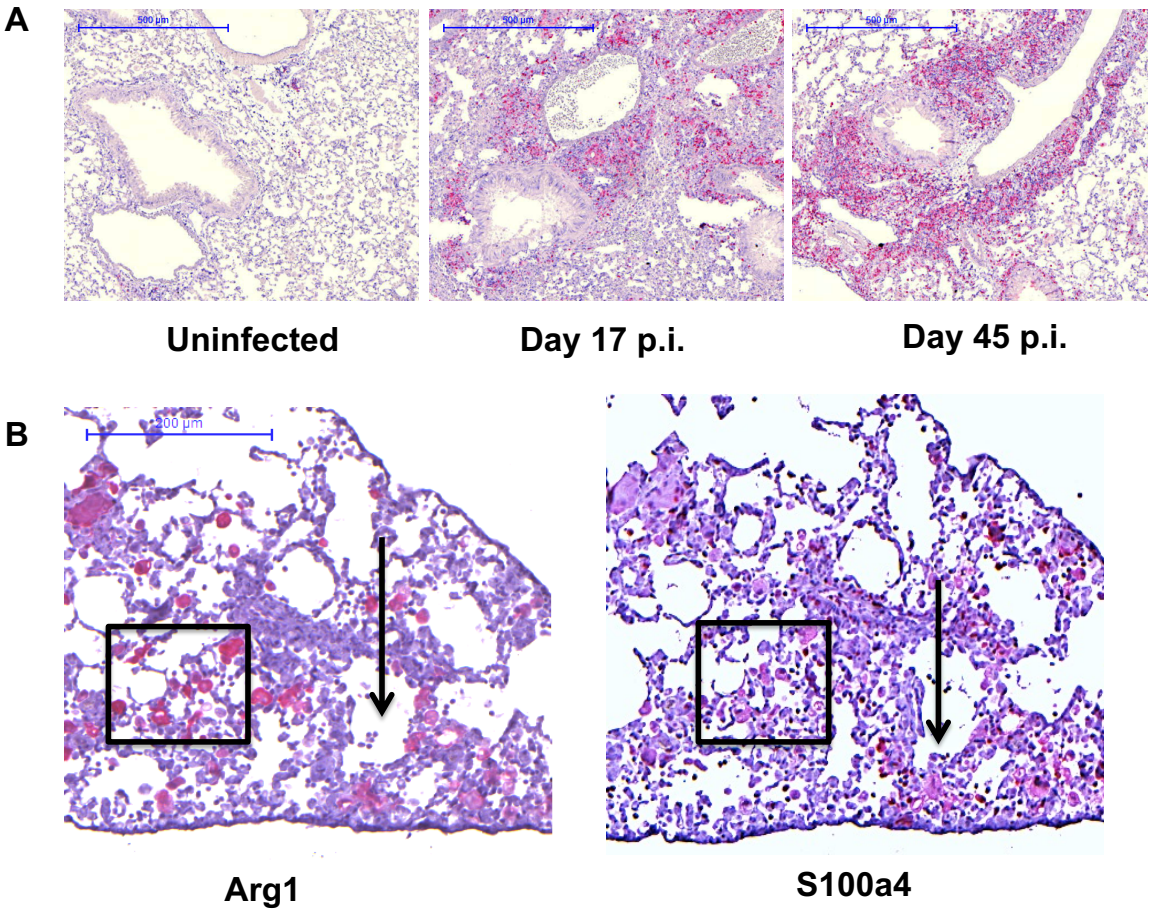

Figure 3.6 Co-localization of S100a4 with alternatively activated macrophages in tissue sections from fibrotic mice.
(A) Representative images of immunohistochemical staining for S100a4 are shown from lung sections of uninfected and MHV-68 infected IFN-γR$^{-/-}$ mice at day 17 and day 45 p.i.. The S100a4 positive cells are denoted by red staining. Positive staining was found in monocytes/macrophages from infected animals. (B) Serial section staining of S100a4 and Arg1 (M2 macrophages) in MHV-68 infected IFN-γR$^{-/-}$ mice at days 45 and 90 p.i.. Arrows and frames indicate co-staining.

Moreover, accumulation of S100a4 positive cells with the characteristic morphology of monocytes/macrophages during fibrosis progression was also found in the bleomycin induced IPF mouse model (Figure 3.7A), and co-localization of S100a4 and Arg1 were also substantiated by immunohistochemical staining of serial lung sections (Figure 3.7B). The bleomycin lung sections were kindly provided by Dr. Melanie Königshoff, CPC.

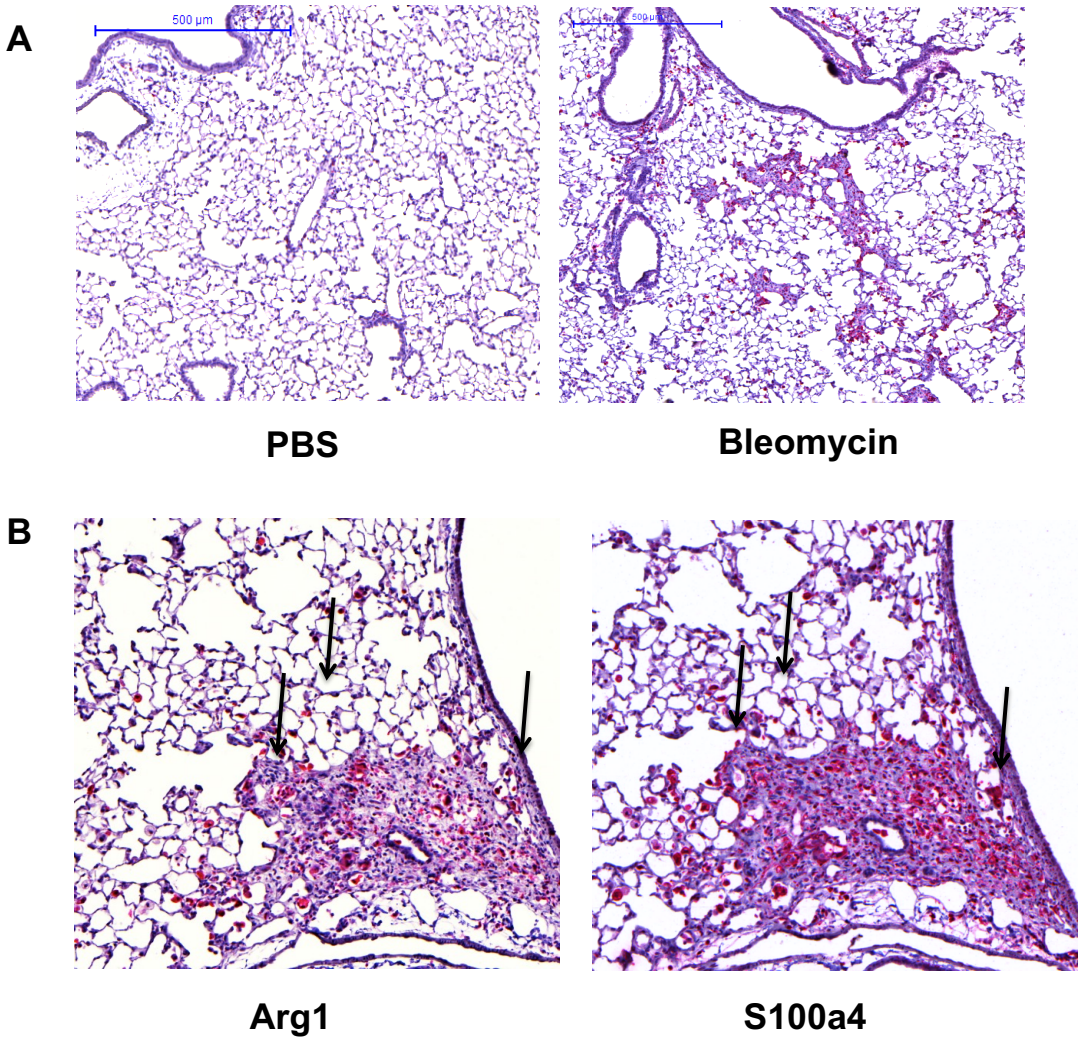

Figure 3.7 Localization of S100a4 in lung tissues of PBS and bleomycin-treated mice. (A) Immunohistochemical staining for S100a4 was performed on lung sections of PBS and bleomycin-treated mice at day 14 after instillation. The S100a4 positive cells are denoted by red staining. (B) Co-staining of S100a4 and Arg1 (M2 macrophages) on the lung serial sections of bleomycin-treated mice at day 14 after instillation. Arrows indicate co-staining.

3.2.4 Expression Analysis of S100a4 in Alveolar Macrophages Isolated from Control or Fibrotic Mice by qRT-PCR

To confirm that S100a4 is expressed by alternatively activated alveolar macrophages, qRT-PCR was performed on freshly isolated alveolar macrophages from uninfected and MHV-68 infected IFN-γR$^{-/-}$ mice when lung fibrosis was well established (days 45 and 90 p.i.). Significant increases of *S100a4* (5-fold) and *Arg1*, the alternatively activated macrophage marker, as well as a decrease of *Tnf*, the typical marker of classically activated macrophages, were found in alveolar macrophages derived from virus infected mice compared with macrophages derived from uninfected mice with equivalent numbers of cells (Figure 3.8A). Furthermore, mRNA levels of *S100a4*, *Arg1* and *Tnf* were also analyzed in the alveolar macrophages isolated from PBS or bleomycin-treated mice. Alveolar macrophages isolated from bleomycin treated mice highly expressed *S100a4* and *Arg1* but lowly expressed *Tnf.* These findings suggest that *S100a4* originates from alternatively activated macrophages during lung fibrosis (Figure 3.8B).

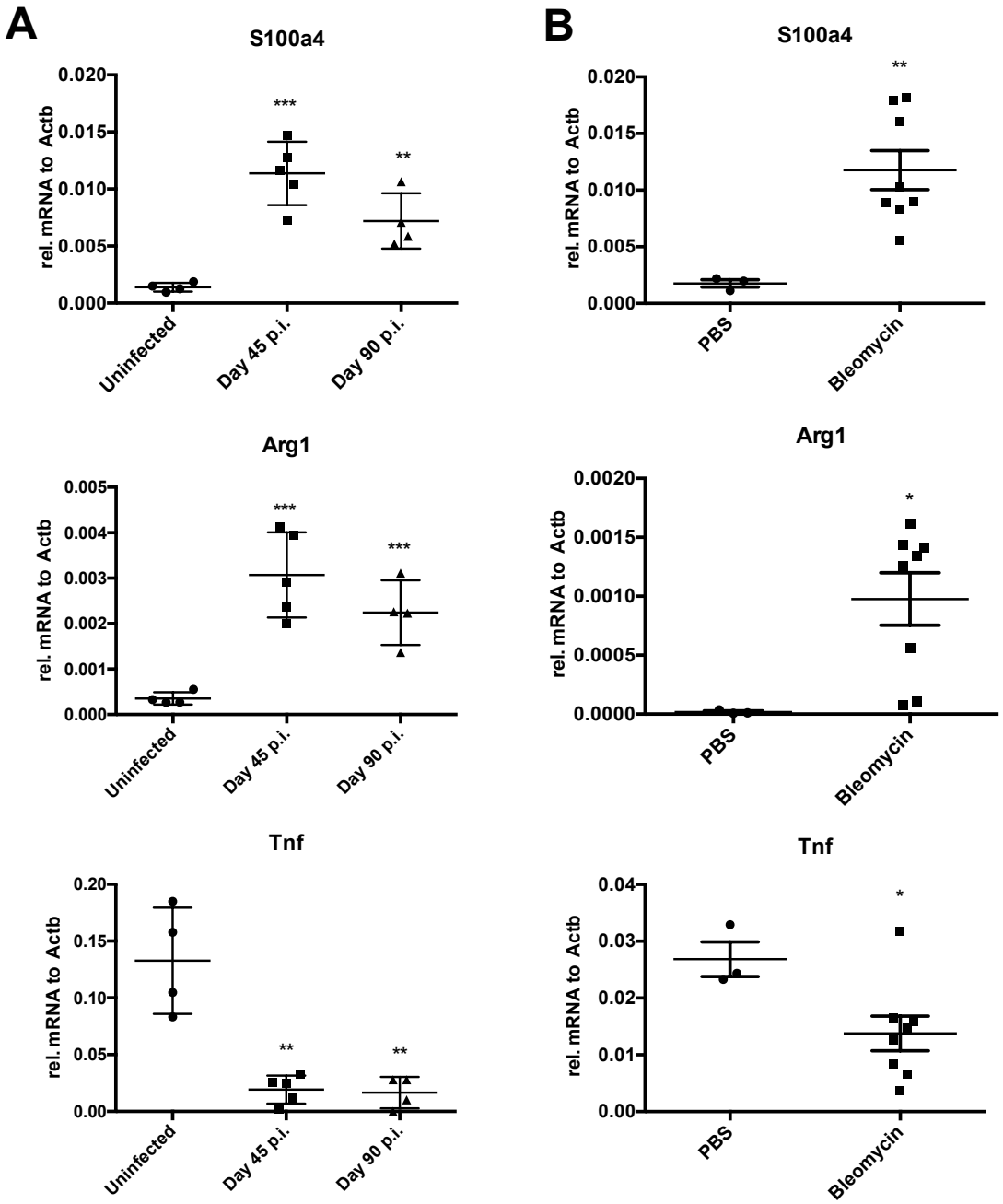

Figure 3.8 Increased S100a4 expression in alveolar macrophages in experimental lung fibrosis.

(A) qRT-PCR was used to determine the levels of *S100a4*, *Arg1* (M2 marker) and *Tnf* (M1 marker) transcripts in alveolar macrophages of uninfected or MHV-68 infected IFN-γR$^{-/-}$ mice at days 45 and 90 p.i.. Expression of target genes was normalized to *β-actin*. Each symbol represents a mouse (n = 4 uninfected group; n = 5 or 4 infected group). Results are shown as mean ± SD. Unpaired t-test was performed for statistical analysis (** denotes p<0.01; ***denotes p < 0.001). (B) Relative mRNA levels of *S100a4*, *Arg1* and *Tnf* in alveolar macrophages isolated from PBS or bleomycin challenged C57BL/6 mice were assessed. Expression of target genes was normalized to β-actin. Each symbol represents a mouse (n=3 PBS group; n=8 bleomycin-treated group). Results are shown as mean ± SD. Unpaired t-test was performed for statistical analysis (* denotes p<0.05; ** denotes p<0.01).

3.2.5 Analysis of S100a4 Gene Expression in Polarized Alveolar Macrophages by qRT-PCR

Recently, the group of Dr. Tobias Stöger (CPC) has demonstrated that the alveolar macrophage, like other subpopulations of tissue macrophages, can be polarized into respective M1 (classically activated) and M2 (alternatively activated) phenotypes *in vitro* (215). To investigate the association of *S100a4* and polarized alveolar macrophages, freshly isolated alveolar macrophages were treated either with LPS (1 µg/ml) and IFNγ (20 ng/ml) to induce M1-like phenotypes or with IL-4 (20 ng/ml) to induce M2 polarization. Cells were harvested for total RNA isolation and qRT-PCR was performed. The expression profile of *S100a4* in polarized alveolar macrophages was in accordance with *Arg1*, the M2 marker. Both *S100a4* and *Arg1* were significantly elevated in M2 polarized alveolar macrophages, when compared to the control M0 and M1 polarized macrophages (Figure 3.9).

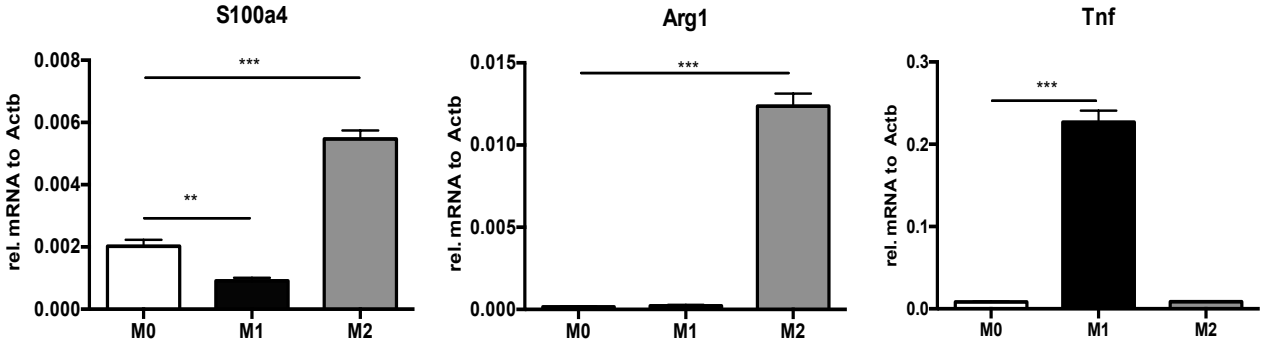

Figure 3.9 Expression profile of S100a4 in polarized alveolar macrophages.
Alveolar macrophages isolated from C57BL/6 mice were treated with LPS (1 µg/ml) and IFNγ (20 ng/ml) or IL-4 (20 ng/ml) for 24 hours and relative mRNA levels of *S100a4*, *Arg1* (M2 marker) and *Tnf* (M1 marker) were assessed using qRT-PCR. Expression of target genes was normalized to *β-actin.* qRT-PCR results are representative of two independent experiments with similar results. Shown are mean ± SD of triplicate samples from one of two representative experiments. Unpaired t-test was performed for statistical analysis (** denotes $p<0.01$; ***denotes $p < 0.001$).

3.2.6 Kinetics of S100a4 Gene Expression during IL-4-driven Alveolar Macrophage Polarization

The above studies focused on a single time point of macrophage polarization and thus do not provide detailed information concerning the dynamic changes of S100a4 during the whole process of polarization. To understand the kinetics of the increased

expression of *S100a4* during IL-4-driven alveolar macrophage polarization, primary macrophages were treated with IL-4 (20 ng/ml) for 6, 24, 48 and 72 hours, respectively. The gene expression analysis by qRT-PCR revealed an elevated trend of expression of *S100a4* from 6 to 72 hours after IL-4 treatment, which reached the maximal level at 72 hours (Figure 3.10A). Additionally, we also determined whether the expression of *S100a4* is IL-4 dose-dependent or not. Primary alveolar macrophages were treated with increasing amounts (10 ng/ml, 20 ng/ml, 50 ng/ml, 100 ng/ml and 200 ng/ml) of IL-4 for 24 hours. Expression levels of S100a4 were estimated by qRT-PCR, which demonstrated IL-4 stimulated *S100a4* expression in a concentration-dependent manner, reaching peak expression at 20 ng/ml. (Figure 3.10B).

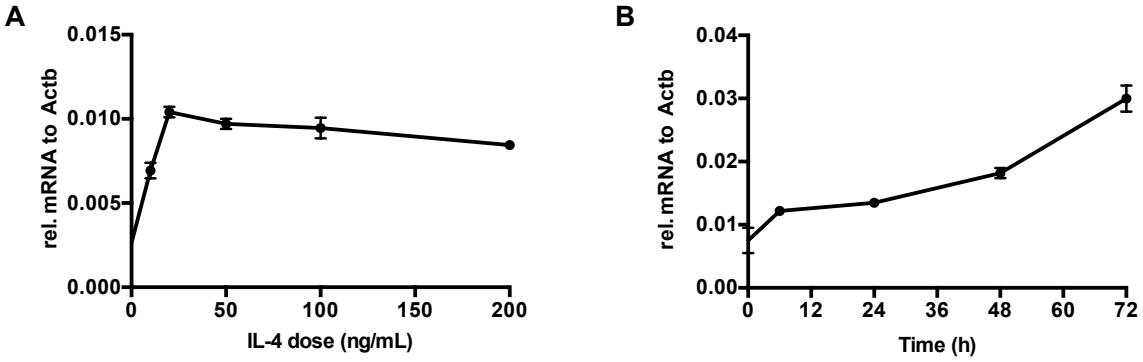

Figure 3.10 Gene expression analysis of S100a4 during primary alveolar macrophage polarization by qRT-PCR

(A) Primary alveolar macrophages from C57BL/6 mice were treated with IL-4 (20 ng/ml). for 6, 24, 48 and 72 hours, respectively, and relative mRNA levels of *S100a4* were analyzed by qRT-PCR. Results are normalized to *β-actin* expression. (B) Primary alveolar macrophages from C57BL/6 mice were treated with 10 ng/ml, 20 ng/ml, 50 ng/ml, 100 ng/ml and 200 ng/ml IL-4, respectively, and relative mRNA levels of *S100a4* were analyzed by qRT-PCR. Results are normalized to *β-actin* expression. Shown are mean ± SD of triplicate samples from one experiment.

3.2.7 Analysis of S100a4 protein Expression during Alveolar Macrophage Polarization by Western Blot

Following the mRNA profile, we also investigated protein expression of S100a4 in primary alveolar macrophages. Cells were treated with LPS (1 µg/ml) or IFNγ (20 ng/ml) and IL-4 (20 ng/ml) or IL-13 (20 ng/ml) for 6, 24, 48 and 72 hours, respectively. It has been well described that the effects of IL-13 on activation of macrophages are similar to IL-4 due to their sequence similarity and similar structure

(216). Additionally, both of them can induce the phosphorylation of STAT6 as they share the common receptor IL-4Ra (217). Thus, phosphorylated STAT6 is used as a marker of M2 polarization. As expected, the S100a4 protein was both detected by 48 hours after IL-4 or IL-13 induced M2 polarization and increased further to 72 hours, but was not detected in M0 or M1 polarized macrophages (Figure 3.11 A and B).

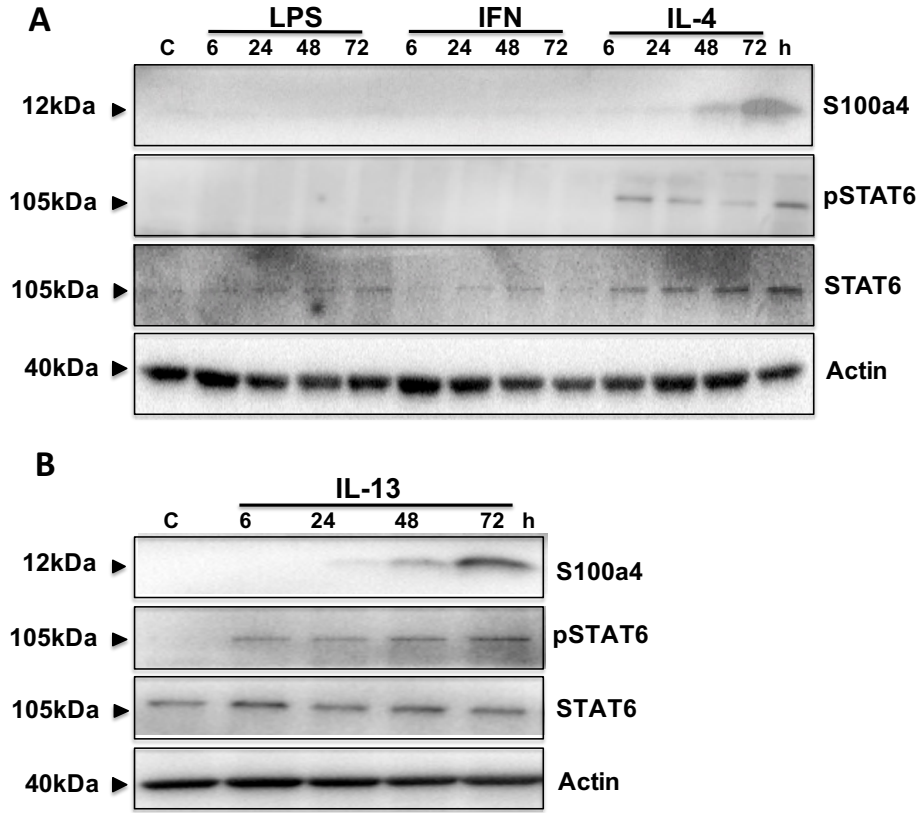

Figure 3.11 Analysis of S100a4 protein expression during alveolar macrophage polarization by Western blot

Primary alveolar macrophages isolated from C57BL/6 mice were treated with LPS (1 µg/ml) or IFNγ (20 ng/ml) and IL-4 (20 ng/ml) or IL-13 (20 ng/ml) for 6, 24, 48 and 72 hours, respectively. Protein expression of S100a4 and phosphorylation of STAT-6 were determined by western blot assay. The phosphorylated STATA6 was used as an indicator for IL-4 or Il-13 induced M2 macrophage polarization. Blots were incubated with an anti-β-actin antibody as loading control. Results are representative of two independent experiments. The control (c) reflects unstimulated alveolar macrophages at 24 hours.

3.2.8 Analysis of S100a4 Protein Expression during Alveolar Macrophage Polarization by ELISA

To confirm that S100a4 is secreted by M2 polarized macrophages, we subsequently performed ELISA tests on supernatants of IL-4 treated primary alveolar macrophages from both IFN-γR$^{-/-}$ and C57BL/6 mice 72 hours after stimulation. The

soluble S100a4 in the supernatant from IL-4 treated macrophages increased five to seven times compared with untreated cells (Figure 3.12). It is notable that significantly higher S100a4 production was found in M2 polarized alveolar macrophages from IFN-γR$^{-/-}$ mice compared to C57BL/6 mice, which indicated that macrophages from IFN-γR$^{-/-}$ mice possess an enhanced capacity for IL-4 stimulation. In addition, enhanced production of S100a4 in M2 macrophages from IFN-γR$^{-/-}$ mice is in accord with previous studies showing that IFN-γ suppressed S100a4 transcription in diverse cancer cell lines (218, 219), and is also consistent with our *in vivo* data (Figure 3.4 and 3.5).

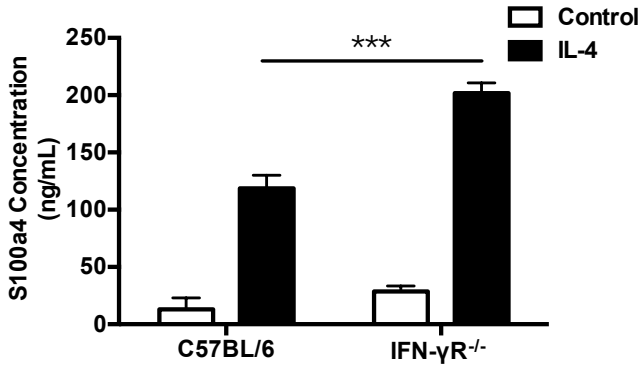

Figure 3.12 Analysis of S100a4 protein secretion during alveolar macrophage polarization by ELISA.
Primary alveolar macrophages from IFN-γR$^{-/-}$ and C57BL/6 mice were treated with IL-4 (20 ng/ml) for 72 hours. The supernatant was collected for the ELISA assay. Results are representative of two independent experiments with similar results. Shown are mean ± SD of triplicate samples from one experiment. Unpaired t-test was performed for statistical analysis (***denotes $p < 0.001$).

3.2.9 Co-localization of S100a4 and Arg1 in M2 Polarized Alveolar Macrophages

To further confirm that all S100a4-expressing alveolar macrophages are indeed M2 macrophages expressing Arg1, we performed double immunofluorescence staining of S100a4 and Arg1 on M2 polarized macrophages (Figure 3.13). These results verified that S100a4 co-localized with Arg1 in each M2 macrophage. Hence, the expression of S100a4 was substantiated by qRT-PCR, Western blot, ELISA and double immunofluorescence staining analysis, providing strong evidence that S100a4 is produced by M2 polarized alveolar macrophages.

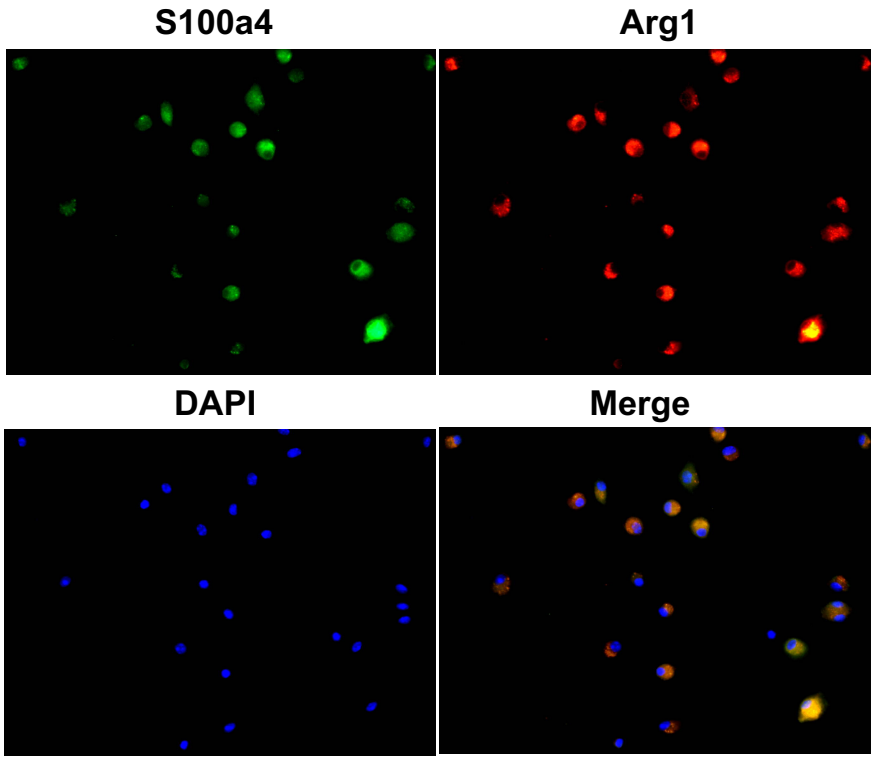

Figure 3.13 S100a4 co-localized with Arg1 in M2 polarized alveolar macrophages. Primary alveolar macrophages from C57BL/6 mice were seeded on coverslips and polarized with IL-4 (20 ng/ml) for 48 hours. Green and red fluorescences reflect S100a4 and Arg1, respectively. Yellow indicates co-localization of these two proteins, whereas DAPI depicts nuclei. Results are representative of three independent experiments.

3.3 Functional Analysis of S100a4 Protein

3.3.1 Effect of S100a4 on the Activation of Primary Lung Fibroblasts

It has been shown in both rodent pulmonary fibrosis models and in IPF patients that alveolar macrophages are alternatively rather than classically activated. An imbalance between T helper 1 and 2 cytokines is evidenced in fibrotic lungs, with Th2 cytokines (IL-4, IL-5, IL-10, IL-3) playing a pivotal role in the pathogenesis of pulmonary fibrosis (115). M2 macrophages secrete Th2 cytokines to promote fibrogenesis via enhancing collagen deposition, angiogenesis and fibroproliferation (220). Therefore, we hypothesized that S100a4 may serve as a cytokine-like factor indirectly promoting the pathogenesis of lung fibrosis.

To investigate the influence of the extracellular S100a4 on lung fibroblasts, primary mouse lung fibroblasts isolated from C57BL/6 mice were starved in DMEM/F-12 medium for 12 hours followed by treatment with S100a4, ranging from 0

to 3 µg/ml for 24 hours. As shown in Figure 3.14A, 0.1 µg/ml to 3 µg/ml S100a4 induced significant expression of alpha-smooth muscle actin (α-SMA, a marker for myofibroblasts) in a concentration-dependent manner. The maximal effect was noted with $\geqslant$ 2 µg/ml S100a4, and we chose a concentration of 2 µg/ml as the optimal dose for the following experiments. Furthermore, primary mouse lung fibroblasts were cultured in the presence of recombinant S100a4 protein or with recombinant S100a4 protein in the presence of a S100a4 neutralizing antibody. After 24 and 48 hours, cells were harvested for western blot analysis of α-SMA and collagen1a (mainly generated and deposited by myofibroblasts during tissue remodeling), respectively. As illustrated in Figure 3.14B, expression levels of α-SMA and collagen1a were elevated after exposure to S100a4 compared with control cells. This effect was blocked by neutralization of S100a4 with specific antibody. These results indicate that S100a4 promotes activation of lung fibroblasts.

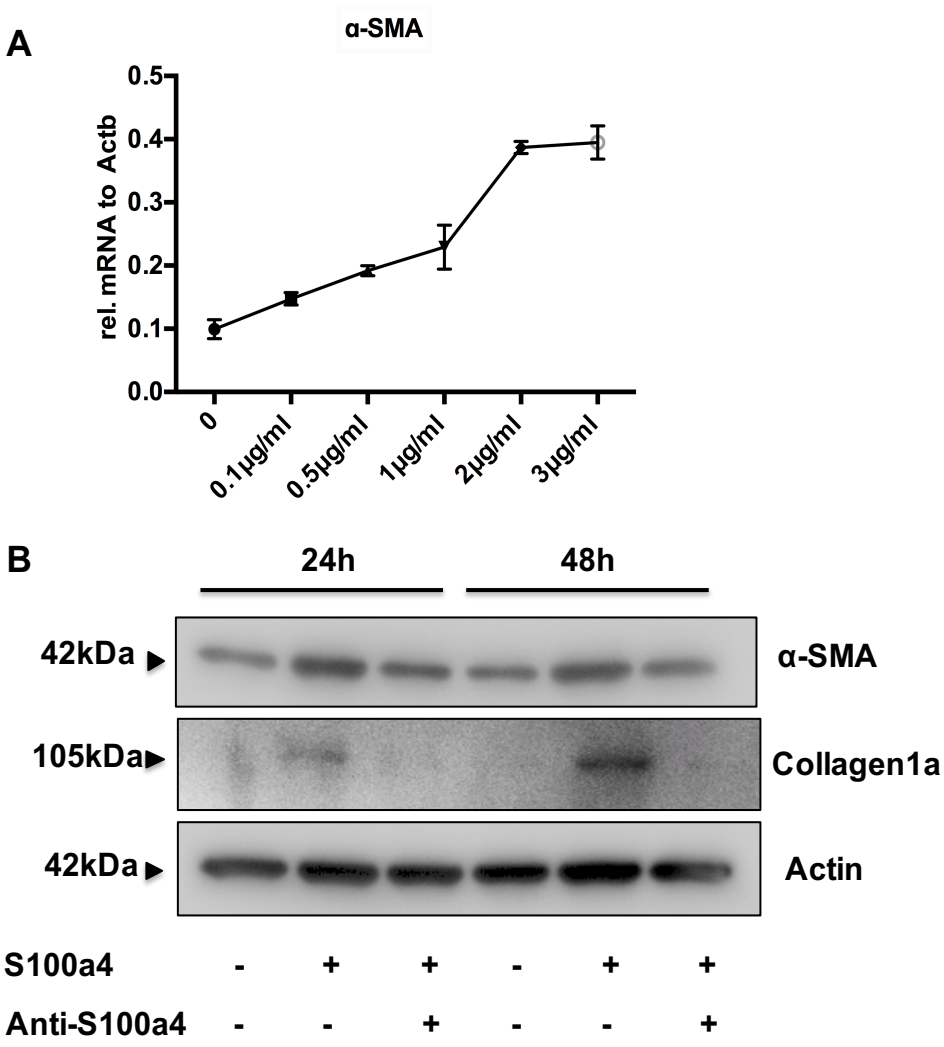

Figure 3.14 S100a4 promotes activation of lung fibroblasts.
(A) Primary lung fibroblasts were treated with various concentrations of recombinant S100a4 (0-3 μg/ml) for 24 hours, and expression of α-SMA was assessed by qRT-PCR. Results are mean ± SD of duplicate samples from one experiment. (B) Cells were treated with 2 μg/ml recombinant S100a4 or with recombinant S100a4 in the presence of a S100a4 neutralizing antibody for 24 and 48 hours, respectively. Cells were harvested and analyzed for expression of α-SMA and collagen1a by western blot. S100a4 neutralization eliminated activation of lung fibroblasts. Results are representative of three independent experiments with similar results.

3.3.2 The Effect of S100a4 on the Proliferation of Primary Lung Fibroblasts

To investigate the effect of S100a4 protein on lung fibroblast proliferation, we employed the XTT assay to measure cell proliferation of lung fibroblasts in response to S100a4 stimulation *in vitro*. As depicted in Figure 3.15, S100a4 significantly accelerated the proliferation of lung fibroblasts by 72 hours after stimulation

compared to the control and antibody treated cells, and neutralization of S100a4 blocked this effect.

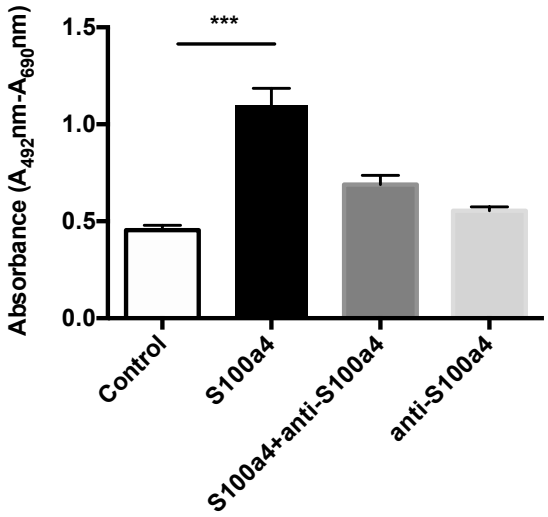

Figure 3.15 S100a4 accelerates lung fibroblasts proliferation.
Primary lung fibroblasts were treated with 2 µg/ml recombinant S100a4 or with recombinant S100a4 in the presence of a S100a4 neutralizing antibody or with antibody alone for 72 hours. Cell proliferation was analyzed using the XTT kit. Results are representative of three independent experiments with similar results. Shown are mean ± SD of five replicates from one experiment. Unpaired t-test was performed for statistical analysis (***denotes $p < 0.001$).

3.3.3 Effect of S100a4 on Wound Healing in Primary Lung Fibroblasts

In fibrotic diseases, fibroblasts migrate to the wound site and participate in the construction of scar tissue. This so-called remodeling is considered to be the vital procedure for the development of fibrosis (221). The role of S100a4 in facilitating migration of a diversity of cancer cells has been broadly reported (178, 222). Hence, we performed the wound healing assay to investigate the influence of S100a4 on the migration of lung fibroblasts. Enhanced cell migration ability was observed in pulmonary fibroblasts after treatment with recombinant S100a4. Additionally, the S100a4-induced cell migration was significantly reduced by blockade with S100a4 neutralizing antibody, which confirmed that S100a4 plays a critical role in cell migration (Figure 3.16).

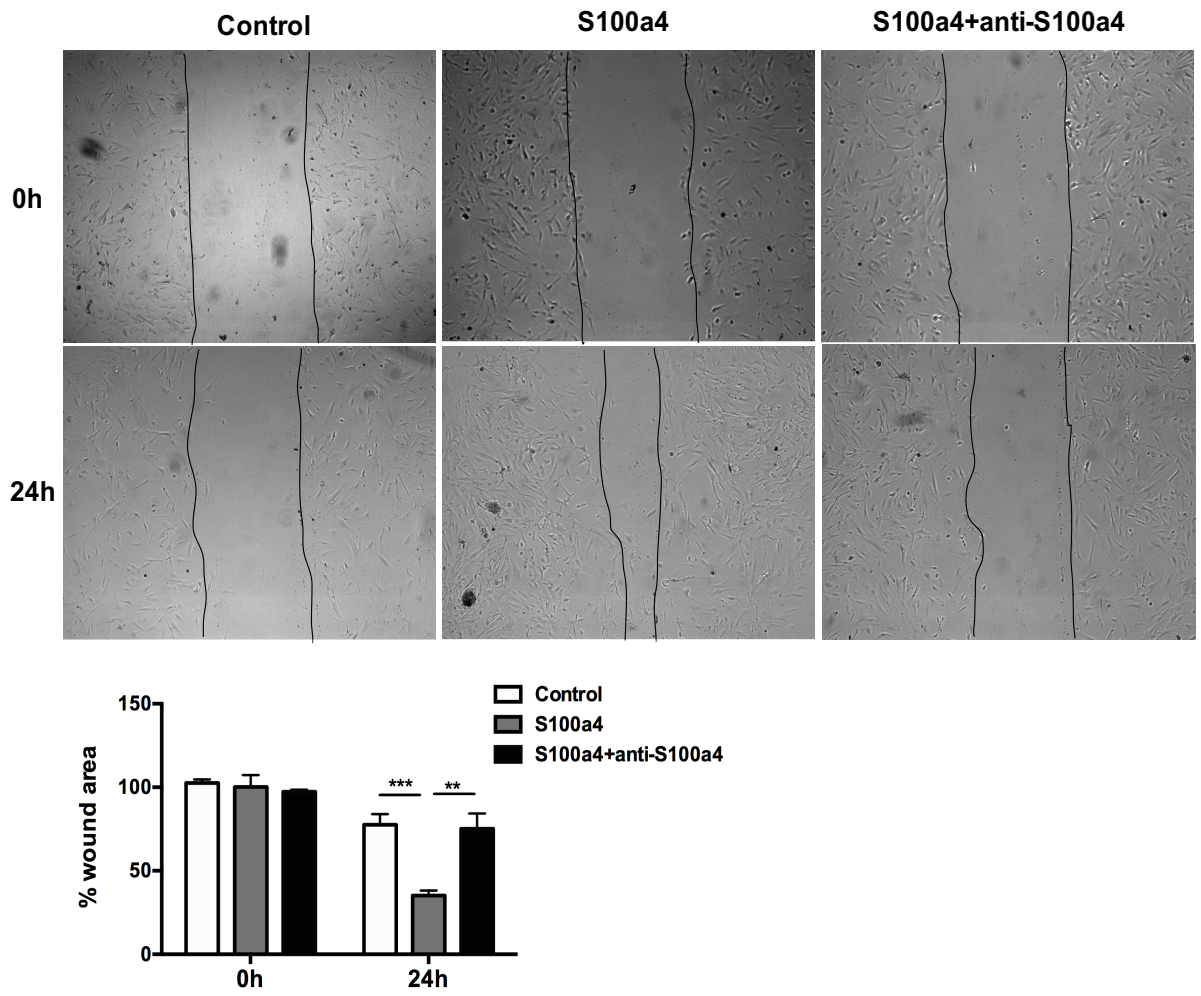

Figure 3.16 S100a4 enhances lung fibroblasts migration in the wound-healing assay. Direct migration of primary lung fibroblasts in the presence of 2 µg/ml recombinant S100a4 or recombinant S100a4 in the presence of the S100a4 neutralizing antibody was analyzed by wound healing assay. Wound closure was determined 24 hours after scratching. Representative phase-contrast pictures of the cells at 0 (immediately after the scratch) and 24 hours after the scratch are shown. The assay was performed three times: one representative experiment is presented. For quantifications, the wound area was measured using ImageJ and normalized to control at 0 hour. Results are representative of three independent experiments with similar results. Shown are mean ± SD of triplicate samples from one experiment. The effect of stimulation by S100a4 was statistically significant in comparison to the control sample, as evaluated by the unpaired t-test (** denotes $p<0.01$; ***denotes $p < 0.001$).

3.4 Inhibition of S100a4 in M2 polarized Alveolar Macrophages

3.4.1 Experimental Approach for Investigation of the Effect of S100a4 Produced by M2 Macrophages on Primary Lung Fibroblasts

Macrophages and fibroblasts are two major cell populations involved in tissue

repair and fibrosis (223). During the proliferation phase of wound healing, fibroblasts proliferate and migrate to the wound site to form granulation tissue; some of these fibroblasts also differentiate into myofibroblasts which chiefly produce ECM and contribute to fibrogenesis (224). Moreover, M2 macrophages are also related to tissue repair and fibrosis through the secretion of paracrine factors (225). However, only limited knowledge is available with regard to the influence of alternatively activated macrophages on the properties of primary lung fibroblasts. Most previous data in the literature has been generated using cell lines (226, 227).

The above experiments have demonstrated that S100a4 is secreted by M2 polarized macrophages during fibrogenesis, and that recombinant S100a4 promotes the proliferation and activation of primary lung fibroblasts. In order to investigate the roles of endogenous S100a4 produced by M2 macrophages on primary lung fibroblasts with respect to proliferation and myofibroblast differentiation, as well as to determine potential therapeutic approaches, the following experiment was performed (Figure 3.17). Alveolar macrophages were isolated *ex vivo* and polarized into M2 macrophages by IL-4 treatment in the presence of anti-S100a4 siRNA or as a control, in the presence of a scrambled siRNA. After 72 hours, the supernatant was harvested and transferred to primary lung fibroblasts. Subsequently, the proliferation of the primary lung fibroblasts was analyzed.

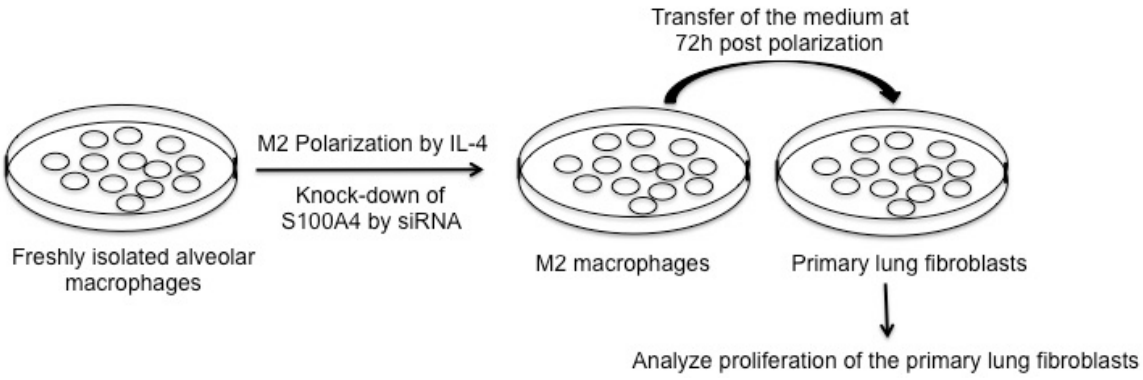

Figure 3.17 Schematic presentation of the experiment for investigation of endogenous S100a4 produced by M2 Macrophages on primary lung fibroblasts.
Diagram shows the conditioned medium transfer system. A total of 3×10^5 freshly isolated alveolar macrophages, isolated from C57BL/6 mice, were plated in a 24-well plate, polarized by IL-4, and transfected with anti-S100a4 siRNA or scrambled control siRNA. The supernatant (conditioned medium) was collected after 72 hours and transferred to primary lung fibroblasts. The proliferation of the primary lung fibroblasts was subsequently analyzed.

3.4.2 Knockdown of S100a4 by siRNA does not interfere with M2-polarization

Since S100a4 is secreted by M2 polarized alveolar macrophages and induced the proliferation and activation of lung fibroblasts, we attempted to downregulate S100a4 production during M2 polarization *in vitro*. For this purpose, transfection of alveolar macrophages with anti-S100a4 siRNAs was employed. Figure 3.18A shows primary alveolar macrophages which were transfected with S100a4-specific siRNA or nonspecific scrambled control siRNA during M2 polarization. It is apparent that the amount of S100a4 mRNA was efficiently downregulated after 72 hours by transient transfection with S100a4 specific siRNAs compared with nonspecific scrambled control siRNA transfection and untransinfected M2 polarized alveolar macrophages. Furthermore, the amount of S100a4 protein in the supernatants of M2 macrophages was also efficiently downregulated after 72 hours by the S100a4 specific siRNAs which is in accordance with the qRT-PCR results (Figure 3.18B). We next investigated whether the reduced amount of S100a4 were duo to a reduced production, or to interference with the macrophage polarization into M2-macrohoages. As shown in Figure 3.18C, inhibition of S100a4 during M2 polarization did not interfere with the expression of Arg1, which suggests that S100a4 is not involved in the polarization of macrophages.

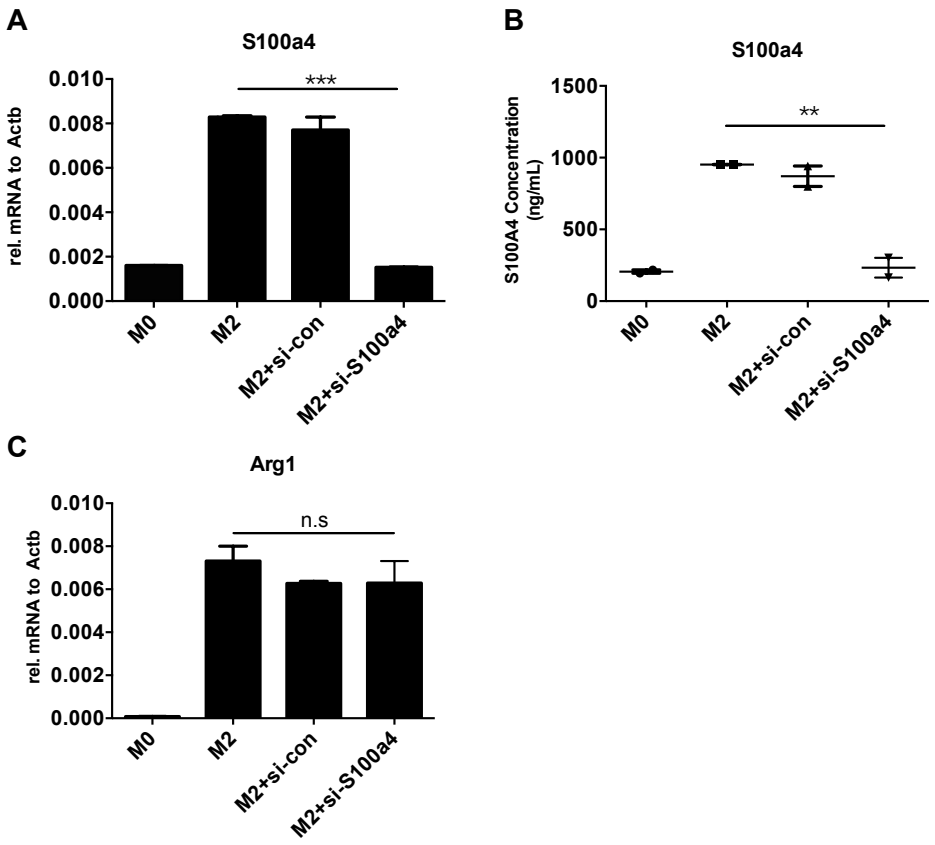

Figure 3.18. Knockdown of S100a4 by siRNA in M2 polarized alveolar macrophages. M2 polarized alveolar macrophages were transfected with nonspecific scrambled control siRNA or S100a4-specific siRNA for 72 hours, and the levels of S100a4 were measured to examine knockdown efficiency. RT-PCR (A and C) was performed for S100a4 and Arg1 mRNA expression analyses. ELISA (B) was performed to measure the amount of S100a4 protein in culture medium. Results are representative of two independent experiments with similar results. Shown are mean ± SD of triplicate samples from one experiment. Unpaired t-test was performed for statistical analysis (* denotes $p<0.05$; ** denotes $p<0.01$; n.s denotes non-significance).

4.4.3 Proliferation of Primary Lung Fibroblasts is Attenuated after Treatment with Conditioned Medium from anti-S100a4 siRNA Transfected M2 Macrophages

It was reported previously that the co-culture of fibroblasts and M2 macrophages can promote the proliferation of fibroblasts, and soluble profibrotic factors secreted by M2 macrophages mediate such an effect, for example IL-4, IL-13 and TGF-β (228). Additionally, the most recent study manifests that S100a4 amplifies TGF-β-induced fibroblast activation and proliferation (229). Therefore, we wanted to investigate the role of S100a4 produced by M2 macrophages on primary lung fibroblasts with respect to proliferation and finally determine potential therapeutic approaches. To address this question, conditioned supernatants from control M2

macrophages or anti-S100a4 siRNA transfected M2 macrophages were transferred to primary lung fibroblast cultures, and the effect on proliferation was evaluated after 24 hours.

The conditioned medium from anti-S100a4 siRNA transfected M2 macrophages caused significantly less proliferation of lung fibroblasts when compared with conditioned medium from scrambled siRNA transfected M2 macrophages. In addition, to confirm the role of S100a4 in cell proliferation and to show that the proliferation is caused by S100a4 contained in the conditioned medium, we first neutralized S100a4 protein in the conditioned medium of M2 macrophages with specific antibody, and then applied it on lung fibroblasts. Neutralization with the specific antibody resulted in reduced proliferation, while the addition of the same amount of control rabbit serum (negative control) had no effect (Figure 3.19). These observations suggested that S100a4 is one of the soluble factors produced by M2 polarized alveolar macrophages which are able to enhance the proliferation of fibroblasts.

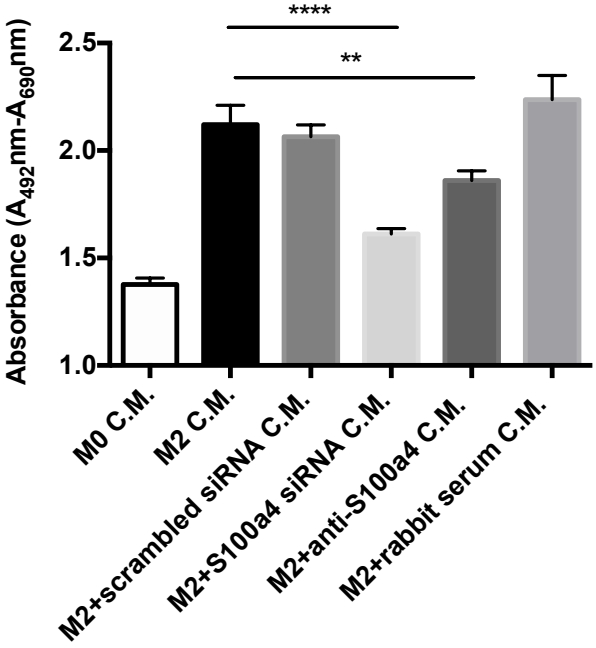

Figure 3.19 Effect of conditioned medium on lung fibroblast proliferation.
Primary lung fibroblasts were treated with conditioned medium (C.M.) from M0, M2 and M2 macrophages transfected with scrambled or S100a4 specific siRNA. In addition, specific S100a4 antibody or isotype control rabbit serum pre-treated M2 conditioned medium were used to stimulate lung fibroblasts. Cell proliferation was analyzed by using XTT kit after 48 hours of treatments. Results are representative of two independent experiments with similar results. Shown are mean ± SD of five replicates from one experiment. Unpaired t-test was performed for statistical analysis (** denotes $p<0.01$; ****denotes $p < 0.0001$).

3.5 Pharmacologic Inhibition of S100a4 Expression

3.5.1 Calcimycin and Niclosamide Interfere with Cell Viability

Previous studies reported that calcimycin and niclosamide, as transcriptional inhibitors of S100a4, bore a great potential to block S100a4 expression in colon cancer cells and therefore hindered cancer metastasis (230, 231). Calcimycin and niclosamide treatment can inhibit cell migration, invasion, wound healing and proliferation capabilities in a S100a4-specific manner in colon cancer cells. Both inhibitors interfere with the constitutively active Wnt pathway. Inhibiting the Wnt/β-catenin pathway activity by calcimycin or interfering with the β-catenin/TCF transcription activating complex by niclosamide resulted in reduced Wnt target gene transcription, among them S100a4 (230, 231). This potential and the applicability of the two small compounds also suggest a novel therapeutic strategy for patients with IPF.

To analyze the inhibitory potential of calcimycin and niclosamide on the expression of S100a4 in alveolar macrophages, we first determined the concentration at which the inhibitors were applicable to MH-S cells, an alveolar macrophage cell line. To cover a broad concentration range, MH-S cells were exposed to thirteen two-fold dilutions of calcimycin and niclosamide, beginning with 200 µM. Cell viability was measured at 24 hours post treatment via XTT kit. Both calcimycin and niclosamide treatment influenced the viability of MH-S cells in a concentration-dependent manner. The half maximal inhibitory concentration (IC50), representing the concentration at which cell viability was decreased to 50%, was calculated to be 5.2µM (95% confidence interval, 4.8-5.7µM) for calcimycin and 0.8µM (95% confidence interval, 0.5-1µM) for niclosamide (Figure 3.20).

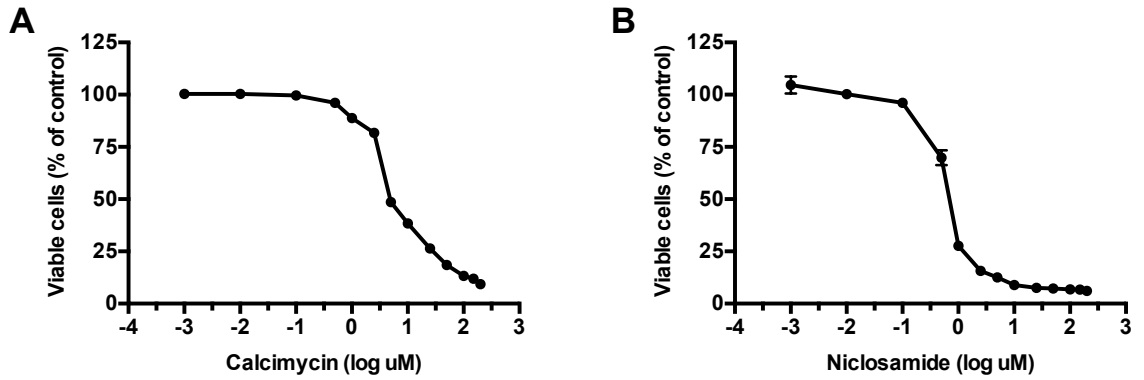

Figure 3.20 Calcimycin and Niclosamide interfere with cell viability in a concentration-dependent manner.

MH-S cells were exposed to increasing concentrations of calcimycin (A), niclosamide (B) or the respective amount of solvent. Cell viability was determined after 24 hours via XTT kit. The IC50s for calcimycin and niclosamide were calculated to be 5.2 µM and 0.8 µM, respectively. Results are representative of two independent experiments with similar results. Shown are mean ± SD of 6 replicates from one experiment.

3.5.2 Inhibition of S100a4 Expression in MH-S cells by Calcimycin and Niclosamide

We next analyzed the capability of calcimycin or niclosamide to reduce the endogenous S100a4 expression in MH-S cells. Exposure of MH-S cells to increasing concentrations of calcimycin or niclosamide for 24 hours resulted in a concentration-dependent reduction of S100a4 mRNA. The concentration of more than 1uM calcimycin significantly reduced the endogenous S100a4 mRNA amount to less than 40% of the solvent treated control (Figure 3.21A). No apparent change in the expression level of S100a4 in MH-S cells was observed when the cells were treated with a concentration lower than 0.5uM calcimycin. Similar to the effects seen for calcimycin, a reduction of the S100a4 mRNA level to about 50% of the solvent treated control was observed when MH-S cells were treated with 0.3uM niclosamide (Figure 3.21B). For further investigation, a concentration with a minimal effect on cell viability and a maximized inhibitory effect on S100a4 expression was selected. A concentration of 1µM calcimycin and 0.3µM niclosamide was sufficient to restrict S100a4 expression to less than 50% of the solvent control. In addition, calcimycin or niclosamide treatment of MH-S cells at those concentrations did not strongly affect cell viability.

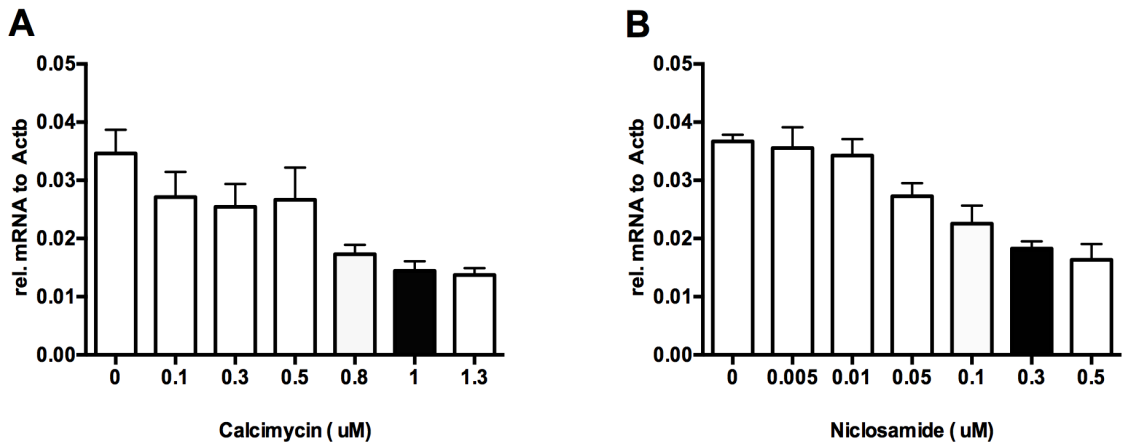

Figure 3.21 Calcimycin and Niclosamide inhibit expression of S100a4 in a concentration-dependent manner.
MH-S cells were exposed to increasing concentrations of calcimycin (A), niclosamide (B) or the respective amount of solvent for 24 hours. mRNA levels of S100a4 were determined by qRT-PCR. 1µM calcimycin or 0.3µM niclosamide were sufficient to inhibit S100a4 expression to less than 50% of solvent-treated cells. Results are representative of two independent experiments with similar results. Shown are mean ± SD of 6 replicates from one experiment.

3.5.3 Inhibition of S100a4 in M2 Polarized Alveolar Macrophages

With the concentrations determined before, we examined the inhibitory effect on S100a4 expression by calcimycin and niclosamide in M2 polarized primary alveolar macrophages. 1µM calcimycin and 0.3µM niclosamide were applied to primary alveolar macrophages during M2 polarization, respectively. Both compounds significantly reduced the S100a4 mRNA expression level (Figure 3.22A). Furthermore, we analyzed the expression of Arg1 in calcimycin or Niclosamide treated primary alveolar macrophages during M2 polarization. As shown in Figure 3.22B, expression of Arg1 was not affected by the treatment with both inhibitors.

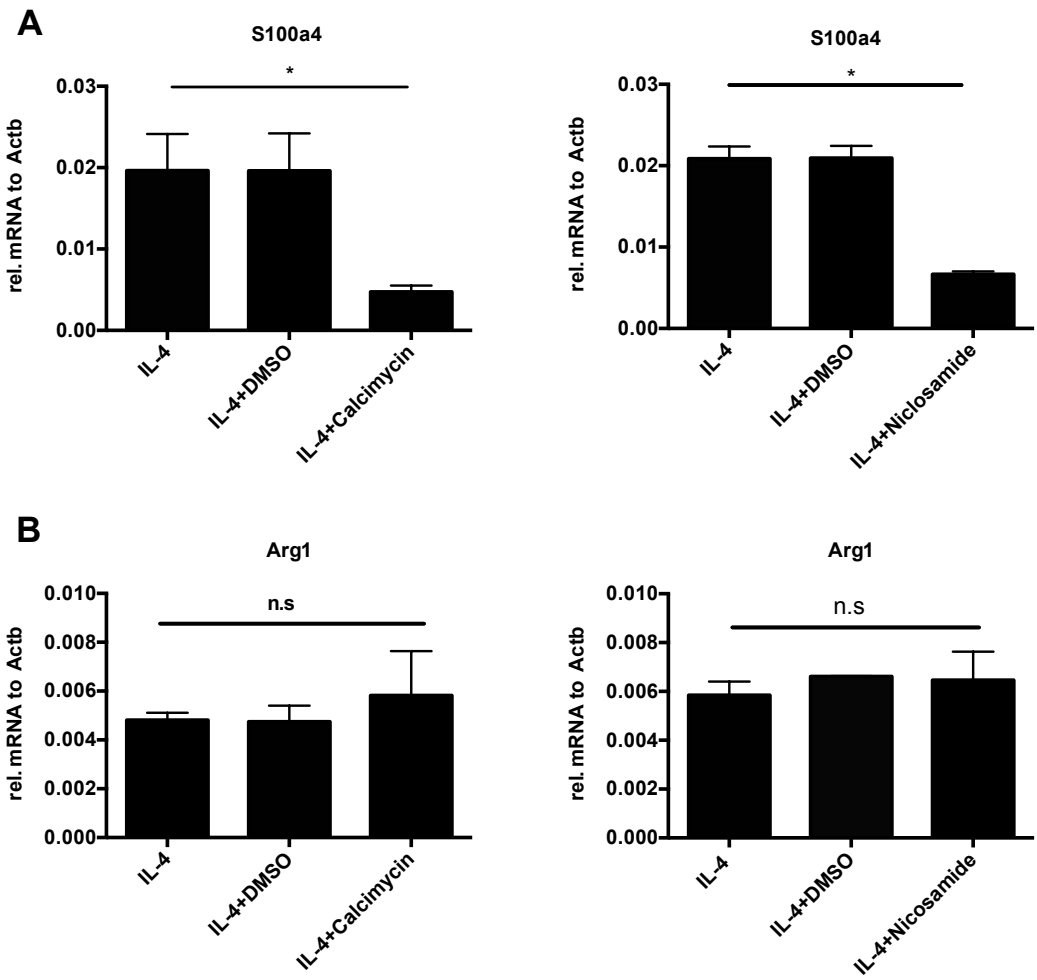

Figure 3.22 Calcimycin and Niclosamide Inhibit expression of S100a4 during M2 polarization.

Alveolar macrophages were treated with IL-4 (20 ng/ml) and 1µM calcimycin or 0.3 µM niclosamide, respectively, for 24 hours. mRNA levels of S100a4 (A) and Arg1 (B) were determined by qRT-PCR. Results are normalized to *β-actin* expression. Results are representative of two independent experiments with similar results. Shown are mean ± SD of duplicates or triplicates from one experiment. (* denotes $p<0.05$; n.s denotes non-significance).

4. Discussion

IPF is the most devastating interstitial lung disease, which is more deadly than most cancers, and death usually ensues 2-5 years after diagnosis due to respiratory failure. Most recently, FDA approved Ofev (nintedanib) and Esbriet (pirfenidone) as two important therapies for the treatment of patients (232, 233). However, new medicines with fewer adverse effects and more efficient attainment of therapeutic outcomes are in short supply. Although the precise molecular mechanisms that drive the pathogenesis of IPF remains elusive, increasing evidence suggests that viral infection, particularly with γ-herpesviruses, is an important factor in the initiation and/or perpetuation of the development of IPF, as EBV protein and DNA are consistently detected in the lung tissue of most cases of IPF patients (21, 199). Moreover, an imbalance between type 1 and type 2 immune responses in the lungs of IPF patients is also observed by the predominance of Th2 cytokines over Th1 cytokines. For example, low levels of IFN-γ have been found in IPF patients (234). Given previous findings, the MHV-68-induced IPF mouse model was established by inoculation of MHV-68 into the respiratory tract of Th2-biased mice, i.e. IFN-γ-receptor-knockout mice. This model recapitulates most histopathological features of pulmonary fibrosis such as emergence of myofibroblast foci, imbalance of Th1 and Th2 cytokines, inflammatory cell infiltrates, excessive deposition of ECM and increased TGF-β. Compared to other animal models, advantages of the MHV-68-induced IPF mouse model are their close relevance to clinical studies and irreversibility. We believe this model will help to reveal pathways involved in the initiation and exacerbation of fibrosis induced by infection.

4.1 Comparative Gene Expression Profiling in the MHV-68-induced IPF model

High-throughput gene expression profiling technology, such as microarrays, is one of the most promising approaches to simultaneously measure the changes in the RNA quantity and to identify key regulatory molecules underlying the disease. Particularly in the cases of complex diseases that associate with altered interactions among numerous genes, expression profiling becomes a prerequisite for the generation of novel hypotheses on mechanisms of diseases and the prioritization of diagnostic and therapeutic candidates. While many hypothesis-driven studies on the mechanisms of IPF were generated in the bleomycin-induced lung fibrosis mouse model, this animal

model is not completely representative of IPF due to the rapid development and resolution with time. Besides, the translation of the current findings into therapeutic candidates has so far been disappointing. Therefore, the generation and verification of novel hypotheses from a more clinically relevant mouse model are of great importance. In this study, we report for the first time genome-wide lung gene expression profiles in the MHV-68-induced IPF mouse model and thereby provide a first step towards a comprehensive view of the complex molecular landscape of initiation and perpetuation of IPF. Allowing robust analysis and statistical selection, a number of differentially regulated genes were identified (Figure 3.2). The composition of this set of genes was analyzed with respect to its association with molecular mechanisms. To dissect processes involved in IPF pathophysiology, we performed various GO and pathway analyses to identify deregulated functions, processes, and pathways (Table 3.1 and 3.2). Enrichment analyses allowed us to pinpoint processes overrepresented among IPF-relevant genes. Consistent with previous studies in the bleomycin-induced IPF mouse model, the result revealed a couple of genes that have been known to be relevant to the pathogenesis of pulmonary fibrosis, such as angiogenesis associated genes. Moreover, there were significant alterations in the expression of many inflammation-related genes including chemokines and cytokines. Interestingly, the upregulation of the chemokines f*CXCL9* and *CXCL10*, that are known to be IFN-γ-inducible and ligands of *CXCR3*, in C57BL/6 mice but not in IFN-γ deficiency mice, supports the notion that IPF is mediated by a Th2 host response. However, IFN-γ treatment in IPF patients has failed to show a survival benefit (235). In order to identify novel candidates for disease-related differentially expressed genes, each gene was prioritized according to the publicly available information in either IPF patients or various animal models, and further analyzed systematically in the literature. Besides the well-known or anticipated IFN-γ-related genes and pathways, a few novel hypotheses have emerged. The gene named S100a4, which has been reported as highly expressed in liver fibrosis, dermal fibrosis and kidney fibrosis, attracted our interest.

4.2 Origin of S100a4-positive Cells in Pulmonary Fibrosis

S100a4, a metastasis-associated gene, is known to be involved in cancer cell motility by virtue of its ability to bind and activate nonmuscle myosin IIA and IIB and actin (236). However, its function in the context of lung injury, repair and fibrosis is unknown. Strong

induction of S100a4 was observed in both IFN-γR$^{-/-}$ and C57BL/6 mice as early as day 14 after MHV-68 infection, and persisted up to day 45 in IFN-γR$^{-/-}$ mice but disappeared in C57BL/6 mice. This induction of S100a4 expression, as detected by microarray analysis, was confirmed by qRT- PCR and western blot in whole lung tissue (Figure 3.3 and 3.4).

S100a4, also termed “fibroblast-specific protein-1”, was considered as a protein that was specifically expressed by fibroblasts but not by other cells, although the protein was known to be highly expressed in cancer cells (180). It was reported that only some S100a4-positive cells were observed in healthy kidneys, while in animal models of renal fibrosis or in patients, a massive increase of S100a4-positive cells in the interstitum and in tubular epithelia was observed, which indicated that fibroblasts, the main ECM producer cells, originated from tubular epithelial cells undergoing EMT (237). Thus, this work introduced S100a4 for identification of fibroblasts in order to demonstrate EMT in many fibrotic diseases. However, in light of our current knowledge, the use of S100a4 as a specific fibroblast marker is not tenable. As a matter of fact, the interstitium of healthy kidneys contains abundant fibroblasts; additionally, myofibroblasts do not express S100a4 (238). Most recently, a similar result was observed in liver fibrosis. In healthy livers from both human and mouse, a few S100a4 cells are found scattered throughout the parenchyma. In contrast, the number of S100a4-positive cells is increased in human and experimental liver fibrosis with scant cytoplasm typically located along fibrotic septa (179, 214). To identify the cellular lineage of S100a4-positive cells, the authors used S100a4-GFP reporter mice. Interestingly, no colocalization of S100a4 and α-SMA or demin, two classical myofibroblast markers, was observed, and the S100a4 positive cells in the injured liver did not synthesize collagen. Instead, S100a4-positive cells clustered with peritoneal macrophages in livers undergoing tissue remodelling (214). Flow cytometry showed that S100a4-positive cells in the mouse model of kidney injury express macrophage-1 antigen (Mac1, also known as CD11b), macrophage-2 antigen (Mac2, also known as Lgals3), macrophage-3 antigen (Mac3, also known as LAMP2), CD45 and CD68 (239). Another group observed coexpression of CD11b, CD68 and F4/80 with S100a4 in mice undergoing unilateral ureteral obstruction (240). A most recent study analyzed S100a4-positive cells at the progression phase of liver fibrosis. These cells expressed the markers of myeloid cells, but not B cells (CD19) or T cells (CD4 and CD8). Immunohistochemistry of fibrotic liver samples confirmed that S100a4-positive cells possess the characteristic

morphology of macrophages (179). In addition, S100a4-positive macrophages have also been reported in various diseases such as peritonitis, cancer and autoimmune encephalitis (241, 242). Our data are in line with these findings. IHC staining of lung sections showed only a few S100a4-positive cells in controls. In the fibrotic lungs, the S100a4-positive cells were widely observed in the lung interstitium. Furthermore, staining of serial lung sections demonstrated that S100a4-positive cells colocalized with Arg1 expressing M2 alveolar macrophages (Figure 3.6 and 3.7). Besides, S100a4 was found to be strongly up-regulated in BALF of IPF experimental mice as compared with controls (Figure 3.5). *In vitro* studies also demonstrated that induction of S100a4 in primary alveolar macrophages via IL-4 or IL-13 was both time and concentration dependent (Figure 3.10). Moreover, expression of S100a4 decreased in LPS or IFN-γ induced M1 macrophages (Figure 3.11).

A Th2-dominant immune response was evidenced in lung tissue from γ-herpesvirus mediated lung fibrosis. Th2 cytokines contributed to the activation of macrophages and differentiation of fibroblasts, and promoted the production of extracellular matrix (201). High expression levels of IL-13 have been reported in BALF from bleomycin-treated mice, and IL-13-deficient mice displayed diminished fibrosis (243).

It is well known that lung fibrosis mediated by chronic herpesvirus infection is associated with the recruitment of alveolar macrophages to the injured lung. These macrophages were exposed to a Th2-dominant immune response environment, activated by the alternative pathway, and expressed a repertoire of pro-fibrotic mediators, such as arginase I, IL-4, IL-13 and TGF-β. Activation of alveolar macrophages via the alternative pathway is considered as an important molecular mechanism promoting the fibrotic process. M2 macrophages produce copious amounts of chemokines, cytokines and growth factors that facilitate the recruitment of multiple cell types involved in damaged tissue repair. In IPF patients, these repair processes failed to restore and resulted in persistent M2 activation and ongoing wound healing responses. Levels of IL-4 and IL-13 are higher in IPF experimental models and patients as compared with controls, and macrophages isolated from fibrotic lungs produce more IL-4 and IL-13 than those isolated from healthy lungs (244). Besides, IL-4 and IL-13 are upstream of STAT6. STAT6 is activated by those cytokines, and promotes IL-4/IL-13-mediated alternative activation of macrophages by producing multiple other wound healing/profibrotic phenotype genes, including the well known TGF-β1 and PDGF, which contribute to proliferation and activation of fibroblasts and enhance expression of

tissue inhibitors of metalloproteinases (TIMPs) that control ECM turnover (245). Moreover, increased multiple products of M2 macrophages have been found in pulmonary fibrosis. Galectin-3, a carbohydrate-binding lectin, which is essential for macrophages alternative activation, was upregulated in BALF from IPF patients compared with that from controls. Galectin-3 is implicated in diverse fibrotic diseases including liver and lung fibrosis. This lectin promotes myofibroblast activation and migration and procollagen 1 synthesis *in vitro* and *in vivo* (246, 247). Studies of macrophage involvement in IPF patients tend to be mostly descriptive, examining the macrophages in samples from patients compared to healthy controls. A more detailed description of M2 macrophages in lung fibrosis was done in experimental models. Depletion of macrophages during the fibrotic phase attenuated the progress of fibrosis. Expression levels of Arg1 and Ym1, M2 markers, were compared before and after depletion of macrophages in the IPF animal model. Depletion of macrophages reduced the expression levels of these two genes. In contrast, iNOS, the M1 marker, did not show a reduction, suggesting that M2 macrophages are essentially responsible for the pathogenesis of fibrosis (248).

4.3 Role of S100a4 in Pulmonary Fibrosis

Extensive studies revealed that S100a4 has both intracellular as well as extracellular functions. Intracellular S100a4 plays a dynamic role in numerous biological processes that are fundamental for cell homeostasis and differentiation including cell growth and survival, cell migration, proliferation and cytoskeletal rearrangement. When secreted extracellularly, S100a4 serves as a cytokine that regulates cell survival and migration, cell differentiation and remodelling of ECM in cancer cells (236). Therefore, in this study, we determined whether the extracellular S100a4 has similar effects on pulmonary fibroblasts, which are the most prominent cellular players in the production of ECM, such as collagen and fibronectin, in the lung. We provided the following lines of evidence to demonstrate the profibrotic role of extracellular S100a4 in pulmonary fibrosis: i) Recombinant S100a4 protein had cell growth-promoting properties on lung fibroblasts. ii) We also found that S100a4 induced the expression of the mesenchymal markers α-SMA and Collagen 1a, indicating that S100a4 promoted lung fibroblasts transition to myofibroblasts which, in turn, synthesized elevated levels of ECM. Therefore, S100a4 might promote pulmonary fibrosis through inducing lung fibroblasts

production of collagen and transition to myofibroblasts. It was noted that blockage of S100a4 with a neutralizing antibody reduced those effects (Figure 3.14). Our results are in agreement with a study by Lin *et al,* reporting S100a4 induced activation of hepatic stellate cells to promote liver fibrosis (179).

Previous studies have investigated the gross mechanisms involved in cell migration caused by extracellular S100a4. Extracellular S100a4 induced migration and proliferation of human pulmonary artery smooth muscle cells through interaction with receptor for advanced glycation end products (RAGE) (249). RAGE is a member of the immunoglobulin superfamily of cell surface molecules, which binds diverse molecules like HMGB1, advanced glycation end products (AGE), and S100 proteins, and plays a potent role in innate immunity (250). The interaction of S100a4 and RAGE resulted in activation of NF-κB, ERK and JNK signaling pathways and is required for cell motility by inducing MMP2 activity (249, 251). Besides S100a4, several other S100 family members (S100A12, S100B, and S100P) were also shown to interact with RAGE. Most recently, Lin and colleagues found that the extracellular S100a4 promoted activation of hepatic stellate cells though upregulation of c-myb, a helix-turn-helix transcription factor that binds to the promoter E box of the *α-SMA* gene (179).

4.4 Inhibition of S100a4 Attenuates Lung Fibroblasts Proliferation *in vitro*

The aforementioned has illustrated that macrophages and fibroblasts are primary effector cells acting in concert in pulmonary inflammation and fibrosis. Macrophages and fibroblasts communicate via soluble autocrine and paracrine signals or juxtacrine signals associated with direct cell contacts. Therefore, both chemical and physical mediators exchanged between macrophages and fibroblasts may modulate wound healing processes such as fibroblast migration and proliferation in the pathogenesis of pulmonary fibrosis. Fibroblasts, reacting to mediators from macrophages, are thought to synthesize extracellular matrix, particularly collagens, resulting ultimately in fibrosis. Both *in vitro* and *in vivo* evidence has demonstrated that classically activated macrophages inhibited fibrogenic properties of fibroblasts by providing antifibrogenic factors, while alternatively activated macrophages enhanced fibrogenesis of fibroblasts by releasing profibrogenic factors such as TGF-β, PDGF, IL-4 and IL-13 (226). Most recently, it was reported that S100a4 is required for TGF-β-induced fibroblast activation (229). Moreover, *in vivo* experiments revealed that S100a4 deficient mice were

protected from liver fibrosis with a reduced accumulation of collagen and a decreased expression level of α-SMA (179). Despite the relevance of macrophages and fibroblasts in tissue homeostasis, the precise role of alternatively activated alveolar macrophages endogenous S100a4 in pulmonary fibrosis has not been fully elucidated to date. Therefore, we performed *in vitro* proliferation assays of lung fibroblasts with conditioned medium from M2 polarized primary alveolar macrophages either left untransfected or transfected with anti-S100a4-siRNA and scrambled control siRNA, respectively. As shown in Figure 3.19, fibroblasts exposed to conditioned medium from M2 macrophages showed increased proliferation, which was in accordance with previous findings (226). In contrast, the conditioned medium from anti-S100a4-siRNA-transfected M2 macrophages induced a significantly lower proliferation rate in lung fibroblasts when compared with conditioned medium from M2 macrophages or control-siRNA-transfected M2 macrophages. In addition, we also neutralized the S100a4 protein in the M2 conditioned medium with an anti-S100a4-antibody. Neutralization with the antibody also reduced the proliferation of the fibroblasts, although not as strong as after siRNA-mediated inhibition. Neutralization with an isotype control antibody had no effect. Based on these findings, we asked whether S100a4 might alter the polarization of macrophages and thereby abrogated the proliferation of lung fibroblast cells. To test this hypothesis, we performed qPCR analysis to determine the expression of Arg1 in alveolar macrophages after knockdown of S100a4 during M2 polarization. As shown in Figure 3.18, no significant change was observed, which indicated that the protein S100a4 was not required for *in vitro* macrophage polarization. It has also been reported that S100a4 induced alterations in the Th1/Th2 polarization balance *in vivo*. T cells challenged with soluble S100a4 displayed a reduced proportion of Th1-polarized cells, shifting the Th1/Th2 balance towards Th2. The imbalance was shown to be the result of S100a4-mediated inhibition of Th1 polarization rather than to be a direct effect on Th2 cell differentiation (252). While M1/M2 paradigms are analogized with Th1/Th2 dichotomy, further studies are necessary to reveal the *in vivo* role of S100a4 in modulating the polarization of macrophages and to get a better understanding of how S100a4 could orchestrate fibrotic remodeling in IPF. Taken together, all these data provided direct evidence that S100a4 produced by M2 macrophages has a prominent profibrogenic effect on the proliferation properties of lung fibroblast cells.

Since the discovery of S100a4, many studies have proven the central role of S100a4 in metastasis formation or fibrogenesis. Hence, targeting S100a4 expression provides a

promising strategy for rational therapies. Previous research showed that inhibition of S100a4 expression in cancer cell lines suppressed cell invasion *in vitro* (254). *In vivo* treatment with anti-S100a4-shRNA or S100a4-neutralizing antibody in fibrotic mice reduced accumulation of myofibroblasts, suppressed deposition of collagen and therefore ameliorated the development of liver fibrosis (179). Furthermore, Sack and colleagues performed high-throughput screening of 1280 pharmacologically active compounds to identify a transcription inhibitor of S100a4 using a human colon cancer cell line. Niclosamide and calcimycin were identified as potential candidates (230, 231). Niclosamide (5-chloro-N-(2-chloro-4-nitrophenyl)-2-hydroxybenzamide) is an FDA-approved anti-helminthic compound used both in humans and animals for the treatment of tapeworm infection since more than forty years (255). Niclosamide is receiving renewed attention due to antiviral effects against severe acute respiratory syndrome virus (SARS) (256). It was reported that Niclosamide inhibited the constitutively active WNT/CTNNB1 signaling pathway by hindering the formation of CTNNB1/TCF transcription activating complex at the S100a4 promoter, thus inhibiting the expression of S100a4 at the transcriptional level. *In vitro* treatment with niclosamide inhibited S100a4-induced migration and proliferation of human colon cancer cells. Besides, niclosamide treatment also attenuated S100a4-induced metastasis formation *in vivo* (231). Calcimycin is one of few natural ionophore antibiotics that specifically transport divalent cations such as calcium and magnesium (257). It has been shown that calcimycin treatment inhibited the constitutively active WNT/β-catenin pathway, thus hindering S100a4 expression and attenuating the S100a4 induced cell migration and invasion both *in vitro* and *in vivo*. Moreover, calcimycin has been reported to reduce the expression of S100a4 at the mRNA level in human monocytes and lymphocytes (258). In line with these findings, both niclosamide and calcimycin suppressed S100a4 in MH-S cells, an alveolar macrophage cell line, in a concentration-dependent manner (Figure 3.21). Moreover, with the determined concentrations, niclosamide and calcimycin were also able to abrogate the expression of S100a4 during M2 polarization without influencing the polarization of macrophages (Figure 3.22).

4.5 Conclusions and Future Perspectives

Our present study provides direct evidence that S100a4 has a significant impact on the proliferation properties of lung fibroblasts. S100a4 could also promote the

differentiation of lung fibroblasts to myofibroblasts and the production of collagen. Moreover, these effects can be attenuated by blockade of S100a4. These results indicate a crucial role of S100a4 in the pathogenesis of lung fibrosis and suggest a novel potential therapeutic target for the treatment of IPF.

Further investigation is required in order to obtain more information about the molecular mechanisms and functions of S100a4 in lung fibroblast cells. It is worth noting that Xu and co-workers have reported that S100A9, a member of the S100 family proteins, promoted human lung fibroblast cells activation and proliferation through RAGE-dependent signaling and subsequent phosphorylation of ERK1/2 MAP-kinase and NF-κB dependent pathways (253). This offers us a clue to the investigation of S100a4 in future studies.

In addition, the possibility that S100a4 is linked to other pathways apart from the RAGE-dependent signaling pathway, such as the Wnt signaling pathway, cannot be excluded. Of much interest in relation to the S100A4 linkup with Wnt signaling is the finding that niclosamide promoted the degradation of the Wnt co-receptor LRP6 (231). Thus, a complex network of signaling cascades that contribute to fibrogenesis is suggested. Therefore, investigation of the role of S100a4 in the Wnt signaling pathway would be necessary and would yield further information about the detailed function of S100a4 in the development of pulmonary fibrosis.

The last but not least, much work is still required to evaluate *in vivo* effects of calcimycin and niclosamide in experimental models. The bleomycin-induced IPF mouse model will provide a powerful tool for investigating the *in vivo* functions of calcimycin and niclosamide. These investigations will further help to clarify the potential benefits of the clinical application of calcimycin and niclosamide in patients with IPF.

5. Appendix

5.1 Abbreviations

°C	degrees celsius
α-SMA	alpha-smooth muscle actin
µl	Microliter
µM	micromolar
Ab	antibody
Actb	Actin, beta
AECs	alveolar epithelial cells
ALI	acute lung injury
AMs	aveloar macrophages
ANG	angiotensin
Arg1	arginase 1
BAL	bronchoalveolar lavage
ccl	chemokine (C-C motif) ligand
cDNA	complementary DNA
Ct	threshold cycle
DMEM	Dulbecco's Modified Eagle Medium
DNA	Deoxyribonucleic acid
d.p.i	days post infection
DPLDs	diffuse parenchymal lung diseases
EBV	Epstein-Barr Virus
ECM	extracellular matrix
EDTA	Ethyldiaminetetraacetate
ELISA	Enzyme-linked immunosorbent assay
EMT	epithelial-mesenchymal transition
ET	endothelin
FBS	fetal bovine serum
g	gram
GM-SCF	granulocyte-macrophage colony stimulating factor
H&E staining	hematoxylin and eosin staining
HRP	horseradish peroxidase
IFN-γ	interferon gamma
IIPs	idiopathic interstitial pneumonias
IL-4	interleukin-4
ILDs	interstitial lung diseases
iNOS	inducible nitric oxide synthase

IPF	idiopathic pulmonary fibrosis
KO, -/-	knock out
KSHV	Kaposi's sarcoma-associated herpesvirus
L	liter
LPS	lipopolysaccharides
M1 macrophages	classically activated macrophages
M2 macrophages	alternatively activated macrophages
MHV-68	Murine gamma-herpesvirus 68
ml	milliliter
mm	millimeter
MMP	matrix metalloproteinases
NF-kB	nuclear factor kappa-light-chain-enhancer of activated B cells
OD	optical density
PBS	Phosphate buffer saline
PBST	Phosphate buffered saline with Tween 20
PCR	Polymerase chain reaction
PFA	phosphate buffered formaldehyde solution
PFU	plaque forming units
PS	pulmonary surfactant
qPCR	quantitative real-time polymerase chain reaction
RAGE	receptor for advanced glycation end products
RIPA	radioimmunoprecipitation assay buffer
RT-PCR	Reverse transcription PCR
S100a4	S100 calcium-binding protein A4
SDS-PAGE	sodium dodecyl sulfate polyacrylamide gel electrophoresis
SD	standard
SP	surfactant proteins
STAT	signal transducer and activator of transcription
TGF	transforming growth factor
Th1 cells	T helper cells type 1
Tnf	tumor necrosis factors
UIP	usual interstitial pneumonia
WT	Wild type

5.2 Acknowledgements

Doing a Ph.D. has always been my dream since I entered the university, as I am very curious about biological sciences and I love learning new things. It's quite clear to all that no one can complete a Ph.D. alone. I really appreciate the selfless and countless help that many people gave me during the last four years. This thesis would not have been completed without their help and encouragement.

Firstly, I would like to express my sincere gratitude to my supervisor Prof. Dr. Heiko Adler for offering me the opportunity to start lung research in Helmholtz Zentrum München, for all his guidance, patience and confidence. He has a great personality and let me always feel being supported. As a superior, he gave me the freedom to conduct my empirical study without any objection. He was always accessible and willing to answer any of my science questions. His perpetual enthusiasm to science extremely inspired me in my studies and makes him an idol.

I would like to thank my thesis committee: Prof. Dr. Klaus Förstemann and Dr. Melanie Königshoff, for their insightful discussions and suggestions throughout the years. In addition, many thanks to Dr. Melanie Königshoff who offered me opportunity to learn H&E and IHC stainings in her lab, and helped me with the animal experiments.

Thanks to all the current and former AG Adler lab members, Dr. Chiristine Sattler, Dr. Martin Strehle, Dr. Dagmar Bunder, Beatrix Steer, that have made my time in the lab enjoyable. I would like to thank colleagues in the Research Unit Gene Vector (AGV) for providing me an international and friendly atmosphere.

Many thanks to colleagues in the group of Dynamics of Pulmonary Inflammation of the Institute of Lung Biology and Disease (iLBD). In particular, Dr. Tobias Stöger, thanks for sharing your broad knowledge and experience in alveolar macrophages, and for inspiring discussions. I would also like to thank my project cooperator Dr. Shanze Chen, from the research group of Dr. Tobias Stöger. Shanze is an energetic person with endless enthusiasm to science. Thanks for teaching me how to collect alveolar macrophages. It is enjoyable to work together with you.

My deepest gratitude goes to my family for their endless love. Dad and Mum, I am so lucky to be your daughter, and my expression of thanks does not suffice. As a

typical Chinese family, you worked hard to support me and provide the possible best environment for me to grow up. You are the best parents in the world.

Above all, I am indebted to my husband, Quan, for his love, understanding and encouragement at all times. Without him it would have been certainly much harder to complete my Ph.D. study in Germany.

6. References

1. Raghu, G., et al., An Official ATS/ERSARS/ALAT Statement: Idiopathic Pulmonary Fibrosis: Evidence-based Guidelines for Diagnosis and Management. Am J Respir Crit Care Med, 2011. **183**(6): p. 788-824.

2. Geiser, T., Idiopathic pulmonary fibrosis--a disorder of alveolar wound repair? Swiss Med Wkly, 2003. **133**(29-30): p. 405-11.

3. Selman, M. and A. Pardo, The epithelial/fibroblastic pathway in the pathogenesis of idiopathic pulmonary fibrosis. Am J Respir Cell Mol Biol, 2003. **29**(3 Suppl): p. S93-7.

4. Visscher, D.W. and J.L. Myers, Histologic spectrum of idiopathic interstitial pneumonias. Proc Am Thorac Soc, 2006. **3**(4): p. 322-9.

5. Gross, T.J. and G.W. Hunninghake, Idiopathic pulmonary fibrosis. N Engl J Med, 2001. **345**(7): p. 517-25.

6. Israel-Biet, D., et al., Idiopathic pulmonary fibrosis: Diagnosis and treatment in 2013. Rev Pneumol Clin, 2014. **70**(1-2): p. 108-117.

7. Hamman, L. and A.R. Rich, Acute diffuse interstitial fibrosis of the lungs. Trans Am Clin Climatol Assoc, 1935. **51**: p. 154-163.

8. Kim, D.S., H.R. Collard, and T.E. King, Jr., Classification and natural history of the idiopathic interstitial pneumonias. Proc Am Thorac Soc, 2006. **3**(4): p. 285-92.

9. King, T.E., Jr., A. Pardo, and M. Selman, Idiopathic pulmonary fibrosis. Lancet, 2011. **378**(9807): p. 1949-61.

10. Travis, W.D., et al., An Official American Thoracic Society/European Respiratory Society Statement: Update of the International Multidisciplinary Classification of the Idiopathic Interstitial Pneumonias. Am J Respir Crit Care Med, 2013. **188**(6): p. 733-748.

11. Agusti, C., American Thoracic Society/European Respiratory Society International Multidisciplinary Consensus Classification of the Idiopathic Interstitial Pneumonias (vol 165, pg 277, 2002). Am J Respir Crit Care Med, 2002. **166**(3): p. 426-426.

12. Esposito, D.B., et al., Idiopathic Pulmonary Fibrosis in US Automated Claims: Incidence, Prevalence and Algorithm Validation. Am J Respir Crit Care Med, 2015.

13. Gribbin, J., et al., Incidence and mortality of idiopathic pulmonary fibrosis and sarcoidosis in the UK. Thorax, 2006. **61**(11): p. 980-5.

14. Hutchinson, J., et al., Global incidence and mortality of idiopathic pulmonary fibrosis: a systematic review. Eur Respir J, 2015. **46**(3): p. 795-806.

15. Coultas, D.B., et al., The epidemiology of interstitial lung diseases. Am J Respir Crit Care Med, 1994. **150**(4): p. 967-72.

16. Baumgartner, K.B., et al., Cigarette smoking: a risk factor for idiopathic pulmonary fibrosis. Am J Respir Crit Care Med, 1997. **155**(1): p. 242-8.

17. Hubbard, R., et al., Occupational exposure to metal or wood dust and aetiology of cryptogenic fibrosing alveolitis. Lancet, 1996. **347**(8997): p. 284-9.

18. Hubbard, R., et al., Risk of cryptogenic fibrosing alveolitis in metal workers. Lancet, 2000. **355**(9202): p. 466-7.

19. Miyake, Y., et al., Occupational and environmental factors and idiopathic pulmonary fibrosis in Japan. Ann Occup Hyg, 2005. **49**(3): p. 259-65.

20. Fahim, A., M. Crooks, and S.P. Hart, Gastroesophageal reflux and idiopathic pulmonary fibrosis: a review. Pulm Med, 2011. **2011**: p. 634613.

21. Tang, Y.W., et al., Herpesvirus DNA is consistently detected in lungs of patients with idiopathic pulmonary fibrosis. J Clin Microbiol, 2003. **41**(6): p. 2633-2640.

22. Wootton, S.C., et al., Viral Infection in Acute Exacerbation of Idiopathic Pulmonary Fibrosis. Am J Respir Crit Care Med, 2011. **183**(12): p. 1698-1702.

23. Allam, J.S. and A.H. Limper, Idiopathic pulmonary fibrosis: is it a familial disease? Curr Opin Pulm Med, 2006. **12**(5): p. 312-317.

24. Hodgson, U., et al., ELMOD2 is a candidate gene for familial idiopathic pulmonary fibrosis. Am J Hum Genet, 2006. **79**(1): p. 149-154.

25. Crystal, R.G., et al., Idiopathic pulmonary fibrosis. Clinical, histologic, radiographic, physiologic, scintigraphic, cytologic, and biochemical aspects. Ann Intern Med, 1976. **85**(6): p. 769-88.

26. Keogh, B.A. and R.G. Crystal, Alveolitis: the key to the interstitial lung disorders. Thorax, 1982. **37**(1): p. 1-10.

27. Phan, S.H., The myofibroblast in pulmonary fibrosis. Chest, 2002. **122**(6): p. 286-289.

28. Tsang, M., Mesenchymal cells emerge as primary contributors to fibrosis in multiple tissues. J Cell Commun Signa, 2014. **8**(1): p. 3-4.

29. Klingberg, F., B. Hinz, and E.S. White, The myofibroblast matrix: implications for tissue repair and fibrosis. J Pathol, 2013. **229**(2): p. 298-309.

30. Hinz, B., et al., The myofibroblast: one function, multiple origins. Am J Pathol, 2007. **170**(6): p. 1807-16.

31. Willis, B.C., et al., Induction of epithelial-mesenchymal transition in alveolar epithelial cells by transforming growth factor-beta1: potential role in idiopathic pulmonary fibrosis. Am J Pathol, 2005. **166**(5): p. 1321-32.

32. Habiel, D.M. and C. Hogaboam, Heterogeneity in fibroblast proliferation and survival in idiopathic pulmonary fibrosis. Front Pharmacol, 2014. **5**: p. 2.

33. Phillips, R.J., et al., Circulating fibrocytes traffic to the lungs in response to CXCL12 and mediate fibrosis. J Clin Invest, 2004. **114**(3): p. 438-46.

34. Bonner, J.C., Regulation of PDGF and its receptors in fibrotic diseases. Cytokine Growth F R, 2004. **15**(4): p. 255-273.

35. Tsukui, T., et al., Qualitative Rather than Quantitative Changes Are Hallmarks of Fibroblasts in Bleomycin-Induced Pulmonary Fibrosis. Am J Pathol, 2013. **183**(3): p. 758-773.

36. Scotton, C.J. and R.C. Chambers, Molecular targets in pulmonary fibrosis: the myofibroblast in focus. Chest, 2007. **132**(4): p. 1311-21.

37. Selman, M. and A. Pardo, Role of epithelial cells in idiopathic pulmonary fibrosis: from innocent targets to serial killers. Proc Am Thorac Soc, 2006. **3**(4): p. 364-72.

38. Aggarwal, N.R., et al., Aquaporin 5 regulates cigarette smoke induced emphysema by modulating barrier and immune properties of the epithelium. Tissue Barriers, 2013. **1**(4): p. e25248.

39. Sadikot, R.T., et al., Targeted immunomodulation of the NF-kappaB pathway in airway epithelium impacts host defense against Pseudomonas aeruginosa. J Immunol, 2006. **176**(8): p. 4923-30.

40. Fereol, S., et al., Cell mechanics of alveolar epithelial cells (AECs) and macrophages (AMs). Respir Physiol Neurobiol, 2008. **163**(1-3): p. 3-16.

41. Williams, M.C., Alveolar type I cells: molecular phenotype and development. Annu Rev

Physiol, 2003. **65**: p. 669-95.

42. Bartlett, J.A., A.J. Fischer, and P.B. McCray, Jr., Innate immune functions of the airway epithelium. Contrib Microbiol, 2008. **15**: p. 147-63.

43. Fehrenbach, H., Alveolar epithelial type II cell: defender of the alveolus revisited. Respir Res, 2001. **2**(1): p. 33-46.

44. Matthay, M.A., H.G. Folkesson, and C. Clerici, Lung epithelial fluid transport and the resolution of pulmonary edema. Physiol Rev, 2002. **82**(3): p. 569-600.

45. Castranova, V., et al., The alveolar type II epithelial cell: a multifunctional pneumocyte. Toxicol Appl Pharmacol, 1988. **93**(3): p. 472-83.

46. Kapanci, Y., et al., Pathogenesis and reversibility of the pulmonary lesions of oxygen toxicity in monkeys. II. Ultrastructural and morphometric studies. Lab Invest, 1969. **20**(1): p. 101-18.

47. Evans, M.J., et al., Transformation of alveolar type 2 cells to type 1 cells following exposure to NO2. Exp Mol Pathol, 1975. **22**(1): p. 142-50.

48. Kapanci, Y., et al., Cytoskeletal protein modulation in pulmonary alveolar myofibroblasts during idiopathic pulmonary fibrosis. Possible role of transforming growth factor beta and tumor necrosis factor alpha. Am J Respir Crit Care Med, 1995. **152**(6 Pt 1): p. 2163-9.

49. Nash, J.R., et al., Expression of tumour necrosis factor-alpha in cryptogenic fibrosing alveolitis. Histopathology, 1993. **22**(4): p. 343-7.

50. Barlo, N.P., et al., Potential role of endothelin-1 in pulmonary fibrosis: from the bench to the clinic. Am J Respir Cell Mol Biol, 2010. **42**(5): p. 633.

51. Mercer, P.F., et al., Pulmonary epithelium is a prominent source of proteinase-activated receptor-1-inducible CCL2 in pulmonary fibrosis. Am J Respir Crit Care Med, 2009. **179**(5): p. 414-25.

52. Uhal, B.D., et al., Alveolar epithelial cell death adjacent to underlying myofibroblasts in advanced fibrotic human lung. Am J Physiol, 1998. **275**(6 Pt 1): p. L1192-9.

53. Waghray, M., et al., Hydrogen peroxide is a diffusible paracrine signal for the induction of epithelial cell death by activated myofibroblasts. FASEB J, 2005. **19**(7): p. 854-6.

54. Blobe, G.C., W.P. Schiemann, and H.F. Lodish, Role of transforming growth factor beta in human disease. N Engl J Med, 2000. **342**(18): p. 1350-8.

55. Kalluri, R. and E.G. Neilson, Epithelial-mesenchymal transition and its implications for fibrosis. J Clin Invest, 2003. **112**(12): p. 1776-84.

56. Pardo, A. and M. Selman, Matrix metalloproteases in aberrant fibrotic tissue remodeling. Proc Am Thorac Soc, 2006. **3**(4): p. 383-8.

57. King, T.E., et al., Idiopathic pulmonary fibrosis - Relationship between histopathologic features and mortality. Am J Respir Crit Care Med, 2001. **164**(6): p. 1025-1032.

58. Cool, C.D., et al., Fibroblast foci are not discrete sites of lung injury or repair - The fibroblast reticulum. Am J Respir Crit Care Med, 2006. **174**(6): p. 654-658.

59. Selman, M., et al., TIMP-1, -2, -3, and -4 in idiopathic pulmonary fibrosis. A prevailing nondegradative lung microenvironment? Am J Physiol Lung Cell Mol Physiol, 2000. **279**(3): p. L562-74.

60. Moodley, Y.P., et al., Fibroblasts isolated from normal lungs and those with idiopathic pulmonary fibrosis differ in interleukin-6/gp130-mediated cell signaling and proliferation. Am J Pathol, 2003. **163**(1): p. 345-354.

61. Pierce, E.M., et al., Therapeutic targeting of CC ligand 21 or CC chemokine receptor 7 abrogates pulmonary fibrosis induced by the adoptive transfer of human pulmonary fibroblasts to Immunodeficient mice. Am J Pathol, 2007. **170**(4): p. 1152-1164.

62. Hu, B., Z. Wu, and S.H. Phan, Smad3 mediates transforming growth factor-beta-induced alpha-smooth muscle actin expression. Am J Respir Cell Mol Biol, 2003. **29**(3): p. 397-404.

63. Saito, A., et al., Potential action of IL-4 and IL-13 as fibrogenic factors on lung fibroblasts in vitro. Int Arch Allergy Immunol, 2003. **132**(2): p. 168-176.

64. Khalil, N., et al., Increased production and immunohistochemical localization of transforming growth factor-beta in idiopathic pulmonary fibrosis. Am J Respir Cell Mol Biol, 1991. **5**(2): p. 155-62.

65. Coker, R.K., et al., Transforming growth factors-beta 1, -beta 2, and -beta 3 stimulate fibroblast procollagen production in vitro but are differentially expressed during bleomycin-induced lung fibrosis. Am J Pathol, 1997. **150**(3): p. 981-91.

66. Akhurst, R.J. and A. Hata, Targeting the TGFbeta signalling pathway in disease. Nat Rev Drug Discov, 2012. **11**(10): p. 790-811.

67. Broekelmann, T.J., et al., Transforming growth factor beta 1 is present at sites of extracellular matrix gene expression in human pulmonary fibrosis. Proc Natl Acad Sci U S A, 1991. **88**(15): p. 6642-6.

68. Khalil, N., et al., Regulation of alveolar macrophage transforming growth factor-beta secretion by corticosteroids in bleomycin-induced pulmonary inflammation in the rat. J Clin Invest, 1993. **92**(4): p. 1812-8.

69. Kapanci, Y., et al., Phenotypic modulation of alveolar myofibroblasts in transplanted human lungs. Mod Pathol, 1997. **10**(11): p. 1134-42.

70. Khalil, N., et al., TGF-beta 1, but not TGF-beta 2 or TGF-beta 3, is differentially present in epithelial cells of advanced pulmonary fibrosis: an immunohistochemical study. Am J Respir Cell Mol Biol, 1996. **14**(2): p. 131-8.

71. Khalil, N., et al., Biological effects of transforming growth factor-beta(1) in idiopathic pulmonary fibrosis may be regulated by the activation of latent transforming growth factor-beta(1) and the differential expression of transforming growth factor-beta receptors. Chest, 2001. **120**(1): p. 48S-48S.

72. Munger, J.S., et al., The integrin alpha v beta 6 binds and activates latent TGF beta 1: a mechanism for regulating pulmonary inflammation and fibrosis. Cell, 1999. **96**(3): p. 319-28.

73. Castelino, F.V. and J. Varga, Interstitial lung disease in connective tissue diseases: evolving concepts of pathogenesis and management. Arthritis ResTher, 2010. **12**(4): p. 213

74. Hu, Y., et al., Role of extracellular signal-regulated kinase, p38 kinase, and activator protein-1 in transforming growth factor-beta1-induced alpha smooth muscle actin expression in human fetal lung fibroblasts in vitro. Lung, 2006. **184**(1): p. 33-42.

75. Caraci, F., et al., TGF-beta 1 targets the GSK-3 beta/beta-catenin pathway via ERK activation in the transition of human lung fibroblasts into myofibroblasts. Pharma Res, 2008. **57**(4): p. 274-282.

76. Dugina, V., et al., Focal adhesion features during myofibroblastic differentiation are controlled by intracellular and extracellular factors. J Cell Sci, 2001. **114**(18): p. 3285-3296.

77. Doucet, C., et al., IL-4 and IL-13 specifically increase adhesion molecule and inflammatory cytokine expression in human lung fibroblasts. Int Immunol, 1998. **10**(10): p.

1421-1433.

78. Mehrad, B., et al., Circulating peripheral blood fibrocytes in human fibrotic interstitial lung disease. Biochem Biophys Res Commun, 2007. **353**(1): p. 104-8.

79. Moeller, A., et al., Circulating fibrocytes are an indicator of poor prognosis in idiopathic pulmonary fibrosis. Am J Respir Crit Care Med, 2009. **179**(7): p. 588-94.

80. Andersson-Sjoland, A., et al., Fibrocytes are a potential source of lung fibroblasts in idiopathic pulmonary fibrosis. Int J Biochem Cell Biol, 2008. **40**(10): p. 2129-40.

81. Bucala, R., et al., Circulating fibrocytes define a new leukocyte subpopulation that mediates tissue repair. Mol Med, 1994. **1**(1): p. 71-81.

82. Hashimoto, N., et al., Bone marrow-derived progenitor cells in pulmonary fibrosis. J Clin Invest, 2004. **113**(2): p. 243-52.

83. Woo, J.I., et al., Spiral ligament fibrocyte-derived MCP-1/CCL2 contributes to inner ear inflammation secondary to nontypeable H. influenzae-induced otitis media. BMC Infect Dis, 2010. **10**: p. 314.

84. Moore, B.B., et al., The role of CCL12 in the recruitment of fibrocytes and lung fibrosis. Am J Respir Cell Mol Biol, 2006. **35**(2): p. 175-81.

85. Sun, L., et al., New concepts of IL-10-induced lung fibrosis: fibrocyte recruitment and M2 activation in a CCL2/CCR2 axis. Am J Physiol Lung Cell Mol Physiol, 2011. **300**(3): p. L341-53.

86. Yokota, T., et al., Bone marrow lacks a transplantable progenitor for smooth muscle type alpha-actin-expressing cells. Stem Cells, 2006. **24**(1): p. 13-22.

87. Martin, T.R. and C.W. Frevert, Innate immunity in the lungs. Proc Am Thorac Soc, 2005. **2**(5): p. 403-11.

88. Bringardner, B.D., et al., The role of inflammation in the pathogenesis of idiopathic pulmonary fibrosis. Antioxid Redox Signal, 2008. **10**(2): p. 287-301.

89. Dethloff, L.A. and B.E. Lehnert, Pulmonary interstitial macrophages: isolation and flow cytometric comparisons with alveolar macrophages and blood monocytes. J Leukoc Biol, 1988. **43**(1): p. 80-90.

90. Cheung, D.O., K. Halsey, and D.P. Speert, Role of pulmonary alveolar macrophages in defense of the lung against Pseudomonas aeruginosa. Infect Immun, 2000. **68**(8): p. 4585-92.

91. Lyons, C.R., et al., Inability of human alveolar macrophages to stimulate resting T cells correlates with decreased antigen-specific T cell-macrophage binding. J Immunol, 1986. **137**(4): p. 1173-80.

92. Fathi, M., et al., Functional and morphological differences between human alveolar and interstitial macrophages. Exp Mol Pathol, 2001. **70**(2): p. 77-82.

93. Laskin, D.L., B. Weinberger, and J.D. Laskin, Functional heterogeneity in liver and lung macrophages. J Leukoc Biol, 2001. **70**(2): p. 163-70.

94. Gordon, S.B. and R.C. Read, Macrophage defences against respiratory tract infections. Br Med Bull, 2002. **61**: p. 45-61.

95. Gong, J.L., et al., Interstitial lung macrophages interact with dendritic cells to present antigenic peptides derived from particulate antigens to T cells. Immunology, 1994. **81**(3): p. 343-51.

96. Hussell, T. and T.J. Bell, Alveolar macrophages: plasticity in a tissue-specific context. Nat Rev Immunol, 2014. **14**(2): p. 81-93.

97. Brieland, J.K., et al., Effect of acute inflammatory lung injury on the expression of monocyte chemoattractant protein-1 (MCP-1) in rat pulmonary alveolar macrophages. Am J Respir Cell Mol Biol, 1992. **7**(2): p. 134-9.

98. Jiang, Y., et al., Monocyte chemoattractant protein-1 regulates adhesion molecule expression and cytokine production in human monocytes. J Immunol, 1992. **148**(8): p. 2423-8.

99. Guilliams, M., et al., Alveolar macrophages develop from fetal monocytes that differentiate into long-lived cells in the first week of life via GM-CSF. J Exp Med, 2013. **210**(10): p. 1977-1992.

100. Schneider, C., et al., Induction of the nuclear receptor PPAR-gamma by the cytokine GM-CSF is critical for the differentiation of fetal monocytes into alveolar macrophages. Nat Immunol, 2014. **15**(11): p. 1026-1037.

101. Gomez Perdiguero, E., et al., Tissue-resident macrophages originate from yolk-sac-derived erythro-myeloid progenitors. Nature, 2015. **518**(7540): p. 547-51.

102. Maus, U.A., et al., Resident alveolar macrophages are replaced by recruited monocytes in response to endotoxin-induced lung inflammation. Am J Respir Cell Mol Biol, 2006. **35**(2): p. 227-35.

103. Janssen, W.J., et al., Fas determines differential fates of resident and recruited macrophages during resolution of acute lung injury. Am J Respir Crit Care Med, 2011. **184**(5): p. 547-60.

104. Erwig, L.P. and P.M. Henson, Clearance of apoptotic cells by phagocytes. Cell Death Differ, 2008. **15**(2): p. 243-50.

105. Bird, L., Innate immunity: calling on the neighbours. Nat Rev Immunol, 2011. **11**(1): p. 2.

106. Scott, C.L., S. Henri, and M. Guilliams, Mononuclear phagocytes of the intestine, the skin, and the lung. Immunol Rev, 2014. **262**(1): p. 9-24.

107. Martinez, F.O., et al., Macrophage activation and polarization. Front Biosci, 2008. **13**: p. 453-61.

108. Biswas, S.K. and A. Mantovani, Macrophage plasticity and interaction with lymphocyte subsets: cancer as a paradigm. Nat Immunol, 2010. **11**(10): p. 889-896.

109. Naessens, T., et al., Innate Imprinting of Murine Resident Alveolar Macrophages by Allergic Bronchial Inflammation Causes a Switch from Hypoinflammatory to Hyperinflammatory Reactivity. Am J Pathol, 2012. **181**(1): p. 174-184.

110. Mills, C.D., et al., M-1/M-2 macrophages and the Th1/Th2 paradigm. J Immunol, 2000. **164**(12): p. 6166-73.

111. Gordon, S. and F.O. Martinez, Alternative activation of macrophages: mechanism and functions. Immunity, 2010. **32**(5): p. 593-604.

112. Gordon, S., Alternative activation of macrophages. Nat Rev Immunol, 2003. **3**(1): p. 23-35.

113. Mora, A.L., et al., Activation of alveolar macrophages via the alternative pathway in herpesvirus-induced lung fibrosis. Am J Respir Cell Mol Biol, 2006. **35**(4): p. 466-73.

114. Martinez, F.O., L. Helming, and S. Gordon, Alternative activation of macrophages: an immunologic functional perspective. Annu Rev Immunol, 2009. **27**: p. 451-83.

115. Balce, D.R., et al., Alternative activation of macrophages by IL-4 enhances the proteolytic capacity of their phagosomes through synergistic mechanisms. Blood, 2011.

118(15): p. 4199-208.

116. Joerink, M., H.F. Savelkoul, and G.F. Wiegertjes, Evolutionary conservation of alternative activation of macrophages: structural and functional characterization of arginase 1 and 2 in carp (Cyprinus carpio L.). Mol Immunol, 2006. **43**(8): p. 1116-28.

117. Itoh, T., et al., Experimental metastasis is suppressed in MMP-9-deficient mice. Clin Exp Metastas, 1999. **17**(2): p. 177-181.

118. Hanania, R., et al., Classically Activated Macrophages Use Stable Microtubules for Matrix Metalloproteinase-9 (MMP-9) Secretion. J Biol Chem, 2012. **287**(11): p. 8468-8483.

119. Ricardo, S.D., H. van Goor, and A.A. Eddy, Macrophage diversity in renal injury and repair. J Clin Invest, 2008. **118**(11): p. 3522-3530.

120. Lu, J.Y., et al., Discrete functions of M-2a and M-2c macrophage subsets determine their relative efficacy in treating chronic kidney disease. Kidney Int, 2013. **84**(4): p. 745-755.

121. Martinez, F.O., et al., Genetic programs expressed in resting and IL-4 alternatively activated mouse and human macrophages: similarities and differences. Blood, 2013. **121**(9): p. e57-69.

122. Raes, G., et al., Arginase-1 and Ym1 are markers for murine, but not human, alternatively activated myeloid cells. J Immunol, 2005. **174**(11): p. 6561; author reply 6561-2.

123. Stein, M., et al., Interleukin 4 potently enhances murine macrophage mannose receptor activity: a marker of alternative immunologic macrophage activation. J Exp Med, 1992. **176**(1): p. 287-92.

124. Mantovani, A., et al., The chemokine system in diverse forms of macrophage activation and polarization. Trends Immunol, 2004. **25**(12): p. 677-86.

125. Biswas, S.K. and A. Mantovani, Macrophage plasticity and interaction with lymphocyte subsets: cancer as a paradigm. Nat Immunol, 2010. **11**(10): p. 889-96.

126. Martinez, F.O. and S. Gordon, The M1 and M2 paradigm of macrophage activation: time for reassessment. F1000Prime Rep, 2014. **6**: p. 13.

127. Boorsma, C.E., C. Draijer, and B.N. Melgert, Macrophage heterogeneity in respiratory diseases. Mediators Inflamm, 2013. **2013**: p. 769214.

128. Migliaccio, C.T., et al., The IL-4Ralpha pathway in macrophages and its potential role in silica-induced pulmonary fibrosis. J Leukoc Biol, 2008. **83**(3): p. 630-9.

129. Murray, L.A., et al., Serum amyloid P therapeutically attenuates murine bleomycin-induced pulmonary fibrosis via its effects on macrophages. PLoS One, 2010. **5**(3): p. e9683.

130. Prasse, A., et al., A vicious circle of alveolar macrophages and fibroblasts perpetuates pulmonary fibrosis via CCL18. Am J Respir Crit Care Med, 2006. **173**(7): p. 781-92.

131. Yogo, Y., et al., Macrophage derived chemokine (CCL22), thymus and activation-regulated chemokine (CCL17), and CCR4 in idiopathic pulmonary fibrosis. Respir Res, 2009. **10**: p. 80.

132. Pechkovsky, D.V., et al., Alternatively activated alveolar macrophages in pulmonary fibrosis-mediator production and intracellular signal transduction. Clin Immunol, 2010. **137**(1): p. 89-101.

133. Wynn, T.A. and L. Barron, Macrophages: master regulators of inflammation and fibrosis. Semin Liver Dis, 2010. **30**(3): p. 245-57.

134. Wynn, T.A., Integrating mechanisms of pulmonary fibrosis. J Exp Med, 2011. **208**(7): p. 1339-50.

135. Dancer, R.C., A.M. Wood, and D.R. Thickett, Metalloproteinases in idiopathic

pulmonary fibrosis. Eur Respir J, 2011. **38**(6): p. 1461-7.

136. Laskin, D.L., et al., Macrophages and tissue injury: agents of defense or destruction? Annu Rev Pharmacol Toxicol, 2011. **51**: p. 267-88.

137. Yang, G., et al., Anti-IL-13 monoclonal antibody inhibits airway hyperresponsiveness, inflammation and airway remodeling. Cytokine, 2004. **28**(6): p. 224-32.

138. Mackinnon, A.C., et al., Regulation of transforming growth factor-beta1-driven lung fibrosis by galectin-3. Am J Respir Crit Care Med, 2012. **185**(5): p. 537-46.

139. Pesce, J.T., et al., Arginase-1-expressing macrophages suppress Th2 cytokine-driven inflammation and fibrosis. PLoS Pathog, 2009. **5**(4): p. e1000371.

140. Liu, T., et al., FIZZ1 stimulation of myofibroblast differentiation. Am J Pathol, 2004. **164**(4): p. 1315-26.

141. Garrett, S.C., et al., S100A4, a mediator of metastasis. J Biol Chem, 2006. **281**(2): p. 677-80.

142. Donato, R., Intracellular and extracellular roles of S100 proteins. Microsc Res Tech, 2003. **60**(6): p. 540-51.

143. Marenholz, I., R.C. Lovering, and C.W. Heizmann, An update of the S100 nomenclature. Biochim Biophys Acta, 2006. **1763**(11): p. 1282-3.

144. Dutta, K., et al., Calcium coordination studies of the metastatic Mts1 protein. Biochemistry, 2002. **41**(13): p. 4239-45.

145. Gingras, A.R., et al., Crystal structure of the Ca(2+)-form and Ca(2+)-binding kinetics of metastasis-associated protein, S100A4. FEBS Lett, 2008. **582**(12): p. 1651-6.

146. Malashkevich, V.N., et al., Structure of Ca2+-bound S100A4 and its interaction with peptides derived from nonmuscle myosin-IIA. Biochemistry, 2008. **47**(18): p. 5111-26.

147. Pathuri, P., L. Vogeley, and H. Luecke, Crystal structure of metastasis-associated protein S100A4 in the active calcium-bound form. J Mol Biol, 2008. **383**(1): p. 62-77.

148. Mazzucchelli, L., Protein S100A4: Too long overlooked by pathologists? Am J Pathol, 2002. **160**(1): p. 7-13.

149. Stein, U., et al., The metastasis-associated gene S100A4 is a novel target of beta-catenin/T-cell factor signaling in colon cancer. Gastroenterology, 2006. **131**(5): p. 1486-1500.

150. Donato, R., S100: a multigenic family of calcium-modulated proteins of the EF-hand type with intracellular and extracellular functional roles. Int J Biochem Cell Biol, 2001. **33**(7): p. 637-68.

151. Kriajevska, M.V., et al., Non-muscle myosin heavy chain as a possible target for protein encoded by metastasis-related mts-1 gene. J Biol Chem, 1994. **269**(31): p. 19679-82.

152. Kriajevska, M., et al., Liprin beta 1, a member of the family of LAR transmembrane tyrosine phosphatase-interacting proteins, is a new target for the metastasis-associated protein S100A4 (Mts1). J Biol Chem, 2002. **277**(7): p. 5229-35.

153. Takenaga, K., et al., Binding of pEL98 protein, an S100-related calcium-binding protein, to nonmuscle tropomyosin. J Cell Biol, 1994. **124**(5): p. 757-68.

154. Li, Z.H., et al., Mts1 regulates the assembly of nonmuscle myosin-IIA. Biochemistry, 2003. **42**(48): p. 14258-66.

155. Endo, H., et al., Methionine aminopeptidase 2 is a new target for the metastasis-associated protein, S10OA4. J Biol Chem, 2002. **277**(29): p. 26396-26402.

156. Li, C.L., et al., A role for CCN3 (NOV) in calcium signalling. J Clin Pathol-Mol Pa, 2002.

55(4): p. 250-261.

157. Grigorian, M., et al., Tumor suppressor p53 protein is a new target for the metastasis-associated Mts1/S100A4 protein - Functional consequences of their interaction. J Biol Chem, 2001. **276**(25): p. 22699-22708.

158. Orre, L.M., et al., S100A4 interacts with p53 in the nucleus and promotes p53 degradation. Oncogene, 2013. **32**(49): p. 5531-40.

159. Donato, R., RAGE: a single receptor for several ligands and different cellular responses: the case of certain S100 proteins. Curr Mol Med, 2007. **7**(8): p. 711-24.

160. Boye, K., et al., Activation of NF-kappaB by extracellular S100A4: analysis of signal transduction mechanisms and identification of target genes. Int J Cancer, 2008. **123**(6): p. 1301-10.

161. Cerezo, L.A., et al., The metastasis-associated protein S100A4 promotes the inflammatory response of mononuclear cells via the TLR4 signalling pathway in rheumatoid arthritis. Rheumatology (Oxford), 2014. **53**(8): p. 1520-6.

162. Schmidt-Hansen, B., et al., Extracellular S100A4(mts1) stimulates invasive growth of mouse endothelial cells and modulates MMP-13 matrix metalloproteinase activity. Oncogene, 2004. **23**(32): p. 5487-95.

163. Mathisen, B., et al., S100A4 regulates membrane induced activation of matrix metalloproteinase-2 in osteosarcoma cells. Clin Exp Metastasis, 2003. **20**(8): p. 701-11.

164. Gao, X.N., S.Q. Tang, and X.F. Zhang, S100A4 antisense oligodeoxynucleotide suppresses invasive potential of neuroblastoma cells. J Pediatr Surg, 2005. **40**(4): p. 648-52.

165. Saleem, M., et al., S100A4 accelerates tumorigenesis and invasion of human prostate cancer through the transcriptional regulation of matrix metalloproteinase 9. Proc Natl Acad Sci U S A, 2006. **103**(40): p. 14825-30.

166. Dahlmann, M., et al., RAGE mediates S100A4-induced cell motility via MAPK/ERK and hypoxia signaling and is a prognostic biomarker for human colorectal cancer metastasis. Oncotarget, 2014. **5**(10): p. 3220-33.

167. Hsieh, H.L., et al., S100 protein translocation in response to extracellular S100 is mediated by receptor for advanced glycation endproducts in human endothelial cells. Biochem Biophys Res Commun, 2004. **316**(3): p. 949-59.

168. Belot, N., et al., Extracellular S100A4 stimulates the migration rate of astrocytic tumor cells by modifying the organization of their actin cytoskeleton. Biochim Biophys Acta, 2002. **1600**(1-2): p. 74-83.

169. Tsukamoto, N., et al., The Expression of S100A4 in Human Pancreatic Cancer Is Associated with Invasion. Pancreas, 2013. **42**(6): p. 1027-1033.

170. Kikuchi, N., et al., Nuclear expression of S100A4 is associated with aggressive behavior of epithelial ovarian carcinoma: an important autocrine/paracrine factor in tumor progression. Cancer Sci, 2006. **97**(10): p. 1061-9.

171. Ismail, N.I., et al., S100A4 overexpression proves to be independent marker for breast cancer progression. Cancer Cell Int, 2008. **8**): p. 12.

172. Saleem, M., et al., S100A4 accelerates tumorigenesis and invasion of human prostate cancer through the transcriptional regulation of matrix metalloproteinase 9. Proc Natl Acad Sci U S A, 2006. **103**(40): p. 14825-14830.

173. Gongoll, S., et al., Prognostic significance of calcium-binding protein S100A4 in colorectal cancer. Gastroenterology, 2002. **123**(5): p. 1478-1484.

174. Kimura, K., et al., Clinical significance of S100A4 and E-cadherin-related adhesion molecules in non-small cell lung cancer. Int J Oncol, 2000. **16**(6): p. 1125-1131.

175. Levett, D., et al., Transfection of S100A4 produces metastatic variants of an orthotopic model of bladder cancer. Am J Pathol, 2002. **160**(2): p. 693-700.

176. Li, Y., et al., Frequent S100A4 Expression with Unique Splicing Pattern in Gastric Cancers: A Hypomethylation Event Paralleled with E-cadherin Reduction and Wnt Activation. Transl Oncol, 2008. **1**(4): p. 165-176.

177. Cerezo, L.A., et al., The metastasis promoting protein S100A4 is increased in idiopathic inflammatory myopathies. Rheumatology (Oxford), 2011. **50**(10): p. 1766-72.

178. Abu El-Asrar, A.M., et al., S100A4 is upregulated in proliferative diabetic retinopathy and correlates with markers of angiogenesis and fibrogenesis. Mol Vis, 2014. **20**: p. 1209-24.

179. Chen, L., et al., S100A4 promotes liver fibrosis via activation of hepatic stellate cells. J Hepatol, 2015. **62**(1): p. 156-64.

180. Okada, H., et al., Early role of Fsp1 in epithelial-mesenchymal transformation. Am J Physiol, 1997. **273**(4 Pt 2): p. F563-74.

181. Iwano, M., et al., Evidence that fibroblasts derive from epithelium during tissue fibrosis. J Clin Invest, 2002. **110**(3): p. 341-50.

182. Strutz, F., et al., Role of basic fibroblast growth factor-2 in epithelial-mesenchymal transformation. Kidney Int, 2002. **61**(5): p. 1714-28.

183. Venkov, C.D., et al., A proximal activator of transcription in epithelial-mesenchymal transition. J Clin Invest, 2007. **117**(2): p. 482-91.

184. Zeisberg, M., et al., BMP-7 counteracts TGF-beta1-induced epithelial-to-mesenchymal transition and reverses chronic renal injury. Nat Med, 2003. **9**(7): p. 964-8.

185. Gauldie, J. and M. Kolb, Animal models of pulmonary fibrosis: how far from effective reality? Am J Physiol Lung Cell Mol Physiol, 2008. **294**(2): p. L151.

186. Moore, B.B. and C.M. Hogaboam, Murine models of pulmonary fibrosis. Am J Physiol Lung Cell Mol Physiol, 2008. **294**(2): p. L152-60.

187. Davison, A.J., et al., The order Herpesvirales. Arch Virol, 2009. **154**(1): p. 171-7.

188. Roizman, B., et al., Herpesviridae. Definition, provisional nomenclature, and taxonomy. The Herpesvirus Study Group, the International Committee on Taxonomy of Viruses. Intervirology, 1981. **16**(4): p. 201-17.

189. Blaskovic, D., et al., Isolation of five strains of herpesviruses from two species of free living small rodents. Acta Virol, 1980. **24**(6): p. 468.

190. Said, J., Kaposi's sarcoma-associated herpesvirus (KSHV): a new viral pathogen associated with Kaposi's sarcoma, primary effusion lymphoma, and multicentric Castleman's disease. West J Med, 1997. **167**(1): p. 37-8.

191. Sunil-Chandra, N.P., S. Efstathiou, and A.A. Nash, Murine gammaherpesvirus 68 establishes a latent infection in mouse B lymphocytes in vivo. J Gen Virol, 1992. **73** (12): p. 3275-9.

192. Nash, A.A. and N.P. Sunil-Chandra, Interactions of the murine gammaherpesvirus with the immune system. Curr Opin Immunol, 1994. **6**(4): p. 560-3.

193. Mora, A.L., et al., Control of virus reactivation arrests pulmonary herpesvirus-induced fibrosis in IFN-gamma receptor-deficient mice. Am J Respir Crit Care Med, 2007. **175**(11): p. 1139-50.

194. Flano, E., et al., Gamma-herpesvirus latency is preferentially maintained in splenic

germinal center and memory B cells. J Exp Med, 2002. **196**(10): p. 1363-72.

195. Stewart, J.P., et al., Lung epithelial cells are a major site of murine gammaherpesvirus persistence. J Exp Med, 1998. **187**(12): p. 1941-51.

196. Vannella, K.M. and B.B. Moore, Viruses as co-factors for the initiation or exacerbation of lung fibrosis. Fibrogenesis Tissue Repair, 2008. **1**(1): p. 2.

197. Egan, J.J., et al., Epstein-Barr virus replication within pulmonary epithelial cells in cryptogenic fibrosing alveolitis. Thorax, 1995. **50**(12): p. 1234-9.

198. Lawson, W.E., et al., Endoplasmic reticulum stress in alveolar epithelial cells is prominent in IPF: association with altered surfactant protein processing and herpesvirus infection. "Am J Physiol Lung Cell Mol Physiol, 2008. **294**(6): p. L1119-L1126.

199. Tsukamoto, K., et al., Involvement of Epstein-Barr virus latent membrane protein 1 in disease progression in patients with idiopathic pulmonary fibrosis. Thorax, 2000. **55**(11): p. 958-61.

200. McMillan, T.R., et al., Exacerbation of established pulmonary fibrosis in a murine model by gammaherpesvirus. Am J Respir Crit Care Med, 2008. **177**(7): p. 771-80.

201. Mora, A.L., et al., Lung infection with gamma-herpesvirus induces progressive pulmonary fibrosis in Th2-biased mice. Am J Physiol Lung Cell Mol Physiol, 2005. **289**(5): p. L711-21.

202. Wallace, W.A., et al., A type 2 (Th2-like) pattern of immune response predominates in the pulmonary interstitium of patients with cryptogenic fibrosing alveolitis (CFA). Clin Exp Immunol, 1995. **101**(3): p. 436-41.

203. Wallace, W.A. and S.E. Howie, Immunoreactive interleukin 4 and interferon-gamma expression by type II alveolar epithelial cells in interstitial lung disease. J Pathol, 1999. **187**(4): p. 475-80.

204. Raghu, G., et al., A placebo-controlled trial of interferon gamma-1b in patients with idiopathic pulmonary fibrosis. N Engl J Med, 2004. **350**(2): p. 125-33.

205. Adler, H., et al., Cloning and mutagenesis of the murine gammaherpesvirus 68 genome as an infectious bacterial artificial chromosome. J Virol, 2000. **74**(15): p. 6964-74.

206. Livak, K.J. and T.D. Schmittgen, Analysis of relative gene expression data using real-time quantitative PCR and the 2(T)(-Delta Delta C) method. Methods, 2001. **25**(4): p. 402-408.

207. Stoeger, T., et al., Instillation of six different ultrafine carbon particles indicates a surface area threshold dose for acute lung inflammation in mice. Environ Health Perspect, 2006. **114**(3): p. 328-33.

208. Lewis, C.C., et al., Disease-specific gene expression profiling in multiple models of lung disease. Am J Respir Crit Care Med, 2008. **177**(4): p. 376-87.

209. Jiang, D., et al., Regulation of pulmonary fibrosis by chemokine receptor CXCR3. J Clin Invest, 2004. **114**(2): p. 291-9.

210. Schneider, M., et al., S100A4 is upregulated in injured myocardium and promotes growth and survival of cardiac myocytes. Cardiovasc Res, 2007. **75**(1): p. 40-50.

211. Chuong, C., et al., RAGE expression and NF-kappaB activation attenuated by extracellular domain of RAGE in human salivary gland cell line. J Cell Physiol, 2009. **221**(2): p. 430-4.

212. Yammani, R.R., D. Long, and R.F. Loeser, Interleukin-7 stimulates secretion of S100A4 by activating the JAK/STAT signaling pathway in human articular chondrocytes.

Arthritis Rheum, 2009. **60**(3): p. 792-800.

213. Konigshoff, M., et al., WNT1-inducible signaling protein-1 mediates pulmonary fibrosis in mice and is upregulated in humans with idiopathic pulmonary fibrosis. J Clin Invest, 2009. **119**(4): p. 772-787.

214. Osterreicher, C.H., et al., Fibroblast-specific protein 1 identifies an inflammatory subpopulation of macrophages in the liver. Proc Natl Acad Sci U S A, 2011. **108**(1): p. 308-13.

215. Chen, S., et al., Immunoproteasome dysfunction augments alternative polarization of alveolar macrophages. Cell Death Differ, 2016. **23**(6): p. 1026-37.

216. Webb, D.C., et al., Integrated signals between IL-13, IL-4, and IL-5 regulate airways hyperreactivity. J Immunol, 2000. **165**(1): p. 108-13.

217. Tachdjian, R., et al., Pathogenicity of a disease-associated human IL-4 receptor allele in experimental asthma. J Exp Med, 2009. **206**(10): p. 2191-204.

218. Takenaga, K., Suppression of metastasis-associated S100A4 gene expression by gamma-interferon in human colon adenocarcinoma cells. Br J Cancer, 1999. **80**(1-2): p. 127-32.

219. Andersen, K., et al., Interferon-gamma suppresses S100A4 transcription independently of apoptosis or cell cycle arrest. Br J Cancer, 2003. **88**(12): p. 1995-2001.

220. Meneghin, A. and C.M. Hogaboam, Infectious disease, the innate immune response, and fibrosis. J Clin Invest, 2007. **117**(3): p. 530-8.

221. Schreier, T., E. Degen, and W. Baschong, Fibroblast migration and proliferation during in vitro wound healing. A quantitative comparison between various growth factors and a low molecular weight blood dialysate used in the clinic to normalize impaired wound healing. Res Exp Med (Berl), 1993. **193**(4): p. 195-205.

222. Cox, T.R. and J.T. Erler, Remodeling and homeostasis of the extracellular matrix: implications for fibrotic diseases and cancer. Dis Model Mech, 2011. **4**(2): p. 165-78.

223. Duffield, J.S., et al., Selective depletion of macrophages reveals distinct, opposing roles during liver injury and repair. J Clin Invest, 2005. **115**(1): p. 56-65.

224. Gurtner, G.C., et al., Wound repair and regeneration. Nature, 2008. **453**(7193): p. 314-21.

225. Martin, P. and S.J. Leibovich, Inflammatory cells during wound repair: the good, the bad and the ugly. Trends Cell Biol, 2005. **15**(11): p. 599-607.

226. Song, E., et al., Influence of alternatively and classically activated macrophages on fibrogenic activities of human fibroblasts. Cell Immunol, 2000. **204**(1): p. 19-28.

227. Ploeger, D.T., et al., Cell plasticity in wound healing: paracrine factors of M1/ M2 polarized macrophages influence the phenotypical state of dermal fibroblasts. Cell Commun Signal, 2013. **11**(1): p. 29.

228. Holt, D.J., L.M. Chamberlain, and D.W. Grainger, Cell-cell signaling in co-cultures of macrophages and fibroblasts. Biomaterials, 2010. **31**(36): p. 9382-9394.

229. Tomcik, M., et al., S100A4 amplifies TGF-beta-induced fibroblast activation in systemic sclerosis. Ann Rheum Dis, 2015. **74**(9): p. 1748-55.

230. Sack, U., et al., S100A4-induced cell motility and metastasis is restricted by the Wnt/beta-catenin pathway inhibitor calcimycin in colon cancer cells. Mol Biol Cell, 2011. **22**(18): p. 3344-54.

231. Sack, U., et al., Novel effect of antihelminthic Niclosamide on S100A4-mediated

metastatic progression in colon cancer. J Natl Cancer Inst, 2011. **103**(13): p. 1018-36.

232. King, T.E., Jr., et al., A phase 3 trial of pirfenidone in patients with idiopathic pulmonary fibrosis. N Engl J Med, 2014. **370**(22): p. 2083-92.

233. Wollin, L., et al., Antifibrotic and anti-inflammatory activity of the tyrosine kinase inhibitor nintedanib in experimental models of lung fibrosis. J Pharmacol Exp Ther, 2014. **349**(2): p. 209-20.

234. Ziesche, R., et al., A preliminary study of long-term treatment with interferon gamma-1b and low-dose prednisolone in patients with idiopathic pulmonary fibrosis. N Engl J Med, 1999. **341**(17): p. 1264-9.

235. King, T.E., Jr., et al., Effect of interferon gamma-1b on survival in patients with idiopathic pulmonary fibrosis (INSPIRE): a multicentre, randomised, placebo-controlled trial. Lancet, 2009. **374**(9685): p. 222-8.

236. Boye, K. and G.M. Maelandsmo, S100A4 and metastasis: a small actor playing many roles. Am J Pathol, 2010. **176**(2): p. 528-35.

237. Strutz, F., et al., Identification and characterization of a fibroblast marker: FSP1. J Cell Biol, 1995. **130**(2): p. 393-405.

238. Picard, N., et al., Origin of renal myofibroblasts in the model of unilateral ureter obstruction in the rat. Histochem Cell Biol, 2008. **130**(1): p. 141-55.

239. Inoue, T., D. Plieth, and E.G. Neilson, Antibodies against macrophages that overlap in specificity with fibroblasts - Reply from the authors. Kidney Int, 2005. **68**(5): p. 2400-2401.

240. Lin, S.L., et al., Pericytes and Perivascular Fibroblasts Are the Primary Source of Collagen-Producing Cells in Obstructive Fibrosis of the Kidney. Am J Pathol, 2008. **173**(6): p. 1617-1627.

241. Li, Z.H., et al., S100A4 regulates macrophage chemotaxis. Mol Biol Cell, 2010. **21**(15): p. 2598-610.

242. Bjork, P., et al., Common Interactions between S100A4 and S100A9 Defined by a Novel Chemical Probe. Plos One, 2013. **8**(5).

243. Kaviratne, M., et al., IL-13 activates a mechanism of tissue fibrosis that is completely TGF-beta independent. J Immunol, 2004. **173**(6): p. 4020-9.

244. Hancock, A., et al., Production of interleukin 13 by alveolar macrophages from normal and fibrotic lung. Am J Respir Cell Mol Biol, 1998. **18**(1): p. 60-5.

245. Walford, H.H. and T.A. Doherty, STAT6 and lung inflammation. JAKSTAT, 2013. **2**(4): p. e25301.

246. Henderson, N.C., et al., Galectin-3 regulates myofibroblast activation and hepatic fibrosis. Proc Natl Acad Sci U S A, 2006. **103**(13): p. 5060-5.

247. Nishi, Y., et al., Role of galectin-3 in human pulmonary fibrosis. Allergol Int, 2007. **56**(1): p. 57-65.

248. Gibbons, M.A., et al., Ly6Chi monocytes direct alternatively activated profibrotic macrophage regulation of lung fibrosis. Am J Respir Crit Care Med, 2011. **184**(5): p. 569-81.

249. Spiekerkoetter, E., et al., S100A4 and bone morphogenetic protein-2 codependently induce vascular smooth muscle cell migration via phospho-extracellular signal-regulated kinase and chloride intracellular channel 4. Circ Res, 2009. **105**(7): p. 639-47, 13 p following 647.

250. Bierhaus, A., et al., Understanding RAGE, the receptor for advanced glycation end products. J Mol Med (Berl), 2005. **83**(11): p. 876-86.

251. Yammani, R.R., et al., Increase in production of matrix metalloproteinase 13 by human articular chondrocytes due to stimulation with S100A4: Role of the receptor for advanced glycation end products. Arthritis Rheum, 2006. **54**(9): p. 2901-11.

252. Grum-Schwensen, B., et al., S100A4-neutralizing antibody suppresses spontaneous tumor progression, pre-metastatic niche formation and alters T-cell polarization balance. BMC Cancer, 2015. **15**: p. 44.

253. Xu, X., et al., S100A9 promotes human lung fibroblast cells activation through receptor for advanced glycation end-product-mediated extracellular-regulated kinase 1/2, mitogen-activated protein-kinase and nuclear factor-kappaB-dependent pathways. Clin Exp Immunol, 2013. **173**(3): p. 523-35.

254. Tarabykina, S., et al., Metastasis-associated protein S100A4: spotlight on its role in cell migration. Curr Cancer Drug Targets, 2007. **7**(3): p. 217-28.

255. Ditzel, J. and M. Schwartz, Worm cure without tears. The effect of niclosamide on taeniasis saginata in man. Acta Med Scand, 1967. **182**(5): p. 663-4.

256. Wu, C.J., et al., Inhibition of severe acute respiratory syndrome coronavirus replication by niclosamide. Antimicrob Agents Chemother, 2004. **48**(7): p. 2693-6.

257. Pressman, B.C., Biological applications of ionophores. Annu Rev Biochem, 1976. **45**: p. 501-30.

258. Grigorian, M., et al., Modulation of mts1 expression in mouse and human normal and tumor cells. Electrophoresis, 1994. **15**(3-4): p. 463-8.